Department of Precision and Microsystems Engineering

A Method for Optimal Component Selection in Impedance-Type Haptic Devices

Erik Jansen

Report no : MSD 2016.024
Coach : ir. A.G.L. Hoevenaars
Professor : Prof. dr. ir. J.L. Herder
Specialization : Mechatronic System Design
Type of report : Master Thesis
Date : 30 June 2016

A Method for Optimal Component Selection in Impedance-Type Haptic Devices

Towards Optimization of Haptic Designs

by

Erik Jansen, BSc
Born on August 7, 1990 in Maasland

in partial fulfillment of the requirements for the degree of

Master of Science
in Mechanical Engineering

at the Delft University of Technology,
to be defended publicly on Thursday June 30, 2016 at 13:30.

Faculty:	Mechanical, Maritime and Materials Engineering (3mE)	
Department:	Precision and Microsystems Engineering (PME)	
Specialization:	Mechatronic System Design	
Student number:	4018397	
Supervisor:	ir. A.G.L. Hoevenaars	
Thesis committee:	Prof. dr. ir. J.L. Herder,	TU Delft, PME
	ir. A.G.L. Hoevenaars,	TU Delft, PME
	To be decided	

This thesis is confidential and cannot be made public until June 30, 2017.

TU Delft Delft University of Technology

Preface

Initially, the goal of this thesis was to develop a low-cost haptic device. Therefore I dove into literature, trying to find structured methods to evaluate choices in the design phase. How to design a haptic device, how to optimize a design for certain desired performance? Those were the main questions when I started this project, early in 2015. Unfortanutly, structured design guidelines could not be found. Therefore, I decided to develop this method myself.

However, the most important discoveries during this project don't have anything to do with the design of haptic devices. This thesis is the result of my first academic research, which proved to be quite a challenge. I learned a lot, especially about myself. Working as an independent researcher proved to be difficult, but the result is here: my MSc-thesis!

Of course, I couldn't have done it without the help and support from family and friends, from which some of them deserve the explicit acknowledgments in this report.

First of all, I would like to thank my fellow MSD-students, for the fruitful discussions in the meetings, but the possibly even better ones during lunch and coffee breaks. I am especially grateful to Gijs, Stefan, Arjan and Bart, for proofreading parts of this thesis.

In addition, the people around me in the Delft Haptics Lab. I would like to thank them for the liters of coffee we drank, and for tolerating my desk getting messier and messier during the continuation of my thesis project. I acknowledge Roel in particular, for helping me to get acquainted with the Gemini Haptic Paddle and the tips during the experiments.

Professor Herder, thank you for being the chair of my exam committee. Additionally, I would like to thank the other members for being part of my exam committee too.
Jo, for giving feedback during this project, and leading the inspiring Jo-meetings on the Monday mornings.

Furthermore, Teun, thanks a lot for supervising my master's project. I admire the structured way you work, and learned a lot from you. I am especially grateful for you ever-lasting positive view and for taking the time for proofreading different versions of my paper and thesis in your own spare time.

And then the three most important people in my life:

Jana, thank you for spending the past six-and-a-half years with me! Thanks for challenging me and for pulling me out of my comfort zone. Thanks for kicking my ass when I needed it during this project, and for your patience of having a graduating boyfriend around, with his constant frustrations about his thesis. I am looking forward to going to Friesland with you!

And finally, my parents. Thank you for being the main sponsors of the project "Eriks Education", which will formally end after almost 22 years. During the last seven year at the university, but even so in the years before, you were there for support and motivation. I couldn't have done it without your support!

Erik Jansen
Delft, June 2016

Table of Contents

Nomenclature

List of Latin Symbols

Symbol	Unit	Description
b	$\mathrm{N\,s\,m^{-1}}$	Viscous damping of a haptic device
B	$\mathrm{N\,s\,m^{-1}}$	Virtual Damping
B_{max}	$\mathrm{N\,s\,m^{-1}}$	Virtual damping corresponding to K_{max}
c	N	Coulomb friction of a haptic device
$D(z)$	[−]	Finite difference derivative estimator
F_{ee}	N	Force at the end-effector
F_a	N	Actuation force
F_h	N	Net force of human operator, applied on the haptic device
h	m	length of pulley haptic paddle
$H(z)$	[−]	Discrete-time velocity filter transfer function
$H_{VE}(s)$	$\mathrm{N\,m^{-1}}$	Continuous-time transfer function of virtual environment
I	$\mathrm{kgm^2}$	Inertia
I_{ax}	$\mathrm{kgm^2}$	Additional inertia on pulley-axis
I_a	$\mathrm{kgm^2}$	Inertia of actuator
I_h	$\mathrm{kgm^2}$	Inertia of handle of the haptic paddle
I_p	$\mathrm{kgm^2}$	Inertia of pulley of the haptic paddle
K	$\mathrm{N\,m^{-1}}$	Virtual stiffness
K_{max}	$\mathrm{N\,m^{-1}}$	Overall maximum stable virtual stiffness
K_q	$\mathrm{N\,m^{-1}}$	Maximum stable stiffness by quantization-error stability
K_s	$\mathrm{N\,m^{-1}}$	Maximum stable stiffness by sampled-data stability
L	H	Inductacne of coils in DC-motor
L_h	m	Length of handle haptic paddle
m	kg	Moving mass of a haptic device, lumped at the end-effector
n	[−]	Order of the velocity filter
N	[−]	Pulses per revolution in the encoder
R	Ω	Resistance of coils in DC-motor
R_h	m	Radius of handle haptic paddle
r_p	m	Radius of pulley haptic paddle
T	s	Sample time
t_a	s	Electrical time delay in the actuator
T_a	N m	Actuator Torque
t_d	s	Total time delay
$V(s)$	$\mathrm{m\,s^{-1}}$	Velocity in s-domain
x	m	True position
$X(s)$	m	True position in s-domain
$\hat{x}$	m	Measured position
$\tilde{x}$	m	Noise on position sensing
$Z(s)$	$\mathrm{N\,s\,m^{-1}}$	Impedance
$Z_{FS}(s)$	$\mathrm{N\,s\,m^{-1}}$	Free Space Impedance
$Z_{max}(s)$	$\mathrm{N\,s\,m^{-1}}$	Maximum stable impedance
$\mathbb{Z}_w$	$\mathrm{N\,s\,m^{-1}}$	Z-Width

List of Greek Symbols

Symbol	Unit	Description
Δ	m	Quantization interval in distance at the end-effector
ρ	kgm^{-3}	Volumetric mass density
$\rho(x_1, x_2)$	[−]	Pearson correlation coefficient of x_1 and x_2
τ_e	s	Electrical time constant
ω_c	$\mathrm{rad\,s}^{-1}$	Velocity filter cut-off frequency
ω_{ES}	$\mathrm{rad\,s}^{-1}$	Effective Stiffness Bandwidth

Abbreviations and subscripts

Notation	Used in	Short for
a	I, t, T	Actuator
c	ω	Cut-off
d	t	Delay
des	$Z(s)$	Desired
DoF		Degree of Freedom
ES	ω	Effective Stiffness
FS	$Z(s)$	Free Space
h	I, L, R	Handle of haptic paddle
LC		Limit Cycles
max	$K, B, Z(s)$	Corresponding to the maximum stable stiffness
p	I, r	Pulley of haptic paddle
q	K	Quantization-error
s	K	Sampled-data
S		Stable Response
VE	$H(s)$	Virtual Environment

1

Introduction

1.1. Background

Telemanipulation is performing an action, over a distance. It consists of a pair of robot manipulators: one to be handled by the operator (the master) and one operating in a remote environment (a slave), that reconstructs the human actions of the operator[1], as visualized in figure 1.1a. When forces of the remote environment felt by the slave, are reconstructed at the master side, this is called "Haptic Force Feedback". The slave robot in a remote environment can be replaced by a virtual environment for virtual reality interaction as depicted in figure 1.1b. Ideally, an operator is not able to distinguish those two scenarios, teleoperation and virtual reality interaction, from the third in 1.1c: interaction with the physical tool directly.

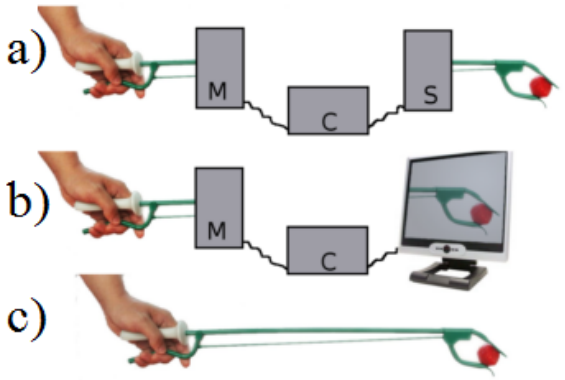

Figure 1.1: The three different scenarios: in a) teleoperation and in b) virtual reality interaction. In the ideal case, with excellent haptic feedback, these two methods feel like there is direct interaction with the tool, scenario c. Here 'M' denotes the master robot, 'C' the controller and 'S' the slave. Figure slightly modified from Christiansson[2].

Teleoperation is typically used in hard-accessible environments, such as minimum invasive surgery, or in hostile environments, e.g. robots for dismantling bombs or robots in radioactive environments, such as explorations robots used in Fukushima. The main application for rendering virtual environments is education, for example in flight simulators or medical training devices.

The two simplest abstractions of interaction with haptic force feedback are the impedance approach and the admittance approach[3], both shown in figure 1.2. For both, and all other approaches, the challenge in haptic devices is to render a broad range of impedances: free motion is desired to feel free, and hard contact is desired to feel stiff.

In impedance controlled force feedback, the haptic device responds to a movement by generating a reaction force. This is visualized in figure 1.2a, where the v's denote velocities and the f's forces of the device, the operators hand and the virtual environment. In an impedance device the forces of hand, device and environment sum to zero, while the velocities are the same. A virtual environment acts as

a mechanical impedance, a force in response to a velocity. It consists of springs and dampers, two of the elementary building blocks of every impedance[4]. With this impedance approach, users feel the combined forces from the dynamics and statics of the device and the simulated environment in response to moving the device[3]. This gives an essential trade off in haptic rendering: In free space motion, the operator only feels the device impedance, which should be as low as possible. However, the same device must be able to render large impedances, for which the device mass and damping prove to be essential.

The other version is the opposite: in an admittance-type haptic device, the virtual environment acts as a mechanical admittance. This is a velocity in response to an applied force. This method is displayed in figure 1.2b. It has the disadvantage that a generally expensive force sensor is needed on the device, and free movement corresponds to high-gain feedback. In an admittance device the velocities of hand, device and environment sum to zero, while the forces are the same.

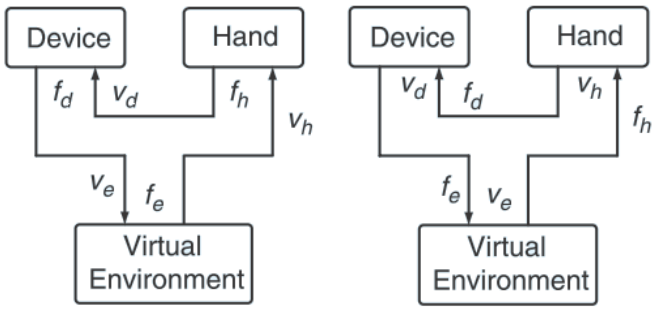

(a) Impedance Approach (b) Admittance Approach

Figure 1.2: The two mechanical circuits that are used in haptic devices. The impedance approach vs the admittance approach. The v's denote velocities, and f's denote forces. In an impedance device the forces of hand, device and environment sum to zero, while the velocities are the same. In the admittance approach, this is the other way around. Picture from Hayward[3].

A more extensive background of this study can be found in some interesting introductory papers such as Hayward and Maclean[3] or Hannaford and Okamura[5]. Appendix E gives an overview of the studied literature and research background for this thesis.

1.2. Problems and Motivation

The ideal haptic device is stable over a large dynamic range of impedances, and generates an accurate force signal. In haptic performance, one can distinguish two important performance metrics: *haptic capability* and *haptic quality*. The haptic capability is the dynamic range of the stable achievable impedances, in literature well-known as the Z-Width[6]. The haptic quality is a measure for accuracy of the rendered (virtual) environment, the resemblance between the desired and the rendered impedance. In haptic teleoperation, this measure is called the transparency[7]. The transparency is good upto the Effective Stiffness Bandwidth[8]. At higher frequencies, the device dynamics will be dominant over the rendered dynamics.

Several performance studies have been done in literature, but those have two things in common.

First, the evaluation is done afterwards, after a design is finished. Some studies focused on direct comparison of devices (like in Rose[9] who compared haptic paddles, Martin[10] who compared three different 6-DoF devices). Other studies are done based on identification and on standardized benchmark tests[11, 12, 13]. A problem here is that a more structured method is desired, such that a designer of haptic devices is able to calculate the consequences of design decisions.

Secondly, the performance evaluation is done based on individual physical parameters only, such as mass, damping and time delay[14, 15, 16].

However, a haptic device is more than a set of physical parameters, it is a mechatronic device consisting of sensors, D/A and A/D convertors, power amplifiers and actuators. A designer should know the impact of choices in a design phase, before a design is finished. For example, Gil et al.[17] concluded that a smaller time delay improves the maximum stable stiffness, but in practice it is not possible to

just affect the time delay with some mechatronic component. A faster actuator might affect the inertia and damping too. Another example is the transmission. The force at the end-effector scales linear with the transmission ratio, but damping and inertia scale quadratically with that ratio. In addition, a transmission reduces efficiency and adds additional damping.

Recent interest in haptics by universities led to the development of simple, 1DOF, low-cost, haptic interfaces to use for educational purposes. Most of these devices are so-called "Haptic Paddles". The first Haptic Paddle is developed by Stanford University in 1997 and is used in undergraduate dynamics courses[18]. Other universities use the haptic paddle for courses in control, haptics and programming. An extensive overview of the different haptic paddles is given in Rose et al.[9].

Apart from the Haptic Paddles, other parties acknowledged the need for low-cost haptic devices. Several strategies are used. Italian scientists designed the 2-Dof OSHAP[19], with the motivation to develop an alternative for expensive commercial interfaces by using low-cost electronic prototyping environments as the Arduino and the Rasberry Pi. The Arduino micro-controller was also used by Beni et al.[20], where they applied different tricks to reduce the torque ripple of an low-cost stepper motor. In Lawrence et al., another strategy used[21]: they used low-cost hardware, but increased the complexity in control to preserve performance. As an alternative, Eilering developed a method to build 3D-printed miniatures of industrial robot for teleoperation: the Robopuppet[22]. Here the financial benefit is in the production.

The mentioned studies have in common that costs are saved by economizing one aspect of the device, but it lacks an overall vision.

In general, most haptic devices on the market are very expensive and therefore not commonly used yet. The growing interest in low-cost haptic devices requires an overall vision for optimizing the performance-to-cost ratio.

This is also illustrated by studies on haptic task performance. Ideal properties of the device hardware are not always necessary. For example, Wildenbeest et al.[23] showed in an experimental study that overall task performance was improved by providing low-frequency haptic feedback, while further increasing the high-frequency content of the feedback force was only marginally improving performance. This is an example of diminishing returns: the performance shows only marginal improvements, with major effort. Therefore, it is an indication that it is possible to make a simpler and therefore more economical design, without suffering from lower performance.

Unfortunately, a method to design for desired haptic performance does not exist yet. A structured design method is needed, such that a designer of haptic devices is able to evaluate design decisions based on the expected consequences in performance.

1.3. Research Objective

This thesis develops a method that relates component level choices to the main performance criteria in impedance-type haptic devices. This allows direct design trade-offs, enabling the designer to optimize for desired closed-loop haptic performance. It consists of three steps: first the Key Performance Indicators (KPI's) are determined: the Z-Width and the Transparency. Then the effect of individual physical parameters on maximum stable rendering and the KPI's is evaluated. The final step is to determine how component level choices affect the physical parameters and thus the KPI's, since the physical parameters are often interrelated in component level choices.

Novelties in this goal are:

- This method can be used to *predict* closed-loop performance based on modeling, instead of performance evaluation of a physically built device.
- The method focuses on the effect of component level choices as complement of the effect of physical parameters only.

These aspects enable designers of haptic devices to optimize for desired performance.

1.4. Scope

As the title of this thesis and the research objective already suggests, this research is restricted to impedance-type haptic devices. Impedance-type haptic devices are force-reflecting, where thee remote or virtual environment then acts as an impedance, which explains the name. These devices are typically simpler and cheaper than admittance type devices, since a generally expensive force sensor is not needed.

Although the theory is also applicable on teleoperation with a perfect slave, all analysis is done where the master is manipulating a virtual environment. Only one degree of freedom is considered. An 1-DoF impedance type device can be seen as probing a virtual environment with a tool, instead of touching it directly[2].

Furthermore, the evaluation of performance is done on an "uncoupled" device, i.e. without a human operator involved. Since a human arm is considered to be a passive system, it is not able to destabilize the system. Uncoupled stability is a subset of stability with an operator, and therefore this is a save choice.

Finally, the demonstration of the effect of component level choices is only done with variations in transmission ratio and choice of actuator. These choices each affect three physical properties of the haptic device, where other components affect less. Both the actuator and transmission ratio affect the end-effector force and the moving mass, while the first also affects time delay, and the second also influences the quantization interval. Therefore, these are the most challenging choices to analyze or use in an optimization.

1.5. Thesis outline

This thesis consists of two main parts: a paper, and the supporting chapters.

Chapter 2 contains the scientific paper, which is the final product of this research. The paper summarizes the most important results. It shows a quantitative method for optimal component selection in impedance-type haptic devices, which consists of three steps:

First the determination of the specific performance metrics, which are the Z-Width (Dynamic range of stably achievable impedances) and the Effective Stiffness Bandwidth (upper bound in frequency where the force-reflecting quality is as desired). The second step is the influence of individual parameters on the performance metrics, which introduces a lot of trade-offs and conflicting interests. The final step is to relate component level design choices to the individual parameters and thereby to the haptic performance metrics. A case study on the haptic paddle shows that choices in actuation system and transmission ratio not only affect the force at the end-effector, but also the intended haptic performance of a device.

The rest of the chapters contain all the background information used in this research. Furthermore, it contains more extensive derivations and additional computations, checks and verification of assumptions.

Chapter 3 will be the start of the background. Here the model used for the haptic performance study is introduced and investigated in more detail. The influence of changing physical parameters on haptic performance is evaluated.

Chapter 4 will be the next step. Here one will see that physical properties are often correlated in component level choices. The influence of component level choices on the physical parameters is investigated, and thereby on the haptic closed-loop performance.

Chapter 5 will apply the method on the Gemini haptic paddle, a set-up developed in the Delft Haptics lab. The results will be validated with experiments on the real device, showing the effectiveness of this method. In addition, different case studies are done to illustrate the impact of component level choices can have on haptic performance.

Finally, in chapter 6 the results of the complete research will be discussed and summarized. In addition, recommendations for further research will be given.

This thesis will end with appendices, containing background information of this research. First, an extensive explanation to the calculation method using the Routh-Hurwitz criterion will be given in appendix A. In addition, appendix B contains the list of used actuators. The results of the experimental validation will be showed in more detail in appendix C, and an overview of the Matlab scripts will be given in appendix D. Finally, appendix E shows a report of the literature background that formed the basis for this study, as written in December 2015.

2

Research Paper: A Method for Optimal Component Selection in Impedance-Type Haptic Devices

In the following 18 pages, the research paper is included: *A method for optimal component selection in impedance-type haptic devices*. This paper forms the core of this master thesis, and summarizes the most important results. It will lead the reader through the essentials of this research.

This paper is meant for designers of haptic devices. Using existing literature, one was not able to evaluate the effect of component level choices, early in the design phase. This paper gives a tool for that, consisting of three steps:

1. Determination of important performance metrics.
2. Modeling the effect of individual physical parameters (mass, damping, time delay etc.) on the performance metrics.
3. Component level choices seldom affect one parameter: i.e. by choosing a component, a designer chooses a set of symbiotic parameters. This model shows how component level choices can be analyzed, and demonstrates how actuator and transmission choices affect the physical properties, and thereby haptic performance.

Using tests on the existing haptic Gemini[24], one will see that the performance prediction is sufficient. And in addition, calculating the stability boundary is computational efficient (50 times faster than using current techniques). Finally, using the Gemini as case study, it demonstrates some of the conflicting interests of the design metrics.

All in all this paper gives an extensive tool for designers of haptic devices, and it enables optimization in the design phase for desired closed-loop haptic performance.

A Method for Optimal Component Selection for Impedance Type Haptic Devices

Erik Jansen, Antonius G.L. Hoevenaars & Just L. Herder
Delft University of Technology (TU Delft)
Faculty of Mechanical, Maritime and Materials Engineering (3mE)
Department of Precision & Microsystems Engineering (PME)
Delft, The Netherlands
Contact: erikjansen90@gmail.com

Abstract

An impedance-type haptic device ideally has a large range of stable achievable impedances, i.e. a small free space impedance, together with a large stable closed-loop impedance. In addition, the rendered force should be accurate: the resemblance between the rendered and desired force should be large. In haptic design, those properties are quantified as the Z-Width and the Transparency. However, the properties to achieve those results, often contradict. This paper develops a method that relates component level choices to those performance criteria. This allows direct design trade-offs, enabling the designer to optimize for desired haptic performance. It consists of three steps: first the Key Performance Indicators, KPI's, are determined: the Z-Width and the Transparency. Then the effect of individual physical parameters on maximum stable rendering and the KPI's is evaluated. The final step is to determine how component level choices affect the physical parameters and thus the KPI's, since the physical parameters are often interrelated in component level choices.

The focus will be on the well-known Haptic Paddle Configuration, and tests will be performed on the Gemini haptic paddle device.

This experimentally validated approach, in combination with the reduction in computational effort, enables designers of haptic devices to optimize for closed-loop haptic performance.

1 Introduction

Haptic feedback is used in teleoperation in remote environments that are difficult accessible, for example in exploration the collapsed nuclear power plant in Fukushima, or in minimal invasive surgery. Another application of haptic force feedback is in combination with a virtual environment in gaming and educational simulators.

A haptic interface is a device that acts as a link between a human operator and this virtual- or remote environment[2]. It consists of mechatronic components, like sensors, actuators and software, aiming to provide computer-controlled, programmable sensations of mechanical nature. A virtual environment can be programmed, such that the haptic device acts like an impedance[23].

In figure 1 a schematic of such device is displayed, where the two basic functions defined by Tan[41] are distinguished: the measurement of the motion of the human operator, and the generation of the reflected forces by the virtual or remote environment. An impedance-type haptic device is used to generate a virtual impedance. A movement is measured, and a force is applied to the operator. A problem here is that the operator feels the combined impedance of the virtual environment *and* the device[23].

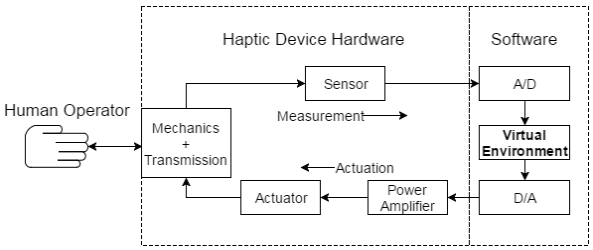

Figure 1: A mechatronic representation of an impedance type haptic device. A user is manipulating a device, his movement is measured and discretized, and a virtual environment force is applied using power amplifiers and actuators. In closed loop, an impedance-type haptic device generates the sense of a virtual environment.

The main challenge in haptic devices is to render a broad range of impedances: free motion should feel free, and hard motion should feel hard. In addition, the generated force is accurate. The haptic capability of rendering a large range range of stable achievable impedances, is in literature quan-

tified as the well-known Z-Width[8]. The accuracy of the rendered force is the resemblance between the desired and the rendered virtual impedance. In haptic teleoperation, this measure is called the transparency[29]. The transparency is good until the Effective Stiffness Bandwidth[12]. At higher frequency, the device dynamics will be dominant over the rendered dynamics.

The qualitative suggestions in literature to design a haptic device, are not sufficient. The ideal haptic device is sometimes modeled as an infinite stiff and mass-less stick[23]. This would implicate that the forces are perfectly reproduced with an infinite bandwidth. A device with that properties is called 'transparent'[29]. In that case, the operator is not able to distinguish haptic telemanipulation from direct manipulation[4]. To achieve those properties, according to literature a designer should strive to a device with very small mass/inertia, no damping and friction[4, 16, 18, 27, 28]. This would ensure the master to have a high force bandwidth, enabling it to reconstruct the environmental forces accurately. However, this proves not to be the full story. A mass-less device with no damping would be unstable[40]: friction, damping and inertia prove necessary for stability.

In addition, the quality of haptic feedback is also reduced by the same parameters. Moving mass is reducing useful frequency range, where the resemblance between the rendered and desired feedback force is good[12]. Therefore, a continuous trade-off between haptic quality and stability exists.

Minsky et. al.[34] were the first to acknowledge those stability problems as the most important problem in force reflecting devices. Instability by sampling delay in rendering hard (virtual wall) environments can be prevented by introducing more damping[21, 42], but this increases the free space impedance. This trade-off is illustrated in figure 2, a schematic of an 1-DoF haptic display rendering a virtual environment. The rendered and the free space impedance are in series, so a user feels the combined impedance[23]. The stable range of impedances is improved and reduced by the same parameters at the same time: damping b, mass m and friction c are necessary for stable rendering the hardest virtual environment possible. However, in free space motion (when B and K are equal to zero), an operator will still experience the device's dynamics.

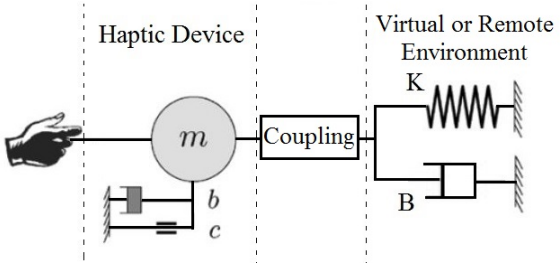

Figure 2: Schematic of an 1-DoF haptic display rendering a virtual environment consisting of a virtual spring K and a virtual damping B. The human operator feels the combined forces of the Virtual Environment and the dynamics of the device itself. The sensing and actuation system form the coupling between the device and the rendered environment. Figure modified from Diolaiti[15]

There are more studies on the influence of physical parameters on haptic device performance. One of the first was Colgate, who did several studies on the maximum impedance that can be rendered passively[8, 9, 10]. However, it is a very conservative measure: passivity is a subset of stability. Therefore, in other papers, different control methods to evaluate stability are used. Examples are the very simplified Routh-Hurwitz criterion by Gil[19], the Nyquist stability criterion as in Minsky[34], the Gain Margin as in Hulin[24].

As an example of a physical parameter study, Gil et al.[20, 21] evaluated the influence of damping and time delay on Z-width and stability. Another example is done by Colonnese and Okamura[13], where among other things the influence of physical mass, stiffness, quantization, sampling rate and time delay on stability and the maximum stable stiffness is evaluated. In another study, Colonnese investigates the influence of the same physical properties on the accuracy of a haptic device[12].

All the mentioned studies have one thing in common: The evaluation is done based on individual physical parameters. However, a haptic device is more than a set of physical parameters, it is a mechatronic device consisting of sensors, D/A and A/D convertors, power amplifiers and actuators, as visualized in figure 1. A designer should know the impact of choices in a design phase, before a design is finished. For example, Gil et al.[20] concluded that a smaller time delay improves the maximum stable stiffness, but in practice it is not possible to just affect the time delay with some mechatronic component. A faster actuator might affect the inertia and damping too. Another example is the transmission. The end-effector force scales linear with the transmission ratio, but damping and inertia go squared with that ratio. In addition, a transmission reduces efficiency and adds additional damping.

In addition, the only performance analysis in

haptics is done afterwards, after a design is finished. For example, some studies focused on direct comparison of devices (like in Rose[38] who compared haptic paddles, or Martin[30] who compared three different 6-DoF devices). Other studies are based on identification and on standardized benchmark tests[22, 39, 44]. However, a method to design for certain haptic performance does not exist yet.

And finally, ideal properties are not always necessary. Wildenbeest et al.[43] showed in an experiment that overall task performance was improved by providing low-frequency haptic feedback, while a high-frequency feedback force was only marginally improving performance. This is an example of diminishing returns: the performance shows only marginal improvements, with major effort. Therefore, it is an indication that it is possible to make a simpler and therefore more economical design, without suffering from lower performance. Ideally, a designer for haptic devices is able to use those insights to make a more economical design.

Therefore, a structured design method is needed, such that a designer of haptic devices is able to judge his design decisions based on the expected consequences in performance.

This paper considers that all physical parameters are coupled by component choices. Therefore, the challenge in this research will be linking the mechatronic components of a haptic device to the physical parameters, and thereby to the performance metrics as discussed before. The goal is to answer the following question: How is the haptic device performance affected by mechatronic component level choices? This will enable a designer of haptic devices to optimize for desired closed-loop haptic performance. In this paper, the actuator and transmission ratio are considered, but other choices could be incorporated as well.

Outline

This will be done in three steps. First, this paper will introduce the model and the Key Performance Indicators, typical performance metrics for haptic devices. The capability of a haptic device (Z-Width) and the quality of the feedback force (Effective Stiffness Bandwidth) will be studied. Those two metrics are chosen as performance indicators for a haptic device. The performance indicators will be explained in more detail and their choice will be motivated. The second step is to combine multiple methods for haptic stability, and the influence of physical parameters on haptic performance is listed. Then the next step is taken: it will be shown that multiple physical properties are coupled by component level choices. Their effect on the performance metrics is evaluated.

Using the well-known haptic paddle configuration, a case study will be done on the haptic Gemini[26], a device developed in the Delft Haptics Lab. Using this device it is shown that the maximum renderable stiffness can be significantly affected by choosing slightly different actuators and transmission ratio. However, trade-offs arise between stable range of impedances and the useful frequency range.

In addition, attention is paid to improving the efficiency of the calculation tools. In combination with the insight in the consequence of component level choices, this will give designers of haptic devices a framework for optimization towards desired haptic performance.

2 Method

First, the model of an impedance-type haptic device will be introduced together with the most important performance metrics. In addition, the calculation methods for the maximum stable rendering of a haptic device will be explained. Finally, the Gemini[26] haptic paddle, subject to the case study, will be introduced.

2.1 Model Description

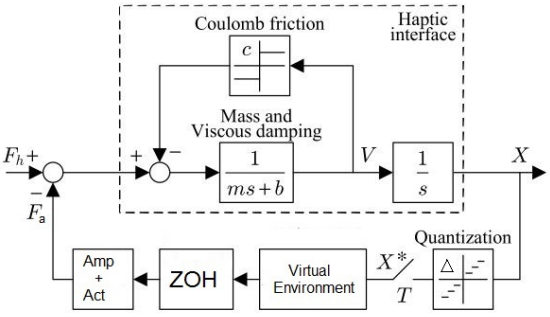

Figure 3: The block diagram of a haptic device, as lumped at the end-effector. It consists of a mass-damper system with a coulomb friction.The device is moved by an operator, and the position sensing is done by a quantization. The feedback force is determined in the virtual environment, and the force is applied after a zero-order-hold and a electrodynamic time delay by amplifiers and actuators. Figure is modified from two papers by Colonnese [11, 12].

For haptic analysis, the block diagram of figure 3 is used, similar to what is used in several other

studies on haptic performance[10, 21, 24, 34]. It consists of a linear model for the mass, damping and friction as lumped at the end-effector. A position signal is measured by a quantization. The haptic device is manipulated by an operator, and the motion is measured. The virtual environment translates the measured position to a desired force at the end effector. Before the feedback force generated by the virtual environment can be applied, the DAC is modeled as a zero-order-hold with sample time T, and the power amplifier together with the actuator introduces a time delay t_a.

The haptic device is modeled as a simple mass-damper system, with mass m and damping b:

$$G(s) = \frac{1}{ms^2 + bs} \tag{1}$$

The Virtual Environment $H_{VE}(s)$ consists of a virtual stiffness K and virtual damper B, a continuous time derivative s and a n^{th} order velocity filter with cut-off frequency ω_c, to attenuate noise introduced by the velocity estimator.

$$H_{VE}(s) = K + Bs\left(\frac{\omega_c}{s + \omega_c}\right)^n \tag{2}$$

The zero order hold is modeled as a time delay of half the sample time:

$$ZOH \rightarrow e^{-\frac{sT}{2}} \tag{3}$$

The actuator and power amplifier together are modeled as an additional time delay t_a, ending up with a total time delay t_d:

$$t_d = \frac{T}{2} + t_a \tag{4}$$

Therefore, the total time delay is implemented as follows:

$$D(s) = e^{-\left(\frac{T}{2} + t_a\right)s} = e^{-t_d s} \tag{5}$$

2.2 Key Performance Indicators: Z-Width and Effective Stiffness Bandwidth

An impedance-type haptic device is an impedance generator. The biggest challenge for the designer is to achieve a large dynamic range of achievable impedances. Colgate and Brown[10] started this approach and called it the *Z-Width*[8], as the dynamic range of *passive* achievable impedances.

Since passivity is a very conservative property (a subset of stability), the term *Z-Width* is currently known and used as the dynamic range of *stable* achievable impedances. This paper will describe the trade-off in this property: inertia and damping positively affect the maximum renderable stiffness, while those properties at the same time harm the free space impedance. Those trade-offs will be explained in table 1 and section 2.5.

The free space impedance of an haptic device is simply determined by the device dynamics, as introduced in equation (1). Written as an impedance, it is as follows:

$$Z_{FS}(\omega) = ms + b \tag{6}$$

The closed-loop impedance, in the continuous domain is as follows:

$$Z_{cl} = \frac{F_h(s)}{V(s)} = \frac{1 + G(s)\,H_{VE}(s)\,D(s)}{sG(s)} \tag{7}$$

With all parameters filled in, the closed loop impedance for a haptic device with a first order velocity filter can be written as:

$$Z_{cl} = \frac{ms^3 + (m\omega_c + b)\,s^2 + (b\omega_c + B\omega_c D + KD)\,s + K\omega_c D}{s\,(s + \omega_c)} \tag{8}$$

To illustrate the Z-width, a fictional haptic device is chosen with mass $m = 50\,\text{g}$, damping $b = 0.1\,\text{N s m}^{-1}$, total time delay $t_d = 1.5\,\text{ms}$, maximum stable virtual stiffness $K = 1000\,\text{N m}^{-1}$ and corresponding virtual damping $B = 5\,\text{N s m}^{-1}$. The Z-Width is displayed in figure 4. The blue dotted line gives the free space impedance, which is only determined by the device dynamics as in (6), the lower limit of the range of impedances. The upper limit is determined by the maximum stable impedance, the green solid line, defined in (8). The filter order is not affecting the Z-Width. The Z-Width (denoted as $\mathbb{Z}_w$ with unit Ns/m) is quantified using the method presented in Christiansson[6], calculating the area in figure 4, where the frequency range of interest is defined from ω_0 until ω_1, in radians per second:

$$\mathbb{Z}_w = \frac{1}{\omega_1 - \omega_0}\int_{\omega_0}^{\omega_1} \left([Z_{max}(\omega)] - [Z_{FS}(\omega)]\right) \mathrm{d}\omega \tag{9}$$

Where $Z_{max}(s)$ is the closed loop impedance from equation (8) with the maximum stable B and K substituted.

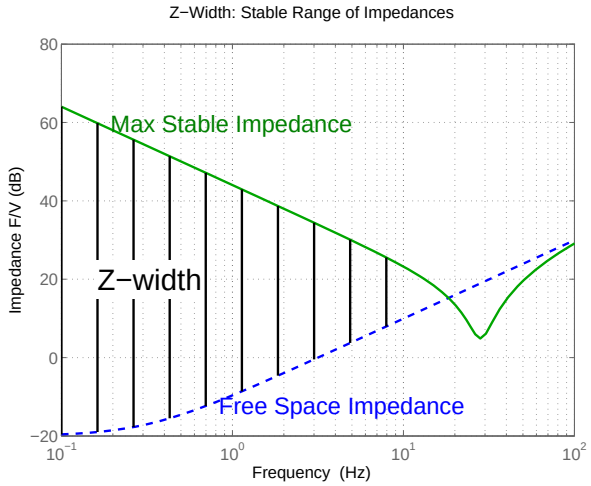

Figure 4: Z-width of a haptic device, the stable range of achievable impedances. The blue dotted line gives the free space impedance, the lower limit. The upper limit is determined by the maximum stable impedance, the green solid line.

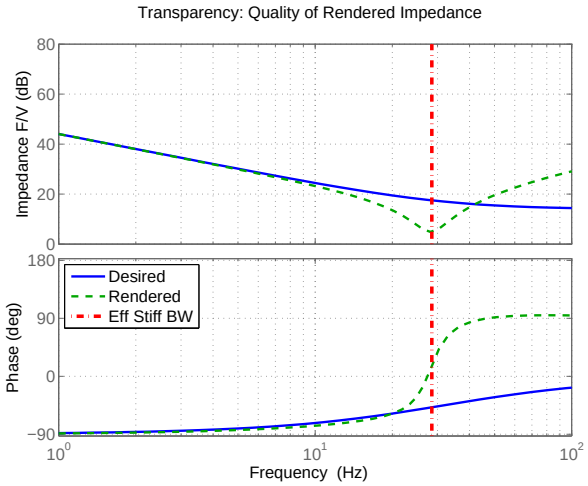

Figure 5: The Transparency of a haptic device, calculated at the maximum stable impedance. The blue solid line represents the desired impedance, which is simply the impedance by B and K. The dashed green line is the rendered impedance, where the dynamics of the device itself also come into play. The resemblance between the desired and rendered impedance is good until the Effective Stiffness Bandwidth defined in (11).

In addition to a large stable range, the quality of haptic rendering must be good. The resemblance between the desired and rendered force should be large. Using the same properties as before, the transparency is visualized in figure 5. The blue solid line represents the desired impedance, which is simply the impedance by B and K as in equation (10). The dashed green line is the rendered impedance from equation (7), where the dynamics of the device itself also come into play. This line is barely affected by the velocity filter.

$$Z_{des} = B + \frac{K}{s} \tag{10}$$

The resemblance between the desired impedance from equation (10) and rendered impedance from equation (8) is good until the Effective Stiffness Bandwidth, which will be the second performance metric.

$$\omega_{ES} = \sqrt{\frac{K}{m}} \tag{11}$$

This effective stiffness bandwidth is a metric introduced by Colonnese et. al.[12], where the rendered impedance is decomposed in "mechanical primitives", as mass, damping and stiffness. In his analysis it is shown that the effective stiffness (the stiffness an operator feels), is equal to the rendered virtual stiffness K until the effective stiffness bandwidth. The same holds for the mass: the operator will experience no feedback on the acceleration, until the effective stiffness bandwidth, where the mass of the device comes into play again. The effective stiffness bandwidth is not affected by the velocity filter.

2.3 Sampled-Data Stability Boundary

Sampling delay and electrodynamic delay cause phase lag and therefore can cause instability. The maximum stable stiffness is called *sampled-data stability boundary*. For sampled data passivity and stability analysis, the block diagram of figure 3 is used. In contrast with most of the existing literature[11, 20, 24], the sampled-data stability analysis is done in the *continuous* domain. This method shows the same accurate results as in the cited studies, but saves a lot in computational effort. Friction is not taken into account in the sampled-data analysis.

Similar to the method used to Gil and Sanchez[21], the total time delay can be approximated by a continuous model, simplifying all further calculations:

$$D(s) = e^{-\left(\frac{T}{2}+t_a\right)s} = e^{-t_d s} \approx \frac{1}{1+t_d s} \tag{12}$$

The complete loopgain $L(s)$ is then calculated by multiplying the three parts in the loop: the haptic device from equation (1), the virtual environment from equation (2) and the approximation of the time delay from equation (12). This gives the following loop-gain:

$$\begin{aligned} L(s) &= P(s)\, H_{VE}(s)\, D(s) \\ &= \frac{K(s+\omega_c)^n + BS\omega_c^n}{(ms^2+bs)(s+\omega_c)^n(1+t_d s)} \end{aligned} \tag{13}$$

For a first order velocity filter, this results in a fourth order characteristic equation. Every order higher in the velocity filter, the characteristic equation is one order higher too. The standard form of the characteristic equation is showed in equation (14).

$$L(s) + 1 = \sum_{n=0}^{4} a_n s_n = 0 \tag{14}$$

With:

$$\begin{aligned} a_4 &= mt_d \\ a_3 &= m + m\omega_c t_d + bt_d \\ a_2 &= m\omega_c + b + b\omega_c t_d \\ a_1 &= b\omega_c + K + B\omega_c \\ a_0 &= K\omega_c \end{aligned} \tag{15}$$

The characteristic equation of (14) is stable when all roots are in the left half of the complex plane. However, computing the roots of a characteristic equation can be computational intensive, especially at higher orders. To reduce the computational effort, the Routh-Hurwitz stability criterion is applied. Using this method, the characteristic equation can be rewritten as terms in a table, for which the number of sign changes in the first column represent the number of unstable poles. This reduces the problem to two simple inequalities:

$$a_3 a_2 > a_4 a_1 \tag{16}$$

$$a_3 a_2 a_1 > a_4 a_1^2 + a_3^2 a_0 \tag{17}$$

And filling in the values of (15), the two stability criteria are as follows:

$$\begin{aligned} &(b + m\,\omega_c + b\,\omega_c\,t_d)\;(m + b\,t_d + m\,\omega_c\,t_d)\cdots \\ &\quad - m\,t_d\;(K + B\,\omega_c + b\,\omega_c) > 0 \end{aligned} \tag{18}$$

And:

$$\begin{aligned} &(b + m\,\omega_c + b\,\omega_c\,t_d)\;(m + b\,t_d + m\,\omega_c\,t_d)\cdots \\ &\quad (K + B\,\omega_c + b\,\omega_c) - m\,t_d\,(K + B\,\omega_c + b\,\omega_c)^2\cdots \\ &\quad - K\,\omega_c\,(m + b\,t_d + m\,\omega_c\,t_d)^2 > 0 \end{aligned} \tag{19}$$

Equations (18) and (19) give a *necessary* and *sufficient* method for the sampled-data stability of the haptic system of figure 3. For higher order characteristic equations, the same method can be used to obtain computational efficient inequalities. A line search algorithm is written to speed up the process even more. As compared to the gain-margin method as used by Hulin[24] and [11], this reduced the computational time 50 times[1].

2.4 Quantization-Error Stability Boundary

Another threat to stability is the quantization error. The noise introduced by a quantization measurement can cause haptic kicks and instability, which can be limiting the rendering of a high stable stiffness. This problem was first discussed by Abbot and Okamura[1] and further analyzed by Diolaiti[15] and Colonnese[11]. The modeling by the latter is used in this research.

For this analysis, the discrete time version of figure 3 is used, with a sample time T. A difference with the continuous analysis of before is the coulomb friction in the model, which will prove to have a stabilizing effect. Another difference is the differentiator, which is a finite difference velocity estimator:

$$s \quad \rightarrow \quad D(z) = \frac{z-1}{Tz} \tag{20}$$

The velocity filter is discrete too:

$$H(z) = \left(\frac{\left(1 - e^{-\omega_c T}\right) z}{z - e^{-\omega_c T}} \right)^n \tag{21}$$

The sensing is done with a position quantization. The true position x will be measured with an accuracy Δ: the worst case error. This is visualized in figure 6a). To calculate the stability boundary, the approximation of figure 6b) is used. Here the measured position $\hat{x}$ is the sum of the true position x and a position noise $\tilde{x} \in \mathbb{R}\,[-\Delta, \Delta]$.

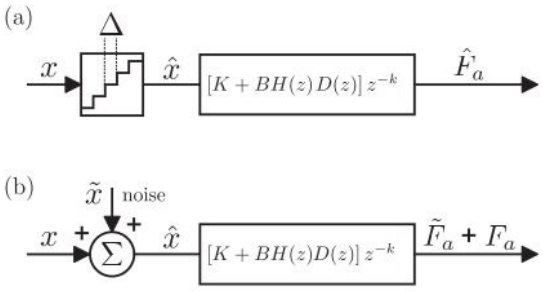

Figure 6: Model used to calculate the quantization error. In a) the true position signal x is quantized with a quantization interval Δ. This leads to an estimation of the position $\hat{x}$, which is used in the virtual environment to generate a actuator force $\hat{F}_a$. In b) a simplification is visualized: the measured position is the sum of the true position and noise $\tilde{x} \in \mathbb{R}\,[-\Delta, \Delta]$. This causes the actuation force to be the sum of the true force and the force caused by noise $\tilde{F}_a$. Figures adapted from Colonnese[11].

Colonnese[11] defined the quantization-error passivity as *sufficiency for no net quantization-*

[1] The details of application the Routh-Hurwitz criterion and the line-search algorithm can be found in appendix A of this report. Higher order characteristic equations are worked out there too.

error energy generation over any sample period. To fulfill this statement, the maximum generated energy by the quantization-error should be lower than the dissipated energy by friction. Therefore, we require the following statement:

$$c > \left\| \left[K + BD\left(z\right) H\left(z\right) \right] \frac{1}{z^k} \right\| \Delta \qquad (22)$$

2.5 Maximum Stable Rendering

In the previous sections, two mechanisms are presented that limit the stable range of a haptic device. First the maximum stiffness limited by sampled-data stability (K_s) was calculated using Routh-Hurwitz stability criterion in (18) and (19). Secondly, the inequality in (22) can be used to obtain the maximum stable stiffness limited by quantization-error: K_q. The maximum stable stiffness is thus:

$$K_{max} = \min\left(K_s,\ K_q\right) \qquad (23)$$

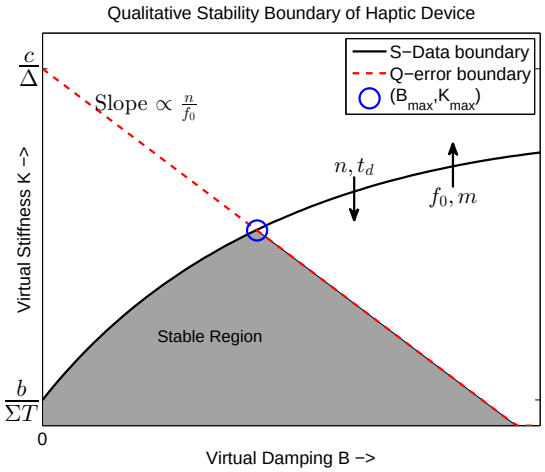

Figure 7: Qualitative visualization of the stability boundary of a haptic device. The maximum stable stiffness is limited by sampled-data stability at lower damping and by quantization-error stability at higher damping. In addition, it is visible how individual physical properties are qualitatively affecting the two stability boundaries.

Figure 7 shows the qualitative stability boundary of a haptic device, with the stable region under the two curves. We see that the maximum stable stiffness is limited by sampled-data stability at lower damping and by quantization error at higher damping. In addition, the effect of individual physical properties is visible. One can see that mass, damping and the filter frequency are improving the sampled-data stability boundary, while the filter order and time delay are diminishing it. In addition, friction and filter order are improving the quantization-error region, while larger velocity filter cut-off or quantization interval are reducing stability. The effects of the physical properties on stability are summarized in the first columns of table 1.

Table 1: Qualitative influence of individual properties on maximum stable stiffness and the free space impedance. Achieving the maximum stiffness proves to be a trade-off between properties, which at their turn diminish the free space impedance. (*The effect of physical damping on maximum stable stiffness is only marginal, it can be neglected as compared to B. They have the same effect on stability, but are typically two orders apart.)

		Effect on:		
Effect of		K_s	K_q	$Z\left(s\right)_{FS}$
Mass	m	+		-
Damping*	b	+*	-*	-
Friction	c		+	-
Delay	t_d	-	-	
Quant. int.	Δ		-	
Vel. filt. cut-off	ω_c	+	-	
Vel. filt. order	n	-	+	

2.6 Effect of Physical Properties on Haptic Performance

Using table 1 one can see that achieving the maximum stable stiffness of a haptic display is a trade-off between individual physical properties. In addition, some properties that are improving the maximum stable stiffness are diminishing the free space impedance. Therefore, it is not that obvious whether a parameter is improving or diminishing the stable range of impedances, the Z-Width. And in addition, the highest possible stiffness is obviously improving the Effective Stiffness Bandwidth from equation (11), and mass is diminishing this value.

Using the calculation method as introduced before, one can calculate the maximum renderable stiffness as a function of fixed device parameters, mass, damping, friction, delays and quantization interval. An optimization algorithm or a brute force parameter study can be used to obtain the desired frequency filter (ω_c and n) to obtain the maximum virtual stiffness K and corresponding damping B, as done in [11] and [5].

2.7 Symbiotic Properties

In the sections so far, it is investigated how individual physical properties affect haptic performance. This is the strategy in most of the literature too, and it proves to end up in a trade-off for maximizing stable stiffness without diminishing bandwidth

and free space impedance.

However, as mentioned before, a haptic device is not only a set of individual properties as displayed in the block diagram of figure 3. It is a mechatronic device consisting of mechanics, a transmission, sensors, power amplifiers and actuators. This is more as displayed in figure 1.

To evaluate design choices in the design phase, the link between component level choices and haptic performance must be known. Therefore, in this study a next step will taken, and the influence of component level choices will be investigated. This is done in two steps. The first step is to determine the influence of physical properties on haptic performance. Results of reviewed literature and modeling is given in the previous sections and summarized in table 1. The second step is to link component level choices to physical properties, where we will see that many physical properties are coupled in design choices, the so-called "Symbiotic properties".

In the next sections, two design options are evaluated. The first option is the transmission ratio in the mechanics. Changing this affects the moving mass (as rotational inertia goes squared with the transmission ratio), force capabilities and sensor quantization, since the sensor is often co-located with the actuator.

The second option is the actuator. By choosing an electrodynamic actuator, a designer affects three properties: moving mass, force capabilities of the haptic device, and the electrodynamic time delay. As mentioned by Millet and Hayward[33], the actuator is what limits the performance from above, where they focus on force capabilities. However, we will see that actuator properties affect Z-width and effective stiffness bandwidth significantly too.

The electrodynamic time delay by the actuator t_a is here defined as five times the electric time constant: the time needed from a current to translate to 99% of the corresponding torque, calculated using the inductance L divided by the resistance R:

$$t_a = 5 \cdot \tau_e = 5\frac{L}{R} \tag{24}$$

Other options can be thought of, a list of design choices is included in table 2. The first two will be discussed in this paper.

Table 2: Design choices in haptic devices and their effect on individual physical properties.

	Affects:				
Choice of:	m	Δ	t_d	T	F_{ee}
Actuator:	x		x		x
Transmission:	x	x	x		x
Sensor:		x			
Controller:			x	x	

The effect of the first two will be discussed in this paper, and the effect of variations in design variables will be verified using a haptic paddle, the Gemini[26] as developed in the Delft Haptics Lab.

2.8 Case: The Haptic Paddle

The haptic paddle, an example of a rotating bar is chosen as a case study, for the following reasons:

- It is a simple 1-DoF example, comparable to what is used in literature.
- The haptic paddle is used at many universities in many different configurations[14, 37, 38] for teaching and studying control, dynamics and haptics.
- As stated in many papers, a parallel mechanism seems to be the preferred choice for haptic devices[18, 23, 27], due to the combination of low moving mass and high structural stiffness[32]. The rotating bar is used actuated link in many parallel mechanisms, such as the Delta Robot[7] in the Novint Falcon [25].

Figure 8 shows a schematic view of the haptic paddle, with the main dimensions indicated. it consists of two parts: the handle and the pulley connected to each other with a capstan drive. The pulley is directly connected to the actuator and the sensor.

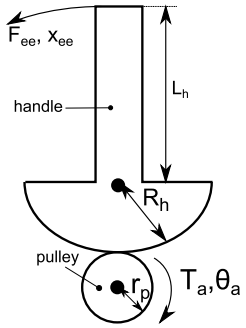

Figure 8: Schematic of the Haptic Paddle Configuration, with the main dimensions indicated.

The paddle in figure 8 consists of a handle with rotational inertia I_h and a pulley with rotational inertia I_p. On the axis of the pulley, the inertia of the actuator contributes, and the inertia of the axis that connects the actuator to the pulley (I_{ax}, including fasteners and the capstan drive). Variables L_h, R_h and r_p denote dimensions as in figure 8. This generates a lumped mass at the end-effector as follows:

$$m = \frac{1}{L_h^2}\left[I_h + \left(\frac{R_h}{r_p}\right)^2 (I_p + I_a + I_{ax})\right] \tag{25}$$

The end-effector force F_{ee} as a function of the actuator torque T_a is as follows:

$$F_{ee} = \frac{R_h}{r_p L_h} T_a \tag{26}$$

And finally, the sensor is co-located with the actuator. An optical encoder with N pulses per revolution, leads to an angle per pulse of $\frac{2\pi}{N}$. Therefore, quantization interval Δ at the end-effector is as follows, in meter:

$$\Delta = \frac{2\pi L_h r_p}{R_h N} \tag{27}$$

2.9 Qualitative case: Gemini

As mentioned before, the Gemini haptic paddle is chosen as subject to this analysis. A render of the device hardware is included in figure 9. The quantitative properties needed for the calculations are listed in table 3. The values of the actuator are simply obtained from datasheets and the dimensions and inertial values from the CAD-software. This strategy enables designers to study the effect of design choices without having to test physical devices.

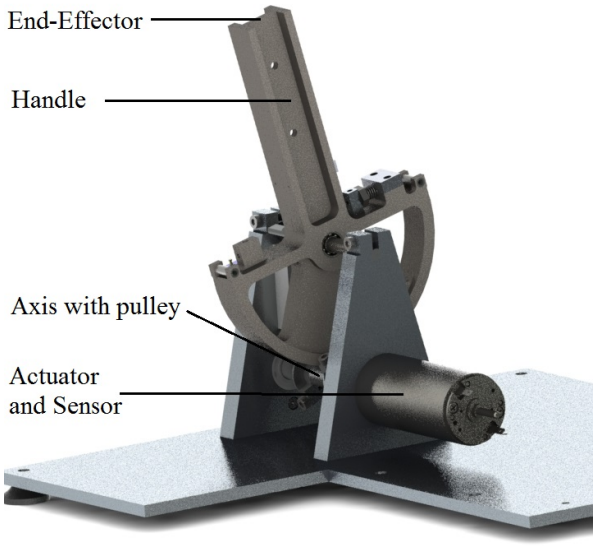

Figure 9: Render of the Gemini Haptic Paddle with the important components annotated.

As concluded in table 1, the physical damping barely contributes to the maximum stable stiffness. Therefore, this value is considered to be constant over the design space, and a value of $b = 0.01\,\mathrm{N\,s\,m^{-1}}$ is taken, which is typical for common devices[15]. The friction is affecting the maximum stable stiffness significantly, but that is a value that is easily enlarged (by adding some friction components), but not easily reduced. Therefore a value of $c = 0.1\,\mathrm{N}$ is chosen, which is a conservative choice compared to common devices[15].

Table 3: Dimensions and properties of the Gemini setup, used for the performance analysis. One might notice that the inertia of the pulley is set to zero, since it is included in I_{ax}. All values are obtained from datasheets and CAD-software.

Part	**Dimensions and Properties**		
Handle	R_h	50	mm
	L_h	100	mm
	I_h	216890	$\mathrm{gmm^2}$
Axis Pulley	I_{ax}	28971	$\mathrm{gmm^2}$
	I_p	(incl in I_{ax}): 0	$\mathrm{gmm^2}$
	r_p	5	mm
	h	19.5	mm
Actuator	Maxon	RE30-60W No. 268216	
	T_a	89.7	mN m
	t_a	1.05	ms
	I_a	3470	$\mathrm{gmm^2}$

Please note that the inertia of the pulley is considered to be zero, since it is included in I_{ax}.

3 Experimental Validation

In literature, some experimental validation of the maximum stable achievable stiffness is already done. The models for sampled-data stability are already tested in Gil[21] and Hulin[24]. In addition, quantization error stability is verified by Colonnese[11].

In addition, the step from component properties to the contribution on individual physical parameters is based on relatively simple mechanics.

However, there are two major differences between the tests in literature and with the analysis in this paper. First, only the "easy-to-test" scenarios are tested. Although electrodynamic time delays are typically in the order of milliseconds, time delays of ten to hundred times higher are tested. And second, the stability of known devices is tested, with all physical properties experimentally identified. In the case of this paper, performance is estimated by modeling component level choices, a priori before a device is tested (or even built), enabling to optimize for certain performance.

Figure 9 shows the Gemini haptic paddle, the setup used for the analysis. The properties of the device are listed in table 3. The black solid line in figure 11 shows the stability margins of the haptic device, as calculated using the methods presented before. The figure is a quantitative version of figure 7.

The test is done as follows: the device is programmed to represent a virtual environment with stiffness K and damping B. The end-effector is

moved manually from the equilibrium position, and then released. In the stable case, the device returns smoothly to its equilibrium position. In the unstable case, the release results in end-less limit cycles, which are only stopped manually. These two scenarios are visualized in figure 10.

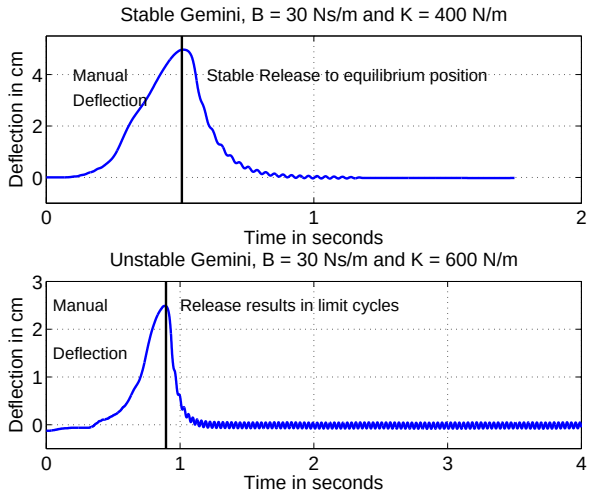

Figure 10: The procedure of the experiment. The end-effector of the Gemini is manually deflected from its equilibrium position and then released. When stable, the device is fast and without many osculations returned to its equilibrium position. In the unstable case, the release results in limit cycles.

The damping is fixed in steps of $2.5\,\mathrm{N\,s\,m^{-1}}$. At every point, this stability is tested as described before. When the device is stable, the stiffness is increased in steps of $100\,\mathrm{N\,m^{-1}}$, until instability occurs. The highest stable value for the stiffness at every damping is saved. The results are shown in figure 11, where the solid black line denotes the calculated stability boundary, and the red crosses the maximum experimentally determined stable value.

Each value is evaluated at least three times, and the results proved to be very reproducible: i.e. every set of stiffness and damping was either stable or showed limit cycles, no combinations occurred. The blue line shows a better approximation of the closed-loop performance, based on the measurements. This is because no osculations where allowed, but in the real tests, some osculations occurred when the device returned to its equilibrium position. This results in a less steep stability boundary. And secondly, the friction was a bit lower than predicted, which results in a lower starting point of the quantization-error boundary.

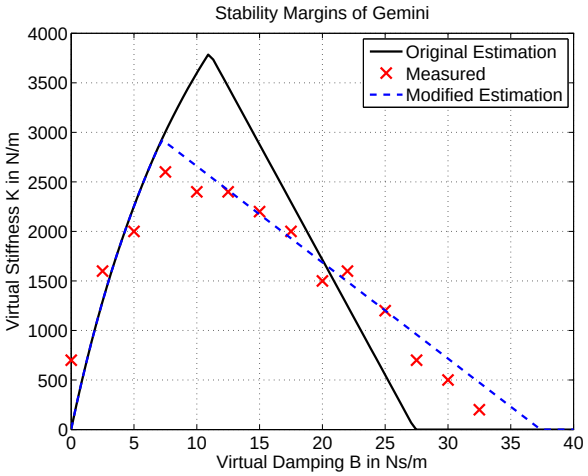

Figure 11: Experimental results: The predicted stability boundary of the Gemini is solid black line, and the maximum stable points as tested on the device. The blue line shows a better approximation of the maximum stable stiffness, based on the experiments.

4 Simulation Results

4.1 Varying the Actuator

An actuator using the Lorentz-force principle for actuation, is the preferred choice in haptic devices[3, 23], due to their linear relationship from current to force, the lack of friction and the back-driveability. To prevent problems as cogging and other non-linearities, generally expensive high performance motors are chosen.

The data of 108 high power density DC-motors are selected from the online catalogs by two manufactures: brushed DC-motors from the *RE-program* and the *DCX-program* by Maxon Motors[31] and motors from the *BLDC-servomotors* range by Faulhaber[17]. From the datasheets, the time-delay is calculated according to (24) and rotational inertia is selected, denoted as I_a. The maximum continuous torque T_a is taken as measure of the maximum torque of the actuator.

The data of the actuators is visualized in a double scatter plot in figure 12, showing the correlations. As a function of the actuator torque T_a the time delay is given as blue crosses with respect to the left vertical axis. On the right axis the rotational inertia is given, as green circles. Two trend-lines are visible, a blue solid one for torque against time delay, and a green dashed line for torque against inertia.

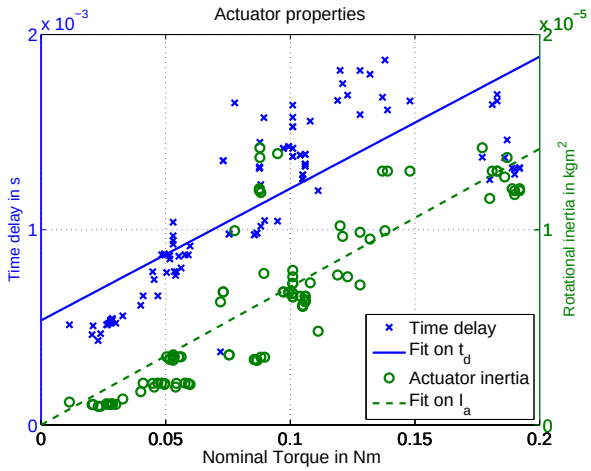

Figure 12: The coupled "symbiotic properties" in 108 DC-motors by Faulhaber and Maxon. A clear correlation is visible between the actuator torque, time delay and inertia. A clear correlation is visible.

In figure 12 a clear correlation between the actuator parameters is visible. Notation $\rho(a_1, a_2)$ is used for the Pearson correlation coefficient between the variables a_1 and a_2. Similar, the following correlation between the motor parameters are showed:

$$\begin{aligned} \rho(T_a, t_a) &= 0.79 \\ \rho(T_a, I_a) &= 0.86 \\ \rho(t_a, I_a) &= 0.80 \end{aligned} \tag{28}$$

The correlation coefficients in equation (28) are high, around 80%. This shows that the three considered actuator properties, the torque, inertia and time delay are highly correlated. This proves the first set of symbiotic properties.

The relations are quantified using a least-squares fit with the actuator torque as a design variable. This gives the following estimated relationships between the three actuator variables:

$$t_a = a_1 \cdot T_a + a_2 \tag{29}$$
$$\text{with:} \quad a_1 = 6.76 \times 10^{-3}\,\mathrm{s\,N^{-1}\,m^{-1}}$$
$$\text{and:} \quad a_2 = 5.35 \times 10^{-4}\,\mathrm{s}$$

and:

$$I_a = a_3 \cdot T_a$$
$$\text{with:} \quad a_3 = 7.07 \times 10^{-5}\,\mathrm{kg\,m\,N^{-1}} \tag{30}$$

Please note that we do not claim that the functions above have any causality or physical meaning. However, the correlations are clear and convenient. Using the lsq-estimations reduces the complexity of the problem. Figure 12 shows that a designer can find an actuator with properties close to the value on the line, so inserting the actuators directly into the optimization problem, would not give a result that is far off with regards to this estimation.

We see that the time delay and the inertia of the actuator scale with the maximum continuous torque. To simplify the calculations, the actuator torque T_a is chosen as a *design variable* in the performance analysis.

4.2 Varying the Transmission Ratio

The influence of the transmission ratio is studied based on the haptic paddle from figure 8.

The variation of the transmission ratio is implemented by varying the radius of the pulley r_p. In table 3, we saw that the initial radius of the pulley is 5 mm. The pulley is a cylinder with an initial pulley radius $r_{p,in}$. Therefore, the variation of the total inertia can be implemented by adding or subtracting the inertia of a hollow cylinder, with an inner radius equal to the initial radius:

$$I_p = \frac{\pi \rho h}{2}\left(r_p^4 - r_{p,in}^4\right) \tag{31}$$

Please note that this value of I_p can also be negative, when $r_p < r_{p,in}$. This is equivalent of subtracting the inertia from the total inertia on the actuator axis.

In equation (25) we saw that the contribution of the components on the pulley-axis to the mass scale squared with the transmission ratio $\frac{R_h}{r_p}$. The inertia of the pulley in equation (31) scales with r_p to the fourth power. Therefore, the mass is significantly affected by the radius of the pulley, and r_p is chosen to be a *design variable* in performance analysis.

Next to its effect on the mass, the radius of the pulley affects the end-effector force via equation (26) and the global sensor resolution via equation (27).

4.3 The Effect of Design Variables on Physical Properties

To evaluate the performance as a function of varying the transmission ratio and the actuator, the first step is to investigate the effect of the design variables to the individual physical parameters from table 1. The radius of the pulley is varied from 3 to 10 mm, so equivalent to a difference from the original setup of -2 and $+5$ mm, where the first value is a minimum determined by practical implementation, and the end-value is twice the original.

The motor torque is varied from 0.01 to 0.2 N m, the range of the motors considered in figure 12 and the range where the estimations in equations (29) and (30) are valid.

Figure 13 shows the variation of moving mass of the Gemini over the design space. The mass is very

sensitive to changes in especially the radius r_p: the minimum and maximum in the figure differ by one order. The sensitivity to actuator choice is lower, due to the relatively heavy axis of the pulley.

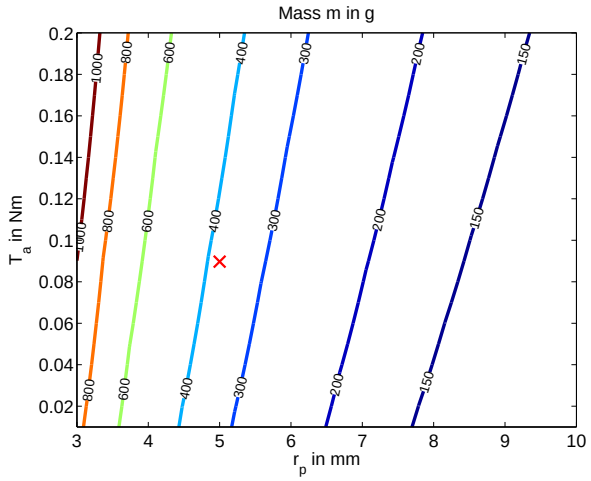

Figure 13: Contour lines of moving mass as affected by design variables r_p and T_a. The red cross denotes the current setup.

In figure 14 the varying time delay over the design space is given. As already stated in the text and table 2, this value is only affected by the actuator choice, not by the transmission ratio. The time delay is doubled over the workspace.

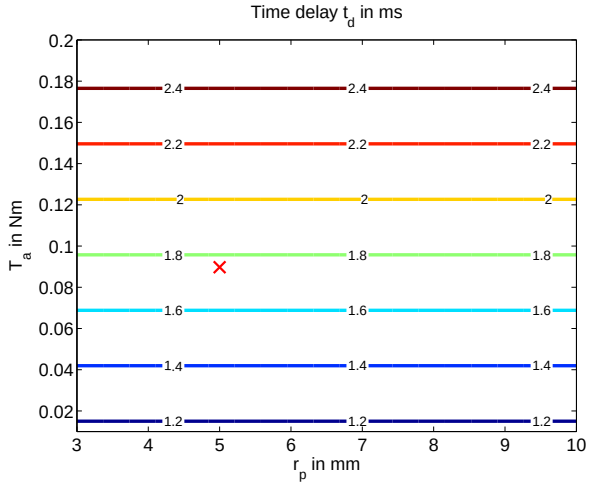

Figure 14: The total time delay as affected by design variables r_p and T_a. The red cross denotes the current setup.

Finally, figure 15 shows how quantization interval Δ is affected by the design variables. As concluded in table 2, it is only influenced by the transmission ratio, as can be seen in the figure too. There is a factor three difference over the design space.

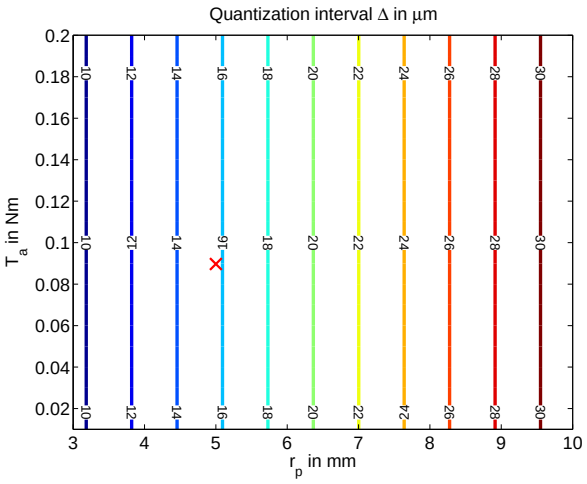

Figure 15: The quantization interval as affected by design variables r_p and T_a. The red cross denotes the current setup.

4.4 The Effect of Design Variables on Haptic Performance

As discussed in section 2.2, the performance of a haptic device will be evaluated with respect to its capabilities (Z-Width, eq. (9), stable range of impedances) and to the quality of the feedback force (Effective Stiffness Bandwidth, eq. (11), resemblance between desired and rendered force).

First, the end-effector over the design space is visualized. As expected, the force at the end-effector is very sensitive to the design variables, as can be seen in figure 16. A smaller r_p leads to a larger amplification of the actuator torque and therefore to a larger end-effector force. A stronger actuator obviously corresponds to a larger force too. The total variation in force is approximately one order.

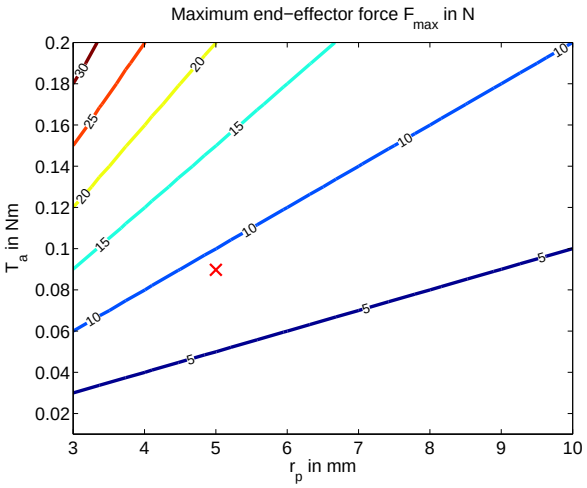

Figure 16: The force at the end-effector as affected by design variables r_p and T_a. The red cross denotes the current setup.

Secondly, the maximum stable stiffness in the design space is showed in figure 17. One can clearly see that the maximum stiffness depends on both design variables. A smaller r_p (so a larger transmission ratio) leads to a larger stable stiffness. A larger actuator has the opposite effect. To render the maximum stable stiffness, a designer should strive to a large transmission ratio in combination with a small motor. However, as seen before in figure 13, this comes at the price of a larger moving mass and thus a larger free space impedance. And, as in figure 16, the smaller motor diminishes the maximum force.

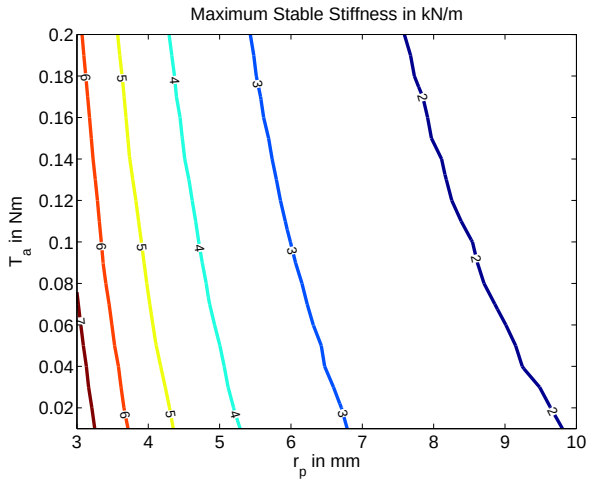

Figure 17: The maximum stable renderable stiffness as a function of the design variables.

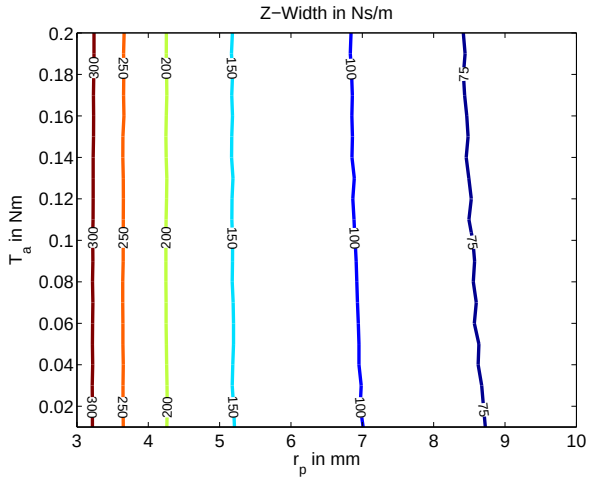

Figure 18: The Z-width as a function of the design variables.

In figure 18, the Z-Width is displayed. This is calculated using a Riemann-approximation of equation (9), where the lower bound of the useful frequency range is chosen to be 0.1 Hz (very slow human movement). The upper bound is set equal to the effective stiffness bandwidth as defined in equation (11). A similar trend as in the maximum stable stiffness is visible: a higher transmission ratio leads to higher Z-Width. The Z-Width is only marginally affected by the choice of actuator.

In figure 19 an opposite trend is visible. The maximum Effective Stiffness Bandwidth is calculated using equation (11), it proves to be affected by both design variables. In contrast with the two figures before, a higher transmission ratio is diminishing the Effective Stiffness Bandwidth. Although the maximum stiffness might be higher, it is increasing effective mass which is increasing the free space impedance and diminishing the effective stiffness bandwidth. A stronger actuator is diminishing the bandwidth even more.

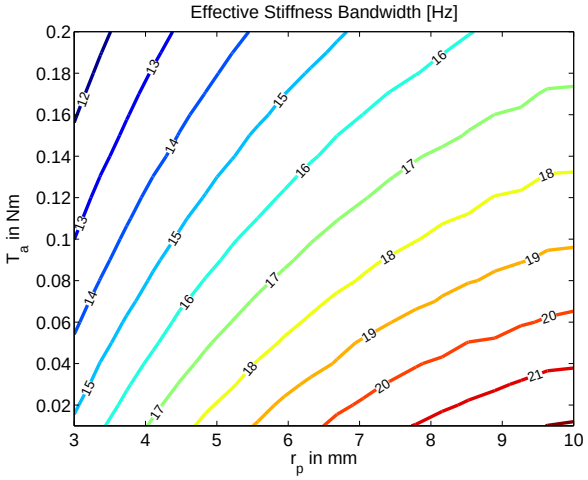

Figure 19: The maximum effective stiffness bandwidth as a function of the design variables.

5 Discussion

The main objective of this paper was to present a method that relates component level choices to closed-loop haptic performance. That is a multi-stage analysis: the component level choices determine the physical properties of a device. Those physical properties enable to calculate the stability boundaries and the free space impedance, which determine the final closed-loop haptic performance.

Closed-loop haptic performance is related to the device's capability of generating an impedance. When a free environment is simulated, it should feel free. So the *free space impedance* (the impedance of the device itself) should be low. On the other hand, when hard contact is simulated, the rendered impedance should be as high as stably possible. In addition, the feedback force should be accurate. Those demands are quantified by the following Key Performance Indicators:

- The maximum stable stiffness of a haptic de-

vice. Limited by phase-lag due to actuator and amplifier time delay on one hand, and by energy generation of the quantization-error on the other hand.

- Z-Width: the stable range of achievable impedances. Limited by free space impedance as minimum and by the maximum stable impedance as maximum.

- Effective Stiffness Bandwidth. Upper limit of the useful frequency range. At lower frequencies, the resemblance between the desired and rendered impedance is good. At higher frequencies on the other hand, the device dynamics dominate.

Figure 7 gives the qualitative stability boundary of a haptic device, where the affect of individual physical parameters can be seen. Physical properties considered here are the moving mass m, physical damping b, viscous friction c, time delay t_d, the quantization interval of the sensor Δ, and the properties of the velocity filter: cut-off frequency ω_c and order n.

Rendering the maximum stable stiffness proves to be a trade-off between those parameters, and as table 1 shows, there are some conflicting interests. Is is shown that the maximum achievable stiffness has two limiting factors. The first one the sampled-data stability boundary, which is positively affected by a shorter time delay, a larger mass, and the filter-cut off frequency. The second one, the quantization error stability boundary, is positively affected by friction and smaller quantization interval.

This conflicting interests of physical properties are even worse for the other KPI's: the Effective Stiffness Bandwidth is increased for higher maximum stable stiffness, but reduced by moving mass. In addition, the Z-Width is also increased by the maximum stable stiffness. Mass and damping are improving the maximum stable stiffness, while diminishing free space impedance. Therefore, their effect on the stable range of impedances (quantified as Z-Width) is not very insightful. The method presented in this paper can be used to quantify these effects.

Here an interesting contradiction is discovered. Conventional design guide-lines for haptic device design are low moving mass, low damping and low friction[16, 18, 23, 28]. However, this study has shown that it is not the full story. Low moving mass, low damping and low friction are indeed beneficial for a low free space impedance, but are reducing the upper limit of the stable region. And despite the fact that higher mass and damping are indeed diminishing the free space impedance, they are improving the maximum stiffness by such level, that the Z-Width could still be improving.

Higher moving mass is improving the maximum stable stiffness and the Z-width, while diminishing the free space impedance and the effective stiffness bandwidth. However, this does not seem as a big problem. Wildenbeest et.al.[43] showed that force feedback improved certain task performance significantly, but that higher bandwidths are not necessarily improving task performance even more. Therefore, the capabilities of the device in terms of achievable impedances might be more important than the frequency range of the feedback force.

Only two physical parameters are improving all haptic performance indicators: a lower time delay t_d and a smaller quantization interval Δ. All other parameters introduce trade-offs with regard to the capabilities of a haptic device (render maximum stable stiffness vs free space impedance: thus Z-Width) and the quality of the feedback force (frequency until where the quality is good: Effective Stiffness Bandwidth).

However, when a designer is optimizing for cost, the smallest quantization error will be achieved using the sensor with the highest resolution, which is probably the most expensive one too. And then we come back to *diminishing returns*: a design might be arrived at the point where it is not limiting by sensor resolution anymore, so improving the resolution will not improve the performance any further.

Therefore, as a next step, the effect of component level choices on the individual physical parameters is investigated, and thereby on the haptic performance metrics. It is shown that component level choices often come with interrelated physical parameters. Figure 12 show that a stronger actuator leads to a larger moving mass and a longer time delay. A similar relation can be seen in the transmission ratio: equation (25) shows the affected mass by the transmission ratio. In the same time, the end-effector force and the quantization interval are affected by the transmission ratio, as can be seen in equations (26) and (27).

To quantify the effect of the component level choices, a case study has been done on a haptic paddle, the Gemini[26]. Two component level choices are worked out in this thesis, the choice of actuator and the transmission ratio. Those are quantified as motor torque (coupled to end-effector force, time delay and moving mass) and radius of the pulley (transmission ratio, coupled to end-effector force, moving mass, and quantization interval).

Using only a-priori knowledge, such as information from data-sheets and values obtained

from CAD-software, the estimation of the stability boundary proved to be quite reliable. This can be seen in figure 11. The predicted and measured data matched within approximately 20%. That the shape is approximately the same, is the most important result, since the stability boundary is used to compare different haptic paddle configurations. The fact that the peak was a bit lower than predicted, has two reasons. First, the slope of the quantization-error stability boundary was lower than predicted. This is because no osculations where allowed. In the real tests, however, some osculations occurred when the device returned to its equilibrium position. This results in a less steep stability boundary. And secondly, the friction was a bit lower than predicted, which results in a lower starting point of the quantization-error boundary. Experiments showed that the friction was approximately 30% lower.

As a general conclusion, it has been demonstrated that the component level choices not only determine the force-capabilities of the device, but they also have a significant effect on closed-loop haptic performance.

The effect of actuator choice on maximum stable stiffness and Z-width does not seem to be that large, as can be seen in figure 17 and 18. This is for a large extend due to the relatively low contribution of the actuator inertia to the total moving mass. The pulley-axis contains all components for fixing the capstan mechanism, and is made out of stainless steel, which explains the high inertia as compared to the actuator. In other configurations, the actuator inertia might play a larger role

On the other hand, the haptic performance proved to be very sensitive to the variation in the radius of the pulley (and thus in the transmission ratio). The maximum stable stiffness can be improved three times over the considered domain, as can be seen in figure 17. In addition, the Z-Width in figure 18 follows the same trend: a larger transmission ratio improves the Z-Width. This seems mainly the result of the reduced quantization interval, since figure 15 and figure 18 have similar contour lines.

The parameters needed for maximum stable stiffness and maximum Z-Width seem to diminish the effective stiffness bandwidth in figure 19. The optimum of the bandwidth correlates to a point with a small stiffness and bandwidth. However, since the effective stiffness bandwidth is well above 10 Hz, it seems reasonable, since literature suggests bandwidths from 10 to 30 Hz for haptic feedback[4, 18, 40, 41]. In figure 19 one can see that bandwidths in that order are indeed achieved. However, this is only when rendering the maximum stiffness that is stably achievable. When rendering a lower stiffness, the Effective Stiffness Bandwidth will be lower too.

Finally, two side-notes are necessary at the choice of performance metrics.

When an impedance is stably achievable, it does not necessarily mean that it is achievable by the haptic device. Actuator- and power-amplifier-saturation can cause the force rendering capability to be a subset of the stable renderable regime. Comparing figure 16 and 17 showed that the maximum end-effector force is not necessarily coinciding with the maximum renderable stiffness.

Although the haptic performance metrics used in this study are generally accepted in literature, all scalar representations are simplifications of the difficult haptic problem. A designer of haptic devices should always investigate the important performance metrics for his problem, which might be different then the ones considered here.

6 Conclusion

This paper developed a method that relates component level choices to the main performance criteria in impedance-type haptic devices. This allows direct design trade-offs, enabling the designer to optimize for desired closed-loop haptic performance. This is done in three steps.

In the first step, the important Key Performance Indicators are determined. Closed-loop haptic performance is related to the device's capability to generate an impedance. The device is desired to be able to generate a very large stable impedance, quantified as the maximum stable stiffness. In addition, when free environments are simulated, it is desired to feel free. The Z-Width is the stable range of achievable impedances, bounded from below by the free space impedance and from above by the maximum stable impedance. Finally, the quality of the feedback force is required to be good. The effective stiffness bandwidth is the upper limit in frequency where this is the case. Therefore, the maximum stable stiffness, Z-Width and Effective Stiffness Bandwidths are the Key Performance indicators.

The second step is to determine the influence of the physical properties on the key performance indicators. A clear relationship between the system parameters of a haptic device (mass, damping, friction, quantization interval and time delay) and the maximum stable stiffness is given in this thesis. At their turn, they affect the other performance indicators, often in multiple ways. The improved stability calculation presented in this paper allows for computational efficient calculations.

The third step is to relate component level choices to changes in physical properties, and thereby to closed-loop haptic performance. A designer can not simply choose a certain mass and damping; a haptic device consists of mechatronic components and software, where physical parameters typically are coupled by component level choices. It is shown that component level choices often come with interrelated physical parameters. Two component level choices are worked out in this paper, the choice of actuator and the transmission ratio.

It is shown that in a set of common DC-motors, there is a clear correlation between motor torque, motor inertia and time delay. Therefore, the choice of actuator affects the maximum end-effector force, the moving mass and the time delay. Those three physical properties have their effect on the closed-loop haptic performance.

The transmission ratio is the amplification of motor torque to end-effector force. Since the motor and sensor are often collocated in haptic design, a higher transmission ratio decreases the quantization interval of the sensor. In addition, the moving mass of the haptic device is affected. All rotational inertia on the motor-axis contributes to the total mass, while multiplied with the transmission ratio squared.

Using the Gemini haptic paddle as case study, it is demonstrated that both design choices not only determine the force capabilities of a haptic device, but have a significant effect on closed-loop haptic performance too.

In every of those three steps, the interconnected properties play a role. This paper presented a method for the quantitative modeling of all steps. In combination with the computational much more efficient calculations, this enables designers of haptic device to optimize for desired closed-loop haptic performance.

6.1 Suggestions for further research

This study has also shown that a higher mass is improving the maximum stable stiffness, while it is diminishing the free space impedance and the useful frequency range. The same holds, to a lower extend, to the physical damping. In addition, friction has a similar effect. In rendering the highest possible stiffness, friction proves to be indispensable.

However, compensation proves to be difficult in impedance-type haptic devices. Generally expensive force sensors are needed to compensate dynamics. Therefore, hybrid designs seems to be a very interesting option for further research, where braking or clutching is applied. Then low friction and damping in free space and some kind of braking mechanism that is increasing friction and damping when rendering harder virtual environments. An interesting choice might be the statically balanced braking mechanism developed for robotic application by Plooij et al.[35], which could generate a very large braking force in comparison with regular brakes. An alternative would be a clutching mechanism, where the actuator or other mass contributions can be decoupled in free space tasks. An example of a clutched actuator for robotic applications is developed by Plooij et al. [36].

Finally, task performance in haptic systems does not only depend on device performance. Human factors play an important role too. Combining studies on human limits with the method presented in this thesis, will lead to optimal designs for certain tasks.

7 Acknowledgments

The author would like to thank Nick Colonnese, Ph.D., for his correspondence and useful tips regarding his paper[11], that proves to be a valuable resource.

In addition, we thank ir. Roel Kuiper for his help on the test-setup, the Gemini[26].

8 Literature

[1] J. J. Abbott and A. M. Okamura. Effects of position quantization and sampling rate on virtual-wall passivity. *IEEE Transactions on Robotics*, 21(5):952–964, 2005.

[2] R. Adams and B. Hannaford. Stable haptic interaction with virtual environments. *IEEE Transactions on Robotics and Automation*, 15(3):465–474, 1999.

[3] P. J. Berkelman and R. L. Hollis. Lorentz Magnetic Levitation for Haptic Interaction: Device Design, Performance, and Integration with Physical Simulations. *The International Journal of Robotics Research*, 19(7):644–667, 2000.

[4] T. Brooks. Telerobotic response requirements. In *IEEE International Conference on Systems, Man, and Cybernetics Conference Proceedings*, pages 113–120. IEEE, 1990.

[5] V. Chawda, O. Celik, and M. K. O'Malley. A Method for Selecting Velocity Filter Cut-Off Frequency for Maximizing Impedance Width Performance in Haptic Interfaces. *Journal of Dynamic Systems, Measurement, and Control*, 137(2):024503, 2014.

[6] G. A. V. Christiansson. *Hard Master, Soft Slave Haptic Teleoperation*. PhD thesis, TU Delft, 2007.

[7] R. Clavel. Device for the movement and positioning of an element in space, 1990.

[8] J. Colgate and J. Brown. Factors affecting the Z-Width of a haptic display. *Proceedings of the 1994 IEEE International Conference on Robotics and Automation*, pages 3205–3210, 1994.

[9] J. Colgate and G. Schenkel. Passivity of a class of sampled-data systems: application to haptic interfaces. *Proceedings of 1994 American Control Conference - ACC '94*, 3(1):37–47, 1994.

[10] J. E. Colgate, M. C. Stanley, and G. Schenkel. Dynamic range of achievable impedances in force reflecting interfaces. In *Proc. SPIE Telemanipulator Technology and Space Telerobotics Conference*, volume 2057, pages 199–210, 1993.

[11] N. Colonnese and A. Okamura. Stability and quantization-error analysis of haptic rendering of virtual stiffness and damping. *The International Journal of Robotics Research*, Oktober 6(2010), 2015.

[12] N. Colonnese, A. Siu, C. Abbott, and A. Okamura. Rendered and Characterized Closed-loop Accuracy of Impedance-type Haptic Displays. *IEEE Transactions on Haptics*, 1412(c):1–1, 2015.

[13] N. Colonnese, S. M. Sketch, and A. M. Okamura. Closed-loop stiffness and damping accuracy of impedance-type haptic displays. *2014 IEEE Haptics Symposium (HAPTICS)*, pages 97–102, 2014.

[14] M. R. Cutkosky, T. Morimoto, A. Okamura, and P. Blikstein. Hapkit by stanford university. `http://hapkit.stanford.edu/index.html`, 2015. Accessed: 03-Dec-2015.

[15] N. Diolaiti, G. Niemeyer, F. Barbagli, and J. K. Salisbury. Stability of haptic rendering: Discretization, quantization, time delay, and Coulomb effects. *IEEE Transactions on Robotics*, 22(2):256–268, 2006.

[16] R. Ellis, O. Ismaeil, and M. Lipsett. Design and evaluation of a high-performance haptic interface. *Robotica*, 14(03):321, 1996.

[17] FaulhaberGroup. Faulhaber brushless dc-motors. `https://fmcc.faulhaber.com/type/PGR_13814_13801/PGR_13822_13814/en/GLOBAL/`, 2016. Accessed: Jan-2016.

[18] P. Fischer, R. Daniel, and K. Siva. Specification and design of input devices for teleoperation. In *Proceedings., IEEE International Conference on Robotics and Automation*, pages 540–545. IEEE Comput. Soc. Press, 1990.

[19] J. J. Gil, A. Avello, acAngel Rubio, and J. Flórez. Stability analysis of a 1 DOF haptic interface using the Routh-Hurwitz criterion. *IEEE Transactions on Control Systems Technology*, 12(4):583–588, 2004.

[20] J. J. Gil and E. Sanchez. Stability Boundary for Haptic Rendering: Influence of Damping and Delay. *IEEE International Conference on Robotics and Automation*, pages 124–129, 2007.

[21] J. J. Gil and E. Sanchez. Stability Boundary for Haptic Rendering: Influence of Damping and Delay. *Journal of Computing and Information Science in Engineering*, 9(1):11005, 2009.

[22] M. Harders, A. Barlit, K. Akahane, and M. Sato. Comparing 6dof haptic interfaces for application in 3d assembly tasks. *Proc. of EuroHaptics'*, pages 3–6, 2006.

[23] B. Y. V. Hayward and K. E. Maclean. Do It Yourself Haptics: Part I. *IEEE Robotics & Automation Magazine*, 14(4):88–104, 2007.

[24] T. Hulin, C. Preusche, and G. Hirzinger. Stability Boundary for Haptic Rendering: Influence of Physical Damping. *Spring*, pages 1570–1575, 2006.

[25] N. T. Inc. Novint falcon technical specifications. `http://www.novint.com/index.php/novintxio/41`, 2015. Accessed: 03-Dec-2015.

[26] R. Kuiper, L. Boerefijn, W. Heij, M. Flipse, W. Vreugdenhil, and K. Wang. Gemini - 1 dof telemanipulator. `http://www.delfthapticslab.nl/device/gemini-1dof-master-slave/`, 2014. Accessed: 09-May-2016.

[27] A. Lavatelli, P. Milano, F. Ferrise, D. Meccanica, and M. Bordegoni. Design of an Open-Source Low Cost 2DOF Haptic Device. In *Mechatronic and Embedded Systems and Applications (MESA), 2014 IEEE/ASME 10th International Conference on*, pages 1–6, 2014.

[28] D. Lawrence and J. Chapel. Performance trade-offs for hand controller design. *Proceedings of the 1994 IEEE International Conference on Robotics and Automation*, 1994.

[29] D. a. Lawrence. Stability and transparency in bilateral teleoperation. *IEEE Transactions on Robotics and Automation*, 9(5):624–637, 1993.

[30] S. Martin and N. Hillier. Characterisation of the Novint Falcon Haptic Device for Application as a Robot Manipulator. In *Australian Conference on Robotics and Automation (ACRA)*, 2009.

[31] MaxonMotor. Maxon motor online catalog. urlhttp://www.maxonmotor.com/maxon/view/catalog/, 2016. Accessed: Jan-2016.

[32] J.-P. Merlet. *Parallel Robots*, volume 208. Springer, 2006.

[33] G. Millet, S. Haliyo, S. Regnier, and V. Hayward. The ultimate haptic device: First step. *Proceedings - 3rd Joint EuroHaptics Conference and Symposium on Haptic Interfaces for Virtual Environment and Teleoperator Systems, World Haptics 2009*, pages 273–278, 2009.

[34] M. Minsky, O.-y. Ming, O. Steele, F. P. Brooks, and M. Behensky. Feeling and seeing: issues in force display. *ACM SIGGRAPH Computer Graphics*, 24(2):235–241, 1990.

[35] M. Plooij, T. Van Der Hoeven, G. Dunning, and M. Wisse. Statically balanced brakes. *Precision Engineering*, 43:468–478, 2016.

[36] M. Plooij, M. Van Nunspeet, M. Wisse, and H. Vallery. Design and evaluation of the Bi-directional Clutched Parallel Elastic Actuator (BIC-PEA). *Proceedings - IEEE International Conference on Robotics and Automation*, 2015-June(June):1002–1009, 2015.

[37] C. Richard, A. M. Okamura, and M. R. Cutkosky. Getting a Feel for Dynamics: using haptic interface kits for teaching dynamics and controls. *ASME Symposium on Haptic Interfaces for Virtual Environment and Teleoperator Systems (Haptics)*, pages 15–21, 1997.

[38] C. G. Rose, J. A. French, and M. K. O'Malley. Design and characterization of a haptic paddle for dynamics education. *IEEE Haptics Symposium, HAPTICS*, pages 265–270, 2014.

[39] E. Ruffaldi, D. Morris, T. Edmunds, F. Barbagli, and D. Pai. Standardized Evaluation of Haptic Rendering Systems. *2006 14th Symposium on Haptic Interfaces for Virtual Environment and Teleoperator Systems*, pages 225–232, 2006.

[40] E. Samur. *Performance metrics for haptic interfaces*. Springer Handbooks, London, 2012.

[41] H. Z. Tan, B. Eberman, M. A. Srinivasan, and B. Cheng. Human Factors for the Design of Force-Reflecting Haptic Interfaces. In C. J. Radcliffe, editor, *Proceedings of the ASME Dynamics Systems and Control Division*, volume 55, pages 353–359, 1994.

[42] D. W. Weir, J. E. Colgate, and M. a. Peshkin. Measuring and increasing Z-width with active electrical damping. *Symposium on Haptics Interfaces for Virtual Environment and Teleoperator Systems 2008 - Proceedings, Haptics*, pages 169–175, 2008.

[43] J. G. W. Wildenbeest, D. a. Abbink, C. J. M. Heemskerk, F. C. T. Van Der Helm, and H. Boessenkool. The impact of haptic feedback quality on the performance of teleoperated assembly tasks. *IEEE Transactions on Haptics*, 6(2):242–252, 2013.

[44] Y. Yokokohji, Y. Iida, and T. Yoshikawa. "Toy problem" as the benchmark test for teleoperation systems. *Proceedings. 2000 IEEE/RSJ International Conference on Intelligent Robots and Systems (IROS 2000)*, pages 996–1001, 2000.

3

Modeling: How Physical Parameters affect Haptic Performance

This chapter will describe the modeling of a haptic device, as used in this research. In addition, it shows how physical parameters affect haptic performance. Therefore, first the model and the performance metrics are discussed. Then a stability analysis is done. This chapter will end with an overview of the influence of the individual parameters on these performance metrics.

3.1. Modeling the Haptic Device

In an impedance-type haptic device, a human operator applies a motion. This motion is measured, and using a computer generated model of an impedance, a force is applied, through power amplifiers and actuators. The sensor- and actuation-system forms a virtual coupling between the operator and the computer generated environment. This is visualized in figure 3.1a. One can see that the impedance of the haptic device itself is in series with the generated impedance, modeled as a virtual spring K and virtual damping B.

In most haptic performance studies, the full control-loop of an 1-DoF impedance-type haptic device is modeled according to figure 3.1b. The haptic device itself is modeled as a mass-damper system with mass m and viscous damping b. In addition, there is a coulomb friction force c which is assumed to be constant over the range of motion. The position is measured with a sample time T and a quantization interval Δ. This measured position is used in the virtual environment to calculate the force to apply.

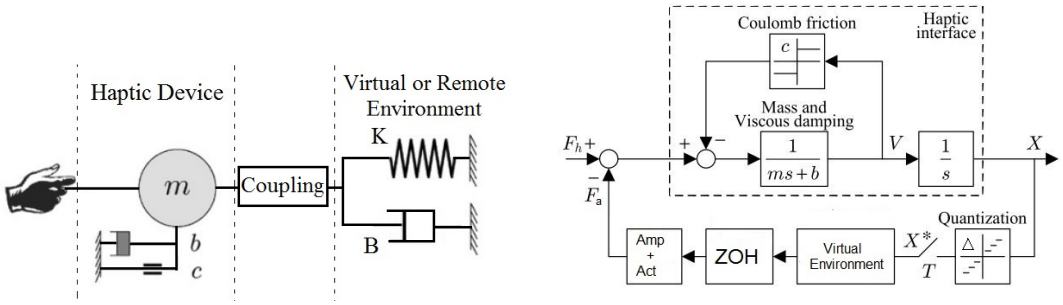

(a) The haptic device as an impedance generator. Modified from [25, 26]

(b) The closed-loop block-diagram of a haptic device. Modified from [6, 16]

Figure 3.1: Two representations of the haptic device. The first in a) shows the human operator moving the haptic device in series with the desired impedance. This indicates the problem that an operator experiences the combined impedance. The actuator and sensor system are a virtual coupling. On the right the block-diagram of a haptic device is visible, which will be used in the closed-loop analysis.

3.2. Performance Metrics of a Haptic Device

According to Tan[27], impedance-type force feedback devices have two basic functions. The first is to measure the position of the human operator, and secondly to display the calculated contact forces to the user. However, it is this bi-directionality in the flow of information and power that makes comparing haptic devices difficult[28].

The ideal haptic device has a large dynamic range of impedances and renders an accurate force. Therefore, this study will focus on both aspects. Two properties of the haptic display will be considered: of which one represent its *Capability* and the other the *Quality*. Both follow from the maximum stable impedance.

An impedance-type haptic device is an impedance generator, and therefore the analysis starts with checking the maximum stable achievable impedance. This is part of the capability of the device, and determines partly the quality of the feedback force. The maximum stable renderable impedance is limited by stability: when the desired virtual stiffness and damping are too high, the haptic device will end up in limit-cycles. The derivation of the maximum stable renderable impedance will be discussed in section 3.3.

Key Performance Indicators are parameters to judge haptic performance. The KPI's here are as follows:

The capability of a haptic device is the range of impedances that can be stably rendered. In haptic literature, this is called the *Z-width*, as introduced by Colgate[6, 14]. The Z-width is limited by the maximum stiffness that can be stably rendered on one hand, and by the *Free Space Impedance* on the other hand, the impedance of the device only. Therefore, the Z-width is the first KPI. This will be discussed in more detail in section 3.4.

The quality of a haptic device is the resemblance between the desired and the rendered feedback force. In the ideal design, the operator is not able to distinguish haptic telemanipulation from direct manipulation[29]. A device with that properties is called 'transparent'[30]. The resemblance between the rendered and the desired force is good upto the *Effective Stiffness Bandwidth*[8]. At higher frequency, the device dynamics will be dominant over the rendered dynamics. Therefore, the Effective Stiffness Bandwidth is the second KPI. This will be discussed in more detail in section 3.5.

The Key Parameters of Interest in this study are thus the *Z-width* and the *Effective Stiffness Bandwidth*. In layman's terms: free motion should feel free, stiff environments should be as stiff as stably possible, and the force signal should be accurate over a suitable frequency range. Table 3.1 gives an overview of these performance metrics, including reference to the sections where they will be discussed in more detail.

In the following sections, those KPI's will be explained in more detail, including the affect of parameters on those KPI's. One will conclude that lots of parameters are improving one KPI while diminishing others. This is the essential trade-off in the mechatronic design of haptic devices.

Table 3.1: Overview of Key Performance Indicators as used in this thesis.

Name	Notation	Description	§
Maximum Stable Achievable Stiffness	K_{max}	The maximum stable stiffness a haptic device. In literature also referred to as *Virtual wall stiffness*. This value is used in the Z-Width and the Effective Stiffness Bandwidth.	3.3
Z-Width	$\mathbb{Z}_w$	The stable range of impedances. Limited from above by the maximum stable stiffness, limited from below by the impedance of the device itself. Term introduced by Colgate and Brown[6]	3.4
Effective Stiffness Bandwidth	ω_{ES}	The frequency upto where the quality of haptic rendering is good. Below this frequency, the rendered force is dominated by the desired force, above this frequency, the device dynamics will dominate. This KPI is introduced by Colonesse et al.[8].	3.5

3.3. Maximum Stable Achievable Impedance

The maximum achievable stiffness of a haptic device is limited by stability. The block diagram of figure 3.1b will be used for the stability analysis. Please note that the *uncoupled* device is modeled, i.e. the impedance of the human is *not* considered. Previous research has shown that the human has a stabilizing effect on the system[16, 17, 26, 31, 32], and therefore it is not taken into account.

The maximum stable achievable stiffness has two limiting mechanisms. At lower damping, the maximum stiffness is limited by *sampled-data stability*: there the phase lag as introduced by sampling and time-delay in the actuation can cause instability. The stability boundary by sampled-data will be discussed in section 3.3.1. At higher damping, the position quantization-error of the sensor can cause the haptic device to generate energy, and therefore cause limit cycles. The quantization-error stability boundary will be discussed in section 3.3.2. Finally, section 3.3.3 will discuss the combined stability boundary of the two mechanisms.

3.3.1. Sampled-Data Stability Boundary

The time delay by sampling and actuation can cause the closed-loop haptic device to become unstable. The maximum impedance that can be stably rendered, limited by this mechanism, is called the *sampled-data stability boundary*.

The stability boundary by sampled-data is first acknowledged by Minsky[33]. Over the years, different ways of calculating the stability boundary are used. An overview of the different control strategies used to analyze sampled-data stability is given in table 3.2.

Table 3.2: Different control strategies used in literature to test sampled-data stability margins.

Introduced by		Control Strategy used
Minsky *et al.*	[33]	Nyquist Stability Criterion
Colgate *et al.*	[14]	Passivity
Gil *et al.*	[31]	Routh-Hurwitz Stability Criterion
Hulin *et al.*	[34]	Gain Margin

Colgate[14] introduced the passivity criterion. Since the human operator can be considered as a passive system, and any combination of passive systems is stable, passivity is sufficient for stability. However, passivity is a very conservative measure, and proves to be a subset of the complete stable range[16, 32].

The Gain-Margin method as introduced by Hulin[34], and used by others[15, 16], is tried in this thesis. However, it is more sensitive to numerical errors than the Routh-Hurwitz Criterion, and much slower. The Nyquist stability criterion also involves calculation of pole locations, and therefore is computational intensive.

Therefore, in this research, the Routh-Hurwitz stability criterion as introduced by Gil[31] is used to examine the stability margins. This method is computational very efficient, and in contrast with other

methods, allows us to use electrodynamic time-delays that are not necessarily multiples of the sample time. In combination with a line-search algorithm, this method proves to be 50 times faster than the Gain-Margin method (see appendix A).

The first step is to determine the transfer functions.

As can be seen in figure 3.1b, the transfer function of the haptic device is modeled as a mass-damper system with mass m and viscous damping b:

$$G(s) = \frac{1}{ms^2 + bs} \tag{3.1}$$

The position signal is measured using an encoder, the signal is quantized using an interval Δ and sampled with sample time T. In an impedance-type haptic device, the virtual environment acts as an impedance. It generates a force as a function of the position and velocity. The virtual environment is modeled as a combination of a virtual spring K and a virtual damper B.

The position signal is differentiated with a finite-difference velocity estimator in combination with a low-pass filter to attenuate noise as introduced by the finite-difference velocity estimator. Although the system in fact is discrete, the modeling is done in the continuous-time domain, since it proves to be faster and reliable[1].

Therefore, the Laplace operator s is used to obtain the derivative information, in combination with velocity filter $H_f(s)$. The transfer function of the virtual environment is then as follows:

$$H_{VE}(s) = K + B\ s\ H_f(s) \tag{3.2}$$

Where the velocity filter $H_f(s)$ is defined in equation (3.3). The cut-off frequency is ω_c in $\mathrm{rad\,s^{-1}}$ and the order is n:

$$H_f(s) = \left(\frac{\omega_c}{s + \omega_c}\right)^n \tag{3.3}$$

The zero order hold is modeled as a time delay of half the sample time:

$$ZOH \rightarrow e^{-\frac{sT}{2}} \tag{3.4}$$

The actuator and power amplifier together are modeled as an additional time delay t_a (with subscript a for *actuation*), ending up with a total time delay t_d, representing all electro-dynamics. This time delay is caused by signal-to-current conversion in the power amplifier and the current-to-force conversion in the actuator.

$$t_d = \frac{T}{2} + t_a \tag{3.5}$$

Similar to the method used to Gil and Sanchez[15], the total time delay can be approximated for low-frequency by a continuous model, simplifying all further calculations:

$$D(s) = e^{-s\left(\frac{T}{2} + t_a\right)} = e^{-st_d} \approx \frac{1}{1 + t_d s} \tag{3.6}$$

With all components known, the loop-gain can be found by multiplying all components in the loop: the haptic device in equation (3.1), the virtual environment in equation (3.2) and the approximation of the time delay of equation (3.6). This gives the following total loop-gain:

$$L(s) = G(s)\, H_{VE}(s)\, D(s) = \frac{1}{ms^2 + bs}\left(K + B\ s\ \frac{\omega_c^n}{(s + \omega_c)^n}\right)\frac{1}{1 + t_d s} \tag{3.7}$$

For the rest of this section, a first-order velocity filter will be used, to illustrate the calculation steps. To see the calculations for $n > 1$, the reader is referred to appendix A.

So for $n = 1$, the loop-gain from equation (3.7) simplifies to:

[1] In appendix A the calculations will be shown in more detail and compared to the discrete-time method of Colonnese[16]. The continuous-method will prove to be 50 times faster, without diminishing the accuracy.

$$L(s) = \frac{K(s+\omega_c) + Bs\omega_c}{(ms^2+bs)(s+\omega_c)(1+t_d s)} \tag{3.8}$$

The characteristic equation can be simply obtained by the loop-gain as follows:

$$L(s) + 1 = 0 \tag{3.9}$$

Which leads to the following characteristic equation:

$$\begin{aligned} &(ms^2+bs)(s+\omega_c)(1+t_d s) + K(s+\omega_c) + BS\omega_c = 0 \\ &mt_d s^4 + (m + m\omega_c t_d + bt_d)s^3 + (m\omega_c + b + b\omega_c t_d)s^2 + (b\omega_c + K + B\omega_c)s + K\omega_c = 0 \end{aligned} \tag{3.10}$$

In (3.10), one can recognize a fourth order characteristic equation. When using a higher order velocity filter ($n > 1$), the order of the total characteristic equation will be higher too. The characteristic equation can be written in the standard form as follows:

$$a_4 s^4 + a_3 s^3 + a_2 s^2 + a_1 s + a_0 = 0 \tag{3.11}$$

With:

$$\begin{aligned} a_4 &= mt_d \\ a_3 &= m + m\omega_c t_d + bt_d \\ a_2 &= m\omega_c + b + b\omega_c t_d \\ a_1 &= b\omega_c + K + B\omega_c \\ a_0 &= K\omega_c \end{aligned} \tag{3.12}$$

Using this standard form, one can fill in the Routh-array. For $n = 1$, it looks as follows (once again, the derivation steps are omitted here, but included in appendix A):

a_4	a_2	a_0
a_3	a_1	0
$-\frac{a_4 a_1 - a_2 a_3}{a_3}$	$\frac{a_0 a_3}{a_3}$	0
$-\frac{a_3 b_2 - a_1 b_1}{b_1}$	0	0
$\frac{b2c1}{c_1}$	0	0

(3.13)

The Routh-Hurwitz stability criterion is as follows: *The number of sign changes in the first column of the Routh-array equals the number of roots of the polynomial in the Closed Right Half-Plane*

As can be observed in (3.12), a_4 obviously is positive. Therefore, all values in the the first column of (3.13) need to be positive too. Working this out, this leads to three inequality constraints:

$$a_n > 0 \quad \text{for} \quad n = 0, 1, 2, 3, 4 \tag{3.14}$$

$$a_3 a_2 > a_4 a_1 \tag{3.15}$$

$$a_3 a_2 a_1 > a_4 a_1^2 + a_3^2 a_0 \tag{3.16}$$

Since all coefficients a_n in (3.12) are built up from summations of strictly positive physical values, the first inequality constraint (3.14) is always satisfied. The other two inequality constraints give the *necessary and sufficient* rules for stability of a haptic display:

$$(b + m\omega_c + b\omega_c t_d)(m + bt_d + m\omega_c t_d) - mt_d(K + B\omega_c + b\omega_c) > 0 \tag{3.17}$$

And:

$$\begin{aligned} &(b + m\omega_c + b\omega_c t_d)(m + bt_d + m\omega_c t_d)(K + B\omega_c + b\omega_c) - mt_d(K + B\omega_c + b\omega_c)^2 \cdots \\ &\quad - K\omega_c(m + bt_d + m\omega_c t_d)^2 > 0 \end{aligned} \tag{3.18}$$

The inequalities (3.17) and (3.18) might not seem very intuitive or insightful, and it does not give any information about the exact location of the closed loop poles. However, the inequalities only contain simple and low-level mathematics, and therefore this is an easy and very computational efficient

method to analyze sampled-data stability boundary of a haptic display.

To give a rough estimation of the sampled-data stability boundary, figure 3.2 shows a qualitative indication in the B, K-plane. Virtual damping has a stabilizing effect at lower values for B, since the virtual damping adds phase. At a certain value, damping is diminishing the maximumm stable stiffness. All points under the curve denote stable achievable impedances.

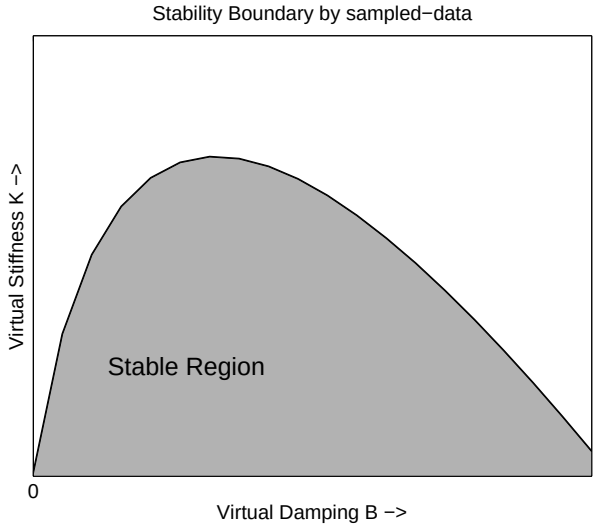

Figure 3.2: Qualitative indication of the sampled-data stability boundary.

3.3.2. Quantization-Error Stability Boundary

Next to the sampled-data stability boundary, a haptic device is also limited by the quantization-error stability. As the virtual environment generates a force from a motion, it can also generate a force from the quantization-error. This quantization-error can cause the system to generate energy, and as a result, limit cycles can occur. Limit cycles can only occur when the generated energy is larger than the dissipated energy. The quantization-error is limiting the maximum stable renderable impedance.

This problem was first discussed by Abbot and Okamura[32], they gave an upper bound for virtual-wall stiffness, where c is the Coulomb friction force. A sufficient condition for stable virtual stiffness limited by quantization-error K_q is as follows:

$$K_q \leq \frac{c}{\Delta} \tag{3.19}$$

In words, with this value for the maximum stiffness the virtual spring environment will not be able to create enough force due to quantization-error to overcome the friction, and therefore the system is stable.

However, the damping is able to generate energy too. Here, we follow the method as introduced by Colonnese[16]. For this analysis, a discrete-time version of the block diagram in figure 3.1b is used, with a sample time T. A difference with the continuous analysis of before is the coulomb friction in the model, which will prove to have a stabilizing effect. Another difference is the differentiator, which is a finite difference velocity estimator:

$$s \quad \rightarrow \quad D(z) = \frac{z-1}{Tz} \tag{3.20}$$

The velocity filter is discrete too, obtained by a bilinear transformation of (3.3):

$$H(z) = \left(\frac{\left(1 - e^{-\omega_c T}\right) z}{z - e^{-\omega_c T}} \right)^n \tag{3.21}$$

The sensing is done with a position quantization. The true position x will be measured with an accuracy Δ: the distance per pulse, and therefore the worst case error. This is visualized in figure

3.3a). To calculate the stability boundary, the approximation of figure 3.3b) is used. Here the measured position $\hat{x}$ is the sum of the true position x and a position noise $\tilde{x} \in \mathbb{R}\,[-\Delta, \Delta]$.

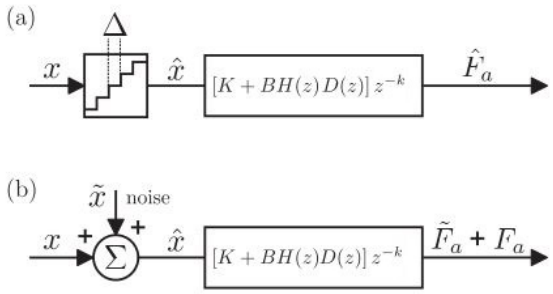

Figure 3.3: Model used to calculate the quantization error. In a) the true position signal x is quantized with a quantization interval Δ. This leads to an estimation of the position $\hat{x}$, which is used in the virtual environment to generate a actuator force $\hat{F}_a$. In b) a simplification is visualized: the measured position is the sum of the true position and noise $\tilde{x} \in \mathbb{R}\,[-\Delta, \Delta]$. This causes the actuation force to be the sum of the true force and the force caused by noise $\tilde{F}_a$. Figures adapted from Colonnese[16].

Colonnese[16] defined the quantization-error passivity as *sufficiency for no net quantization-error energy generation over any sample period.* To fulfill this statement, the maximum generated energy by the quantization-error should be lower than the dissipated energy by friction. Therefore, we require the following statement to be true:

$$c > \left\| \left[K + BD\left(z\right) H\left(z\right)\right] \frac{1}{z^k} \right\| \Delta \tag{3.22}$$

Where $\|\cdot\|$ represented the norm of a signal. A spring-damper virtual environment can not produce enough energy to overcome the friction force as a reaction of the quantization error, when inequality (3.22) holds. In addition, one can see that equation (3.19) is still valid as the maximum virtual stiffness when no virtual damping is applied.

Figure 3.4 gives a qualitative indication of the quantization-error stability boundary. A higher value for B represents a higher energy generation of the virtual environment, and therefore the maximum stable stiffness decreases with increasing virtual damping.

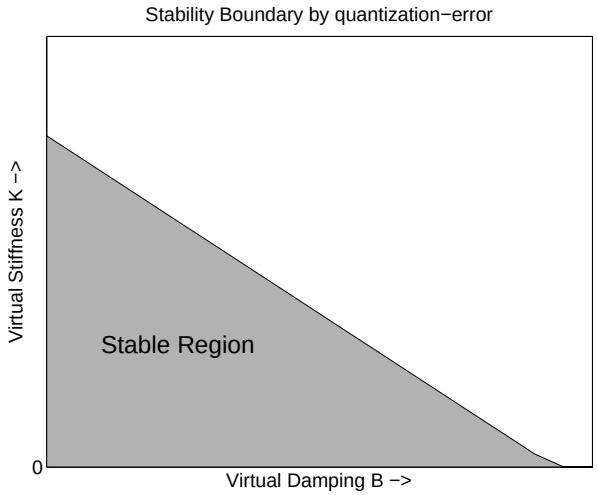

Figure 3.4: Qualitative indication of the quantization-error stability boundary.

3.3.3. Combined Stability Boundary

In the previous sections, one could see that the maximum stable stiffness has two limiting mechanisms. The stability boundaries determined by sampled-data and by quantization-error are derived. When

the maximum virtual stiffness limited by stability is denoted as K_s and the maximum virtual stiffness limited by quantization error denoted as K_q, then the total maximum stiffness is the smallest of the two:

$$\boxed{K_{max} = \min\left(K_s, K_q\right)} \tag{3.23}$$

3.4. Dynamic Range of Stable Impedances: Z-Width

An impedance-type haptic device is an impedance generator. The biggest challenge for the designer is to achieve a large dynamic range of achievable impedances. Colgate and Brown[14] started this approach and called it the *Z-Width*. It is bounded from below by the free space impedance, and bounded from above by the maximum stable impedance, as determined in the previous sections.

The free space impedance of a haptic device is simply determined by the device dynamics, as introduced in equation (3.1). Written as an impedance, it is as follows:

$$Z_{FS}\left(\omega\right) = ms + b \tag{3.24}$$

The closed-loop impedance, in the continuous domain is as follows:

$$Z_{cl} = \frac{F_h\left(s\right)}{V\left(s\right)} = \frac{1 + G\left(s\right) H_{VE}\left(s\right) D\left(s\right)}{sG\left(s\right)} = \frac{\left(bs + Ke^{-t_d s} + ms^2\right)\left(s + \omega_c\right)^n + Bs\omega_c^n e^{-t_d s}}{s\left(s + \omega_c\right)^n} \tag{3.25}$$

The maximum stable renderable impedance, $Z_{max}\left(s\right)$, is the closed loop impedance from equation (3.25), with the maximum stable achievable stiffness from equation (3.23) and the corresponding damping substituted.

To illustrate the Z-width, a fictional haptic device is chosen with mass $m = 50\,\mathrm{g}$, damping $b = 0.1\,\mathrm{N\,s\,m^{-1}}$, total time delay $t_d = 1.5\,\mathrm{ms}$, maximum stable virtual stiffness $K = 1000\,\mathrm{N\,m^{-1}}$ and corresponding virtual damping $B = 5\,\mathrm{N\,s\,m^{-1}}$. The Z-Width is displayed in figure 3.5. The blue dotted line gives the free space impedance, which is only determined by the device dynamics as in (3.24), the lower limit of the range of impedances. The upper limit is determined by the maximum stable impedance, the green solid line, defined in (3.25). The Z-Width (denoted as $\mathbb{Z}_w$ with unit Ns/m) is quantified using the method presented in Christiansson[2], calculating the area in figure 3.5, where the frequency range of interest is defined from ω_0 until ω_1, in radians per second:

$$\mathbb{Z}_w = \frac{1}{\omega_1 - \omega_0}\int_{\omega_0}^{\omega_1}\left(\left[Z_{max}\left(\omega\right)\right] - \left[Z_{FS}\left(\omega\right)\right]\right)\mathrm{d}\omega \tag{3.26}$$

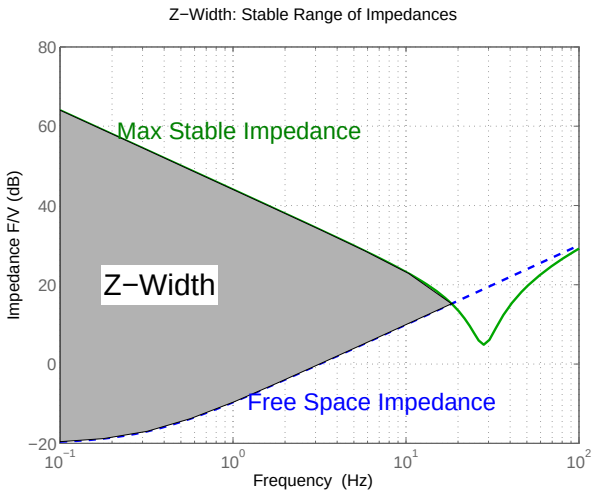

Figure 3.5: Z-width of a haptic device, the stable range of achievable impedances. The blue dotted line gives the free space impedance, the lower limit. The upper limit is determined by the maximum stable impedance, the green solid line. The area in between the two lines, visualized in gray, denote the Z-Width.

3.5. Quality of Feedback Force: Effective Stiffness Bandwidth

In haptic devices, the discrepancy between the desired force and the rendered force must be small. This is the accuracy of a haptic device, in literature about teleoperation also known as *transparency*[7]. However, in an impedance type haptic device, the user feels the combined forces from the dynamics and statics of the device and the simulated environment in response to moving the device[3]. This problem was illustrated with figure 3.1a, where the impedance of the device is in series with the rendered impedance.

The rendered closed loop impedance was already determined in equation 3.25. The desired impedance is simply the the impedance of the virtual environment: the combination of the virtual spring K and virtual damper B:

$$Z_{des}(s) = B + \frac{K}{s} \tag{3.27}$$

Using the same properties as before by analyzing the Z-Width, the transparency is visualized in figure 3.6. The blue solid line represents the desired impedance as in equation (3.27). The dashed green line is the rendered impedance from equation (3.25), where the dynamics of the device itself also come into play.

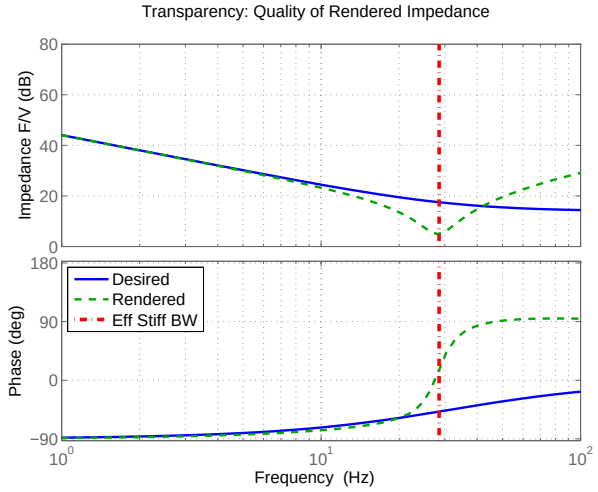

Figure 3.6: The Transparency of a haptic device, calculated at the maximum stable impedance. The blue solid line represents the desired impedance, which is simply the impedance by B and K. The dashed green line is the rendered impedance, where the dynamics of the device itself also come into play. The resemblance between the desired and rendered impedance is good until the Effective Stiffness Bandwidth defined in (3.28).

The resemblance between the desired impedance from equation (3.27) and rendered impedance from equation (3.25) is good until the Effective Stiffness Bandwidth, as can be seen in figure 3.6. Therefore, the Effective Stiffness Bandwidth will be the second performance metric.

$$\omega_{ES} = \sqrt{\frac{K}{m}} \tag{3.28}$$

This effective stiffness bandwidth is a metric introduced by Colonnese et. al.[8], where the rendered impedance is decomposed in "mechanical primitives", as mass, damping and stiffness. This makes it a very convenient tool to compare the real closed loop impedance with the desired one. In this analysis it is shown that the effective stiffness (the stiffness an operator feels), is equal to the rendered virtual stiffness K until the effective stiffness bandwidth. The same holds for the mass: the operator will experience no feedback on the acceleration, at a frequency lower than effective stiffness bandwidth. At higher frequency the mass of the device comes into play again.

3.6. Effect of Physical Parameters on Haptic Performance

The individual physical parameters of a haptic device are thus as follows: mass m, damping b, friction c, sample time T, quantization interval Δ and total time delay t_d. In addition, one can tune the velocity filter by changing the cut-off frequency ω_c or the order n. In the following paragraphs, the sensitivity of the performance metrics to the individual parameters is investigated.

Sensitivity of sampled-data stability to damping

As a starting point for discussing the results, a device is chosen with the following properties: mass $m = 50\,\mathrm{g}$, damping $b = 0.1\,\mathrm{N\,s\,m^{-1}}$, total time delay $t_d = 1.5\,\mathrm{ms}$ and frequency filter cut-off is 50 Hz. The stability criteria are evaluated for this fixed device, varying the damping, to demonstrate its effect. Figure 3.7 shows the result. The maximum renderable stiffness does strongly depend on the virtual damping.

We see that the virtual damping has the same effect as the D-action in a PID-controller. It adds phase, and therefore, upto a certain B, increasing B leads to a larger stable renderable Stiffness.

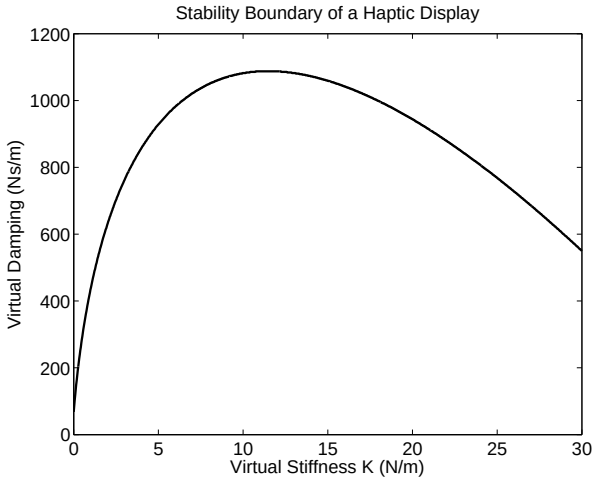

Figure 3.7: Sampled-data stability boundary of a haptic display using $m = 50$ g, damping $b = 0.1$ Ns/m, total time delay $t_d = 1.5$ ms and frequency filter cut-off is 50 Hz. The stable region is *under* the curve.

Gil et al[31] gave a strict measure for the maximum renderable stiffness:

$$K < \frac{b + B}{\frac{T}{2} + t_a} \tag{3.29}$$

Or in words: the strict maximum of the virtual stiffness is the sum of all damping divided by the sum of all time delays. This strict maximum is the initial slope of the curve in figure 3.7. From this one can conclude that virtual damping and physical damping contribute in the same way to the maximum stiffness. However, the contribution of the virtual damping is one to two orders higher than that of the physical damping for typical values in haptic devices (for which some can be found in Diolaiti[26]). Therefore the physical damping will not be taken into account in the analysis as a separate value.

On the other hand, as can be seen directly in equation (3.24) of the free space impedance, damping is diminishing the free space impedance.

Sensitivity of sampled-data stability to mass

Using the passivity approach by Colgate, mass does not affect the maximum stable renderable stiffness[6, 14]. This is the same when virtual damping is not applied. For a static maximum stiffness, mass does not affect the stability margins[16].

In figure 3.8 the stability boundaries of a haptic device is given, with a varying mass. Other physical values were set as follows: physical damping was set to $b = 0.1\,\mathrm{N\,s\,m^{-1}}$, total time delay of $t_d = 1.5\,\mathrm{ms}$ and frequency filter cut-off is 50 Hz.

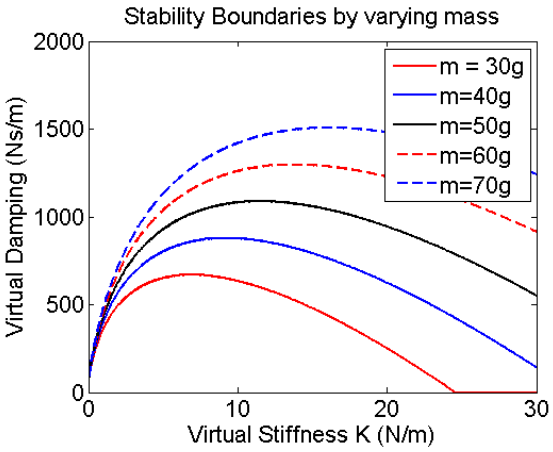

Figure 3.8: The sampled-data stability boundary of a haptic display for varying mass. The stable region is significantly enlarged for a higher mass. The physical damping was set to $b = 0.1$ Ns/m, total time delay of $t_d = 1.5$ ms and frequency filter cut-off is 50 Hz.

In figure 3.8 one can see that a higher moving mass improves the stable region, even for small variations. This is in contrast with statements by Gil[31]. However, the maximum renderable stiffness does only depend on mass in the domain with larger damping. The initial value of the slope is the same for all different mass-values, which is the slope given by equation (3.29).

This result is similar to what is found in literature: Hulin finds a fixed normalized maximum stiffness:

$$\alpha = \frac{KT^2}{m} \tag{3.30}$$

In (3.30) one can see that the the maximum stiffness K at a fixed normalized maximum stiffness is proportional to mass.

Using equation (3.28), one can see that mass reduces the effective stiffness bandwidth. In addition, it diminishes the free space impedance of a haptic device.

Hereby one can conclude that one the traditional guidelines for haptic design: low moving mass[30, 35, 36], is not always true. For rendering maximum stable impedances, mass plays a benificial role.

Sensitivity of sampled-data stability to time delay

Time delay severely hinders stability especially for non-aggressively filtered virtual damping[16].

The influence of time delay on the maximum stable renderable stiffness can already be seen in equation (3.29). The time delay in the denominator suggests that larger time delay diminishes stable region. This is similar to what has been found in literature[16, 31, 34]. In addition, it is also what is seen in simulations for this thesis. Figure 3.9 shows the same fixed haptic device ($m = 50\,\mathrm{g}$, $b = 0.1\,\mathrm{N\,s\,m^{-1}}$, $\omega_c = 50 \cdot 2\pi$ rad/s) for a varying time delay. As expected, one can see that the time delay is decreasing the stability boundary

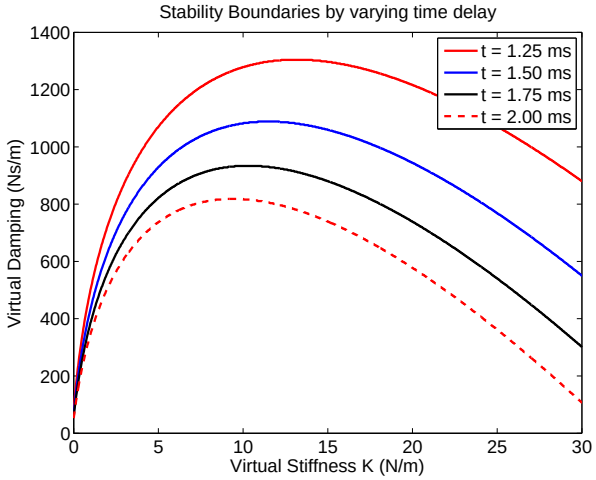

Figure 3.9: The stability boundaries of a haptic display by sampled data, for varying time delays. A very straightforward conclusion is that the time delay is diminishing the stable region.

This could also be seen, when one considers the normalized maximum stiffness from (3.30). Here one can conclude that the maximum stiffness is inversely proportional to the time delay *squared*. Due to the squared relationship, time delay is significantly reducing the maximum renderable stiffness.

Sensitivity of sampled-data stability to velocity filter cut off frequency

In contrast with the original Routh-Hurwitz usage from Gil[31], the characteristic equation in (3.10) is one order higher than the one from Gil, due to the velocity filer. This filter is inserted for noise reduction that is introduced by the finite difference velocity estimator, as suggested and used by Chawda[37] and Colonnese[16] among others.

The stability criterion with an unfiltered velocity estimator by Gil is as follows:

$$(m + bt_d) - Kmt_d \tag{3.31}$$

Therefore, if the filter cut-off frequency is set very high, the two methods give the same results. This is the case as we can see in figure 3.10. A larger filter cut-off will theoretically lead to a larger stable impedance range. However, in practice the low pass filter is needed for noise attenuation.

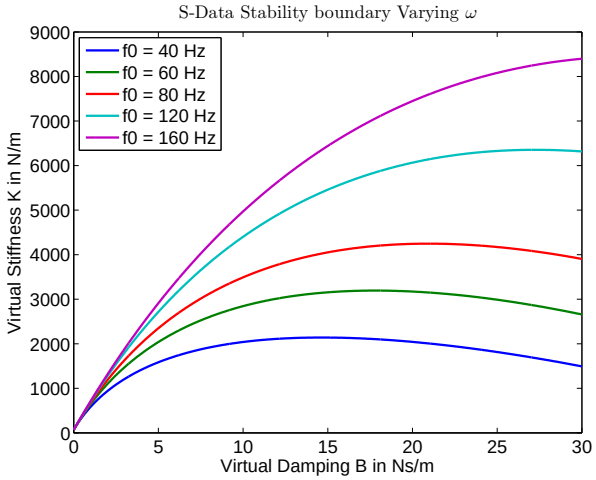

Figure 3.10: The stability boundary of a haptic device as limited by sampled-data. It is clearly visible that a higher velocity filter cut-off frequency enlarges the stable region.

Sensitivity of quantization-error boundary to physical properties

The sensitivities of the quantization-error stability boundary are more insightful than those of the other performance metrics. Therefore, these are visualized in one figure, figure 3.11. Here one can see the

starting point of the boundary was already derived in equation (3.19). A smaller quantization interval will reduce the maximum quantization-error, and therefore increase the stability boundary. In addition, a higher friction will increase the stability boundary, since more energy is dissipated. This is in contrast with traditional haptic design philosophy, where low friction is prefered[30, 35, 36].

Furthermore, a higher velocity filter cut-off allows a broader range of frequencies to pass. Therefore, more energy needs to be dissipated and the quantization-energy boundary in equation (3.22) will be lower. The filter order will have the opposite effect.

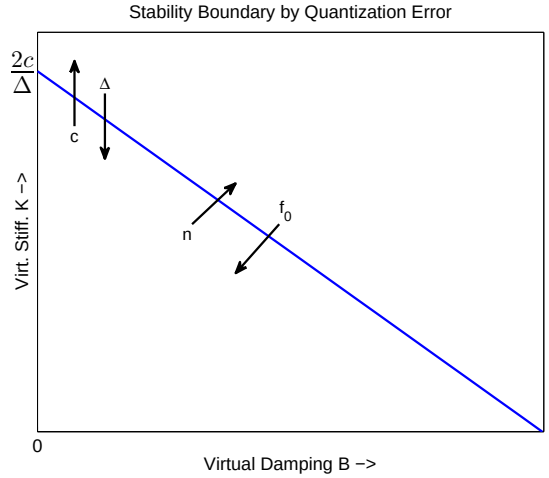

Figure 3.11: Qualitative indication of the quantization-error stability boundary. The starting point of the function is the friction divided by the quantization interval, as already derived in equation (3.19)

3.7. Discussion

The Key Parameters of Interest in this study are thus the *Maximum Stable Stiffness*, the *Z-width* and the *Effective Stiffness Bandwidth*. In layman's terms: free motion should feel free, stiff environments should be as stiff as possible, and the force signal should be accurate over a suitable frequency range. The device should be stable for a large dynamic range of impedances.

The method for calculating these values is as displayed in the flow diagram figure 3.12. The individual physical parameters of a haptic device, $(m, b, c, \Delta, T, t_d)$ determine, together with the velocity filter, the maximum stable renderable stiffness. In addition, the physical parameters determine the free space impedance. As a next step, the Z-Width follows from those two combined, it is bounded from below by the free space impedance and from above by the maximum stable rendering. Finally, the effective stiffness bandwidth is determined by the maximum stable stiffness and the mass of the device.

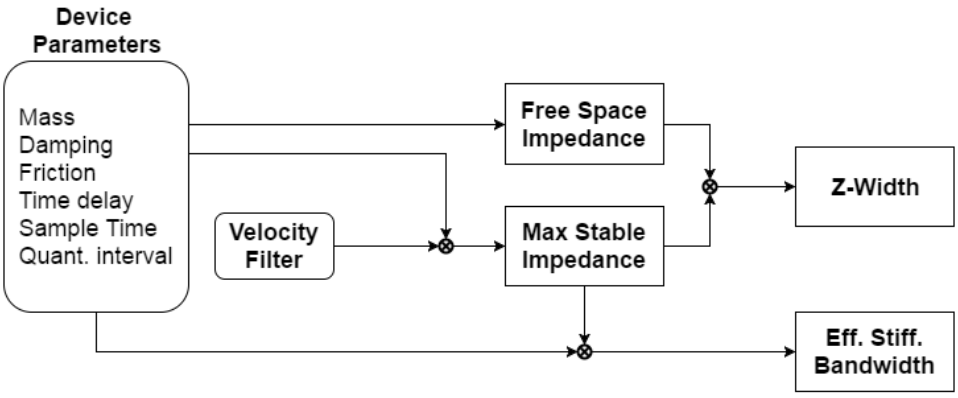

Figure 3.12: This flow diagram summarizes the interconnected relationships, from physical parameters of a haptic device to the performance metrics, as discussed in this chapter. The physical parameters determine the free space impedance. Together with the velocity filter, the physical parameters lead to a maximum stable stiffness, which, combined with the free space impedance, determine the Z-Width. In addition, the maximum stable stiffness combined with the mass of the device, determine the effective stiffness bandwidth.

This multistage calculations make the problem not very insightful. Therefore, in the previous sections sensitivities are calculated. This showed the often conflicting interests of some of the physical properties. Some properties are increasing one performance metric, while diminishing others. An example is the mass, which is diminishing the free space impedance, but needed for sampled-data stability. All direct influences are summarized in table 3.3.

This is also visible in figure 3.13, which shows the qualitative stability boundary of a haptic device, limited by both sampled-data stability and quantization-error stability. One can see that mass and filter cut-off are beneficial for the sampled-data stability boundary, and filter order and time delay are diminishing the stable region. In addition, a higher filter cut-off reduces quantization-error stable range, and the filter order improves it. Higher friction and smaller quantization increase the starting point of the the quantization-error stable range too.

Table 3.3 gives the qualitative influences of the individual physical parameters on haptic performance. For the closed-loop haptic performance metrics Z-Width and Effective Stiffness Bandwidth, it is not directly clear how they are affected by the change of physical parameters. This is due to the ambiguity in the effect of physical parameters on the maximum stiffness, which thereby affects the KPI's. Therefore, a trade-off between the parameters and their effect on the KPI's should be made.

Table 3.3: Qualitative influence of individual parameters on maximum stable stiffness and the free space impedance. Achieving the maximum stiffness proves to be a trade-off between parameters, which at their turn diminish the free space impedance. (*The effect of physical damping on maximum stable stiffness is only marginal, it can be neglected as compared to B. They have the same effect on stability, but are typically two orders apart.)

		Effect on:				
Effect of		K_s	K_q	$Z(s)_{FS}$	$\mathbb{Z}_w$	ω_{ES}
Mass	m	+		-	+ and -	+ and -
Damping*	b	+*	-*	-	+ and -	
Friction	c		+	-	+	+
Delay	t_d	-	-	-	-	
Quant. int.	Δ		-		-	-
Vel. filt. cut-off	ω_c	+	-		+ and -	+ and -
Vel. filt. order	n	-	+		+ and -	+ and -

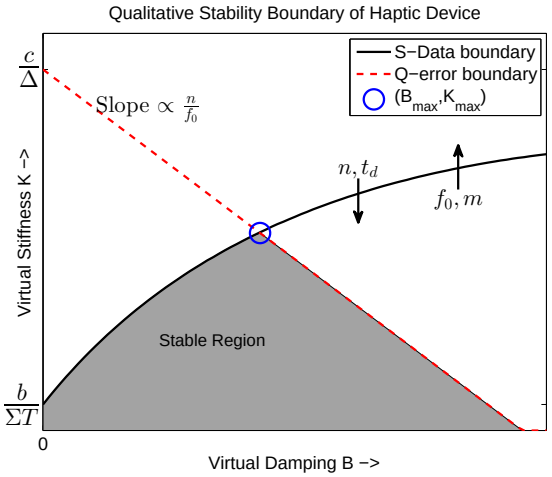

Figure 3.13: Qualitative Stability Boundary of a haptic device, where the influence of the physical parameters is indicated by arrows.

4

The Influence of Component Level Choices on Haptic Performance

In the previous chapter, the link between physical properties and haptic performance is made. However, a haptic device is more than just a set of physical parameters, it is a mechatronic device consisting of several components. This chapter will take the next step, and will make the link from mechatronic component level choices to physical properties, and thereby to haptic performance.

This chapter will start with a motivation. After that it will be shown that component level choices often affect multiple properties, the so-called "symbiotic properties". Some examples will be given, with the focus on the haptic paddle design.

4.1. Motivation

The traditional analysis of a haptic device is graphically visualized in figure 4.1. Individual physical parameters are taken into account to determine the performance indicators: the maximum stable stiffness, the Z-Width and the Effective Stiffness Bandwidth from the previous chapter.

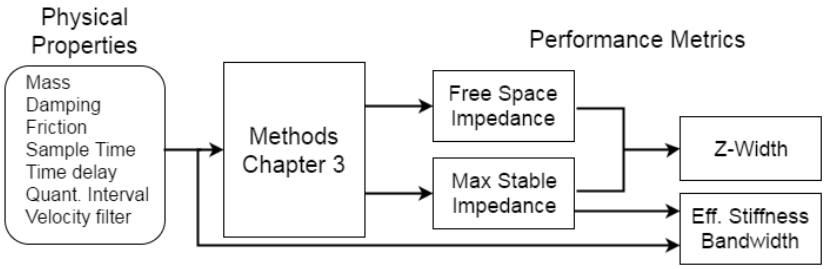

Figure 4.1: Overview of the method from the previous chapter: how physical parameters affect haptic performance.

The model used for haptic performance studies was displayed in figure 3.1b. The haptic device is modeled by a mass-damper system with coulomb friction. The measurement system is modeled as sensor quantization and a switch as A/D convertor. The virtual environment consists of a spring and a damper, and the force is applied after a zero order hold and a time delay, representing all electro-dynamic components.

All the research presented in the previous chapter is focused on the influence of physical parameters, like mass, damping and time delay. However, a haptic device is a mechatronic device, consisting of sensors, actuators, power amplifiers and controllers, like in figure 4.2. In this mechatronic building blocks, many individual parameters are correlated.

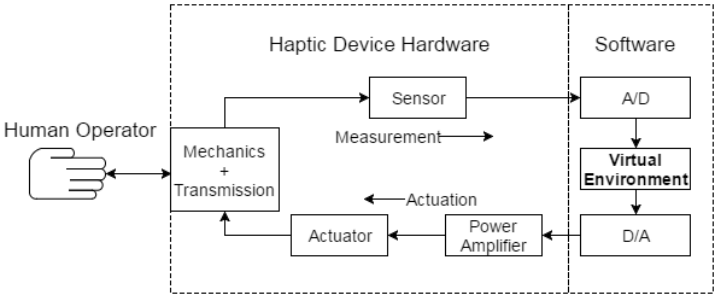

Figure 4.2: The Mechatronic overview of an impedance type haptic device. A position is measured, and as a reaction to the virtual impedance, a force is applied.

A conclusion might be that a larger time delay will reduce the stability boundary as concluded in the previous chapter, but there is a problem. It is not convenient to just affect the time delay with some mechatronic component. A faster actuator might affect the inertia and damping too.

Another example is the transmission. The force goes linear with the transmission ratio, but damping and inertia go squared with that ratio. In addition, a transmission reduces efficiency and adds additional damping.

This can be seen in figure 4.2. The transmission ratio is in the sensing *and* in the actuation part. In addition, sensors and actuators are often co-located, and therefore the transmission ratio also affects the sensing capabilities of a haptic device. And although the actuator is not displayed in the measurement subsystem, the mechanics of the actuator contribute to the total free space impedance too.

4.2. Symbiotic Properties

In the previous chapter, the influence of changing parameters is discussed. A problem of this method is the fact that it is most often not possible to change one property with certain design choices. Changing one property, affects others. This will be proven in the coming sections. In addition, the actuator and the transmission ratio determine the force-reflecting capabilities. The actuator is considered to bound the force-capabilities from above[38]. Therefore, those two are the most important properties in haptic performance analysis.

4.2.1. Symbiotic Properties in the Actuator

Most haptic devices use DC-motors, due to their linearity from force to current, the low friction and good backdriveability[39, 40].

A DC-motor is a electromagnetic actuator, and therefore it acts as a low-pass filter with an electrodynamic time constant.

$$\tau_e = \frac{L}{R} \tag{4.1}$$

The electrical time constant corresponds to the time needed for the torque to reach 63% of its final value. The time delay is equal to *five* times the time constant. This is were the torque reaches 99% of its final value.

$$t_d = 5 \cdot t_e \tag{4.2}$$

In contrast with DC-motors in normal operation, the mechanical time constant does not play a role in impedance-type haptic devices, since force control is applied.

The working principle of the DC-motor is the Lorentz force:

$$F = BIL \tag{4.3}$$

So force is the multiplication of the magnetic field strength, the current and the length of the coils in the magnetic field. From this formula, we have the following hypotheses:

1. A motor with a higher torque, will require more coils, or coils farther from the axis of rotation (larger radius). Thus: a higher toque will come at the cost of a larger moment of inertia.

2. A motor with a higher torque, will require larger and more powerful coils. This will increase the inductance, and therefore increase the time delay.

Both hypotheses are tested on a range of commonly used, high performance DC-motors (see appendix B). Figure 4.3 shows the actuator properties from 108 DC-motors, which are usually used in haptic systems. Two correlations can be observed, so choosing another motor, affects the nominal torque, the time delay and the rotational inertia. Selecting a motor with a higher nominal torque, leads to an actuator with a larger time delay and a larger rotational inertia.

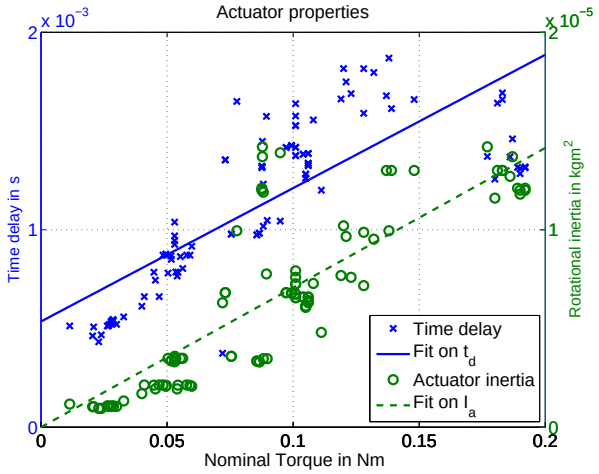

Figure 4.3: Actuator properties from 108 motors, giving the relationship between the actuator torque on the x-axis, the time delay on the left y-axis and the rotational inertia on the right y-axis. With two different least-squares estimations, showing large correlations.

In figure 4.3 a clear correlation between the actuator parameters is visible. When $\rho(a_1, a_2)$ denotes the Pearson correlation between the variables a_1 and a_2, we show the following correlation between the motor parameters, where T_a denotes the maximum continuous torque of the actuator, t_a the time delay, and I_a the rotational inertia:

$$\begin{aligned} \rho(T_a, t_a) &= 0.79 \\ \rho(T_a, I_a) &= 0.86 \\ \rho(t_a, I_a) &= 0.80 \end{aligned} \tag{4.4}$$

The correlation coefficients in equation (4.4) are high, around 80%. This shows that the three considered actuator properties, the torque, inertia and time delay are highly correlated. So in lay-mans terms: a stronger actuator typically is slower and heavier. This proves the first set of symbiotic properties.

4.2.2. Symbiotic Properties in the Transmission Ratio

The transmission ratio, or 1-DoF Jacobian, is the ratio between the motor torque and the end-effector torque or force (the latter depends on orientation of end-effector). Changing this ratio affects multiple properties:

- The transmission ratio determines amplification from actuator torque to the end-effector force/-torque.
- The transmission ratio determines the mass as felt by the end-effector in two different ways:
  1. The size of the pulley must be adjusted. This affects the inertia of the pulley
  2. The inertia of all rotating parts on the actuator-axis is added to the total inertia by the transmission ratio squared.

- The transmission ratio, together with the sensor resolution, determines the quantization interval (distance per pulse) at the end-effector

Using a transmission, it is possible to amplify the torque of the actuator linearly. However, due to the larger rotational speeds, the motor inertia is contributing to the total inertia by the transmission ratio squared. The same holds for the damping and friction forces. In addition, the sensor is mostly collocated with the actuator. An torque-amplifying transmission will also increase the accuracy of the measured value: The number of pulses per unit of distance by the end-effector is increased.

The effect of the transmission ratio can be illustrated using the Haptic Paddle as case. This is a simple 1-Degree of Freedom mechanism, used at many universities in many different configurations[9, 18, 41] for teaching and studying control, dynamics and haptics. In addition, is can be seen as a rotating bar, which is used as an input in many parallel mechanisms[1], such as the Delta Robot[43] in the Novint Falcon [44].

Figure 4.4 shows a schematic view of the haptic paddle, with the main dimensions indicated. it consists of two parts: the handle and the pulley connected to each other with a capstan drive. The pulley is directly connected to the actuator and the sensor.

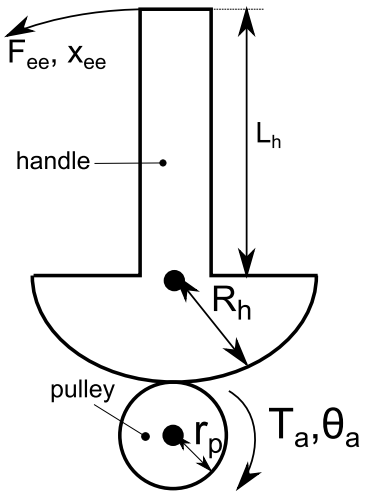

Figure 4.4: Schematic of the Haptic Paddle Configuration, with the main dimensions indicated. Pulley and handle form the transmission from actuator torque θ_a to end-effector force F_{ee}.

The paddle in figure 4.4 consists of a handle with rotational inertia I_h and a pulley with rotational inertia I_p. On the axis of the pulley, the inertia of the actuator contributes, and the inertia of the axis that connects the actuator to the pulley (I_{ax}, including fasteners and the capstan drive). Variables L_h, R_h and r_p denote dimensions as in figure 4.4. This generates a lumped mass at the end-effector as follows:

$$m = \frac{1}{L_h^2}\left[I_h + \left(\frac{R_h}{r_p}\right)^2 (I_p + I_a + I_{ax})\right] \tag{4.5}$$

The end-effector force F_{ee} as a function of the actuator torque T_a is as follows:

$$F_{ee} = \frac{R_h}{r_p L_h} T_a \tag{4.6}$$

And finally, the sensor is collocated with the actuator. An optical encoder with N pulses per revolution, leads to an angle per pulse of $\frac{2\pi}{N}$. Therefore, quantization interval Δ at the end-effector is as follows, in meter:

[1] As stated in many papers, a parallel mechanism seems to be the preferred choice for haptic devices[3, 19, 36], due to the combination of low moving mass and high structural stiffness[42].

$$\Delta = \frac{2\pi L_h r_p}{R_h N} \tag{4.7}$$

In these three equations, one can see what is described before: The torque-to-force ratio scales linear with the dimension, and the same holds for the transmission from sensor resolution as displacement at the end-effector. However, the inertia of everything at the pulley-axis, contributes to the total mass multiplied by the dimensions squared.

4.2.3. Symbiotic Properties in Other Components

Other components typically do not come with symbiotic properties. The control system (hardware of the controller) only affects the sample time and time delay. The same holds for the D/A and A/D convertors and the power amplifier.

Another example is the sensor. In this study, it is considered to be a rotational encoder, since it is the most used sensor in haptic design[3]. It simply affects the quantization interval in the model.

One could think of other sensors, like hall sensors or accelerometers, but that is out of the scope of this project.

4.3. Discussion

A haptic device is more than a set of physical properties, it is a mechatronic device build from components. A designer builds a haptic device from physical components, with which it is difficult to affect single physical properties. The properties prove to be highly correlated in design choices. Table 4.1 gives an list of the mechatronic components in a haptic device, indicates the physical properties they are affecting.

Table 4.1: Design choices in haptic devices and their effect on individual physical parameters.

	Affects:				
Choice of:	m	Δ	t_d	T	F_{ee}
Actuator:	x		x		x
Transmission:	x	x	x		x
Sensor:		x			
Controller:			x	x	

Next to the influence on physical parameters, the transmission ratio and actuator together determine the force capabilities of an haptic device. A complete schematic overview is given in figure 4.5, which indicates the steps from component level choices, via physical parameters, to haptic performance indicators.

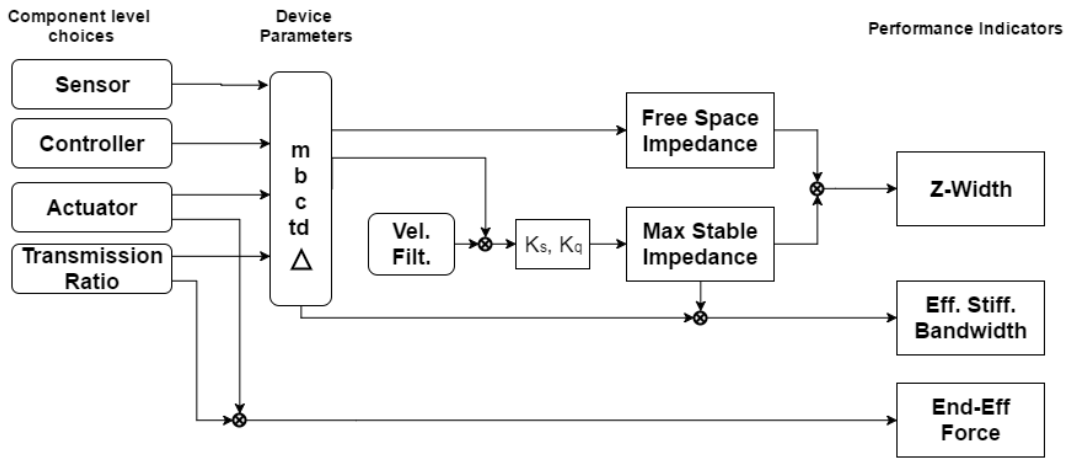

Figure 4.5: Schematic overview of the steps that are taken from component level choices, via physical parameters, to haptic performance indicators.

5

Case Study: Quantitative Modeling of the Gemini Haptic Paddle

This chapter will bring the developed model alive, by applying it on a real device. As a case study, the traditional haptic paddle design is chosen, in the form of the Gemini as developed at the Delft Haptics Lab[1]. First, the Gemini will be analyzed and its performance will be evaluated using the methods developed in the previous chapters. Experiments will we done to validate this the stability boundary of the device.

The next step is the performance analysis of variations of the Gemini, that will be done in section 5.2. Here the effect of even small component level variations will prove to have a clear effect on haptic performance.

5.1. The Gemini

The Gemini haptic paddle[24] is one half of a haptic teleoperation system, which consists of two identical systems. It is developed at the Delft Haptics Lab[1] in the haptic paddle configuration, as displayed in figure 4.4. The Gemini itself is visualized in figure 5.1.

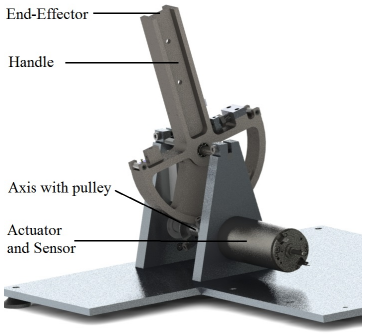

Figure 5.1: The Gemini Haptic Paddle with the important components annotated.

5.1.1. Properties of the Gemini

The properties of the Gemini are listed in table 5.1. Using equation (4.5), one can determine the mass lumped at the end-effector to be $m = 346\,\mathrm{g}$, and using an encoder with 4000 pulses per revolution and equation (4.7), the quantization interval is $\Delta = 16\,\mu\mathrm{m}$. The physical damping barely contributes, so it is assumed to be low: $b = 0.01\,\mathrm{N\,s\,m^{-1}}$ and the friction is assumed to be similar to existing devices (from which the data is listed in Diolaiti[26]): $c = 0.1\,\mathrm{N}$.

[1]The Delft Haptics Lab consists of several researchers affiliated with the Department of BioMechanical Engineering, Faculty of 3mE, Delft University of Technology in the Netherlands. The lab is also part of the Delft Robotics Institute. http://www.delfthapticslab.nl/.

Table 5.1: Dimensions and properties of the Gemini set-up, used for the performance analysis. One might notice that the inertia of the pulley is set to zero. This is because the inner and outer radius are the same. When varying r_p, it will be handled as an additional or subtracted inertia.

Part	**Dimensions and Properties**		
Handle	R_h	50	mm
	L_h	100	mm
	I_h	216890	gmm^2
Axis	I_{ax}	28971	gmm^2
Pulley	I_p	0	gmm^2
	r_p	5	mm
Actuator	Maxon	RE30-60W No. 268216	
	T_a	89.7	mN m
	t_a	1.05	ms
	I_a	3470	gmm^2

Using this values, the maximum stable stiffness can be determined according to the methods in section 3.3. This is visualized by the solid black line in figure 5.3. At lower virtual damping, the sampled-data stability boundary dominates as limiting factor for the maximum stiffness, and at higher damping the quantization error dominates.

The maximum stable stiffness of the is $K_{max} = 3800\,\mathrm{N\,m^{-1}}$ at damping $B = 10.9\,\mathrm{N\,s\,m^{-1}}$. These values are obtained using a second order velocity filter with a cut-off frequency of 100 Hz.

5.1.2. Experimental Validation

Different aspects of the methods used in chapter 3 are already tested, in [15, 16, 32, 34, 37]. However, there are three important notes:

- All tests in the cited research are "easy-to-test" scenarios. For example, the system is tested using programmed time delays in the order of tens of milliseconds. However, real electrodynamic time delays are one order lower.
- All tests are performed on existing devices, from which the physical parameters are obtained by identification instead of modeling.
- In these cited tests, only one of the limiting mechanisms is tested, either sampled-data stability or quantization-error stability.

Due to those three reasons, new tests have been performed. The procedure is as follows: a virtual damping and stiffness are programmed, which are expected to be stable judged on modeling. The end-effector is moved manually from the equilibrium position, and then released. In the stable case, the device returns smoothly to its equilibrium position. In the unstable case, the release results in end-less limit cycles, which are only stopped manually. These two scenarios are visualized in figure 5.2.

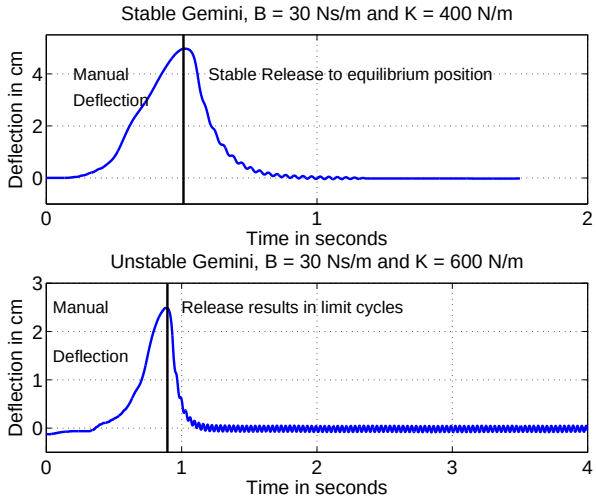

Figure 5.2: The result of two individual tests, with the same virtual damping and a different virtual stiffness. The experimental procedure is simple: the end-effector is retracted from its equilibrium position, and released. The behavior is observed and measured: whether it is stable returning to its equilibrium position (the upper plot) or it results in limit cycles (the lower plot).

When the device proves to be stable for a certain B and K, the virtual stiffness is enlarged and the stability is tested again. The stiffness is increased with steps of $K = 500\,\mathrm{N\,m^{-1}}$ initially, and when the stability boundary is closer, in steps of $K = 100\,\mathrm{N\,m^{-1}}$. This is done at various values for the virtual damping in steps of $B = 2$ or $2.5\,\mathrm{N\,m^{-1}}$.

The resulting experimental determined stability boundary can be seen in figure 5.3. The solid black line denotes the predicted stability boundary, and every red cross denotes the maximum stable stiffness at a certain damping. Data of the complete test can be found in appendix C. Every measurement is at least done three to five times. In every test the same result was obtained. Therefore, no distribution is indicated in the figure.

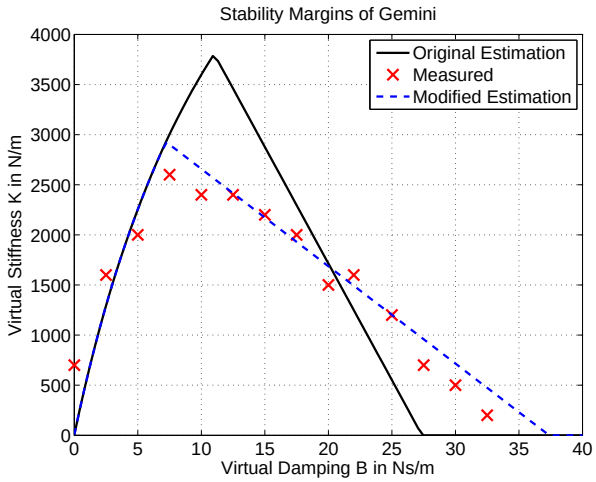

Figure 5.3: Experimental results: The predicted stability boundary of the Gemini is solid black line, and the maximum stable points as tested on the device.

Figure 5.3 shows a good resemblance between the predicted and measured data. The shape of the two is similar. The differences are caused by the following reasons:

First of all, the sharp peak in the predicted stability boundary means that two stability-limiting mechanisms play a role close together, and they might interfere. As one can be seen in the figure, the measured data deviates a bit from the prediction in that regime.

Second, the quantization-error stability boundary seemed to start a bit lower than expected. Probably, the friction is slightly lower than expected.

And finally, the slope of the quantization-error stability boundary is less steep than expected. This might be the case since some small oscillations could occur before reaching a stable equilibrium. That suggests that a bit more quantization energy is allowed, explaining the smaller gradient. This would be in line with Colonnese's research[16]: the system might be able to generate energy over some periods, but dissipates energy on average over all periods.

A modified stability boundary is also indicated in figure 5.3, where the friction is set 30% lower than before, and some generation of energy is allowed in the system[2].

All in all, this experiments showed that the stability boundary could be predicted based on only calculations, modeling and datasheets, before anything on a device is tested. No identification-measurements where performed, and still the results show sufficient resemblance. The fact that no physical measurements are needed for a rough prediction of performance, is an important step for a design tool.

5.2. Redesigning the Gemini

The motivation for the modeling in the previous chapters was to develop a design tool, which can be used to evaluate the effect of component level choices on haptic performance. In this way, a designer could optimize for certain haptic performance.

This is what will be done in this section. A case study will be done to study the effect of two different design choices (the actuator and the transmission). One will see that small changes in those to design choices will lead to large steps in performance.

5.2.1. Choice of Design Variables

In a design process, every component level choice can be considered as a design variable in an optimization problem. As seen in the chapter 4, every change in design variable implies multiple affected physical properties. In this section, two design variables are chosen, and their influence on physical properties and on haptic performance are discussed.

The two variations in the design that will be considered, are the choice of actuator, and the transmission ratio. These two options have an effect on multiple physical properties together (as seen in table 4.1), and are thereby affecting the performance metrics in different ways.

The first one is the actuator. In figure 4.3 the properties of 108 DC-motors were given. Equation (4.4) showed correlations around 80% between the stall torque, the time delay and the rotational inertia. By choosing the actuator torque T_a as a design variable, the inertia and time delay are implicitly changed at the same time.

The relations are quantified using a least-squares fit with the actuator torque as a design variable. This gives the following estimated relationships between the three actuator variables:

$$t_a = a_1 \cdot T_a + a_2 \tag{5.1}$$
$$\text{with:} \quad a_1 = 6.76 \times 10^{-3}\,\mathrm{s\,N^{-1}\,m^{-1}}$$
$$\text{and:} \quad a_2 = 5.35 \times 10^{-4}\,\mathrm{s}$$

and:

$$I_a = a_3 \cdot T_a$$
$$\text{with:} \quad a_3 = 7.07 \times 10^{-5}\,\mathrm{kg\,m\,N^{-1}} \tag{5.2}$$

Please note that we do not claim that the functions above have any causality or physical meaning. However, the correlations are clear and convenient. Using the lsq-estimations reduces the complexity of the problem. Figure 4.3 shows that a designer can find an actuator with properties close to the value found by those functions. Therefore, inserting the actuators directly into the optimization problem, would not give a result that is far off with regards to this estimations in (5.1) and (5.2).

[2] By choosing the condition for no *continuous* generation of energy instead of the condition for no generation of energy in his paper on quantization error[16]

The second design variable is the radius of the pulley r_p, representing a change in the transmission ratio. This is implemented as follows: The inertia of the complete axis, including the pulley, was given in table 5.1. On that axis, the length of the pulley is defined as $h = 19.5\,\text{mm}$. The initial radius of the pulley is $r_{p,in} = 5\,\text{mm}$. The pulley is made of stainless steel, so the density is $\rho = 7800\text{kgm}^3$.

The varying radius of the pulley r_p affects the total inertia then as a simple change in inertia with the following value:

$$I_p = \frac{\pi \rho h}{2}\left(r_p^4 - r_{p,in}^4\right) \tag{5.3}$$

Please note that this is simply an additional inertia, which can be added to the total inertia around that axis, as done in equation (4.5). This is also valid when $r_p < r_{in}$. Then the total inertia at the total axis is lower so the resulting value of equation (5.3) can be subtracted from the total inertia. In addition, as also visible in equation (4.5), r_p also affects the factor at which the rotational inertia of the pulley-axis contributes to the total mass. Furthermore, the maximum end-effector force changes linearly with r_p.

The choice of actuator are varied around the known values for the Gemini. The design choices and their modeling as design variables are summarized in table 5.2. The design variable T_a will be varied over the range of actuators considered. In figure 4.3, one can see that the range in maximum continuous torque is approximately $0.02 - 0.2\,\text{mN m}$. The radius of the pulley will be varied from 3 mm (2 mm smaller than the original design, much smaller than that would be difficult due to the minimal radius of a capstan drive for example) to ten.

Table 5.2: Design variables of the performance analysis of the haptic paddle.

Design option	**Modeled as variation in:**		**Original Gemini**	**Range**
Actuator	Max. cont. Torque	T_a	$90\,\text{mN m}$	$0.02 - 0.2\,\text{mN m}$
Transmission ratio	Pulley radius	r_p	$5\,\text{mm}$	$3 - 10\,\text{mm}$

5.2.2. Results on Individual Physical Parameters

Using the design variables in table 5.2, the design space can be explored. Figure 5.4 shows the variation of moving mass of the Gemini over the design space as a result of changin design variables. The mass is very sensitive to changes in especially the radius r_p: the minimum and maximum in the figure differ by one order. The sensitivity to choice of actuator is lower. This is due to the fact that the inertia of the actuator is small as compared to that of the total axis, and therefore the contribution to the total moving mass is limited.

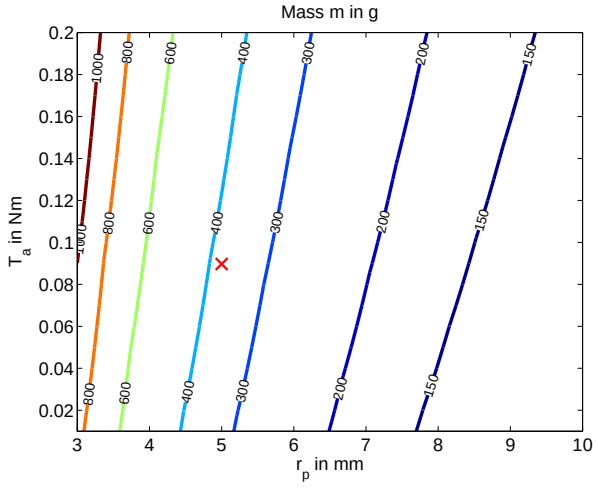

Figure 5.4: Contour lines of moving mass as affected by design variables r_p and T_a. The red cross denotes the current setup.

In figure 5.5 the varying time delay over the design space is given. As already stated in the text and table 4.1, this value is only affected by the actuator choice, not by the transmission ratio. The time delay is doubled over the workspace.

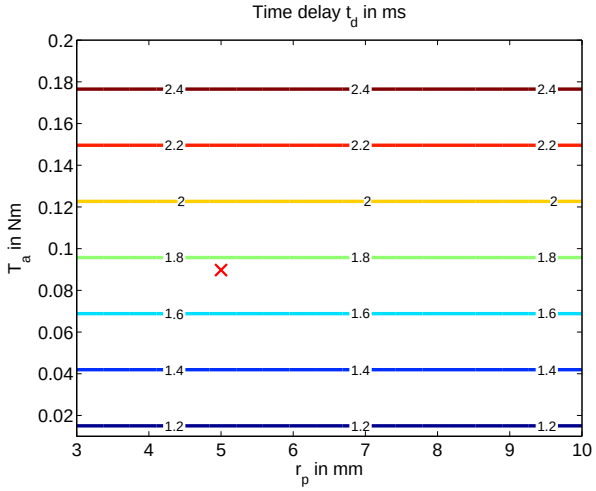

Figure 5.5: The total time delay as affected by design variables r_p and T_a. The red cross denotes the current setup.

Figure 5.6 shows how quantization interval Δ is affected by the design variables. As concluded in table 4.1, it is only changed by the transmission ratio, as can be seen in the figure too. There is a factor three difference over the design space.

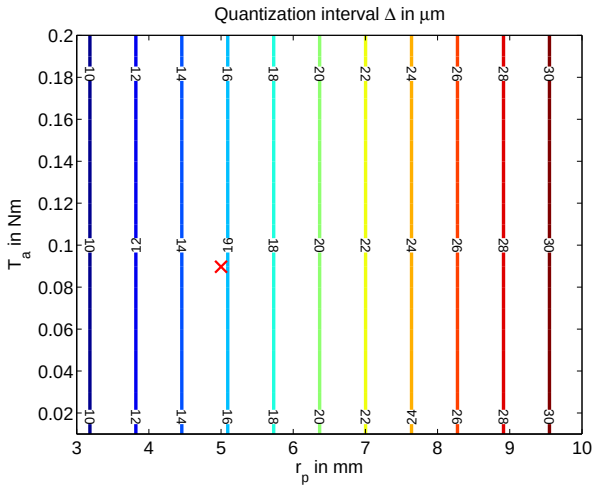

Figure 5.6: The quantization interval as affected by design variables r_p and T_a. The red cross denotes the current setup.

Judging on the three graphs in this section, the influence of even small variations in the design variables can lead to large variations in the physical properties of a device.

5.2.3. Results on Haptic Performance

As discussed in section 3.2, the performance of a haptic device will be evaluated with respect to its capabilities (Z-Width, eq. (3.26), stable range of impedances) and to the quality of the feedback force (Effective Stiffness Bandwidth, eq. (3.28), resemblance between desired and rendered force).

First, the force of the end-effector is displayed in figure 5.7

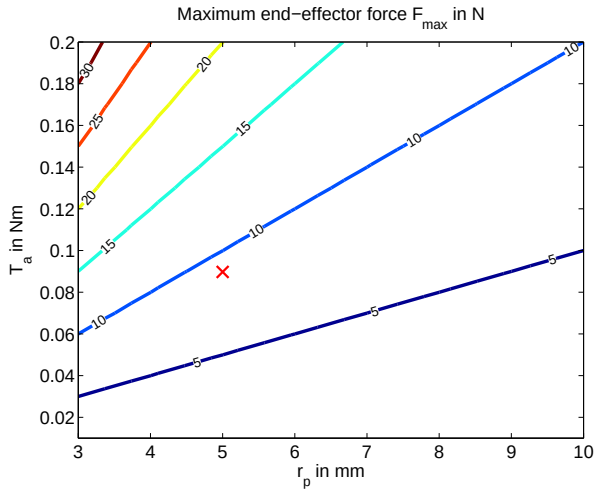

Figure 5.7: The force at the end-effector as affected by design variables r_p and T_a. The red cross denotes the current setup.

As expected, the force at the end-effector is very sensitive to the design variables, as can be seen in figure 5.7. A smaller r_p leads to a larger amplification of the actuator torque and therefore to a larger end-effector force. A stronger actuator obviously corresponds to a larger force too. The total variation in force is almost one order.

The maximum stable stiffness in the design space is showed in figure 5.8. One can clearly see that the maximum stiffness depends on both design variables. A smaller r_p (so a larger transmission ratio) leads to a larger stable stiffness. A larger actuator has the opposite effect. To render the maximum stable stiffness, a designer should strive to a large transmission ratio in combination with a small motor. However, as seen before in figure 5.4, this comes at the price of a larger moving mass and thus a larger free space impedance. And, as in figure 5.7, the smaller motor diminishes the maximum end-effector force.

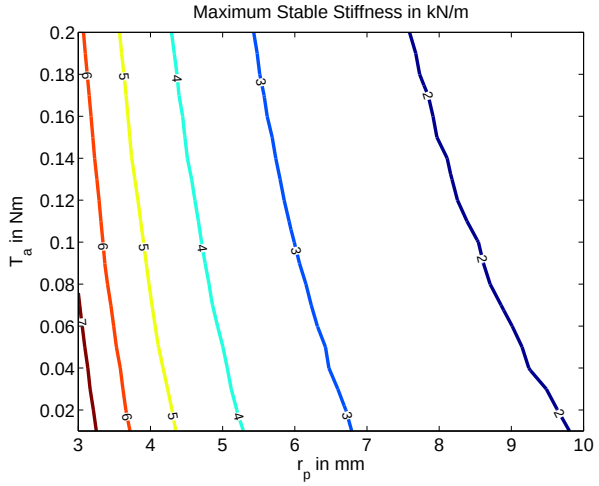

Figure 5.8: The maximum stable renderable stiffness as a function of the design variables.

In figure 5.9, the Z-Width is displayed. This is calculated using a Riemann-approximation of equation (3.26), where the lower bound of the useful frequency range is chosen to be 0.1 Hz (very slow human movement). The upper bound is set equal to the effective stiffness bandwidth as defined in equation (3.28). A similar trend as in the maximum stable stiffness is visible: a higher transmission ratio leads to higher Z-Width. The Z-Width is only marginally affected by the choice of actuator.

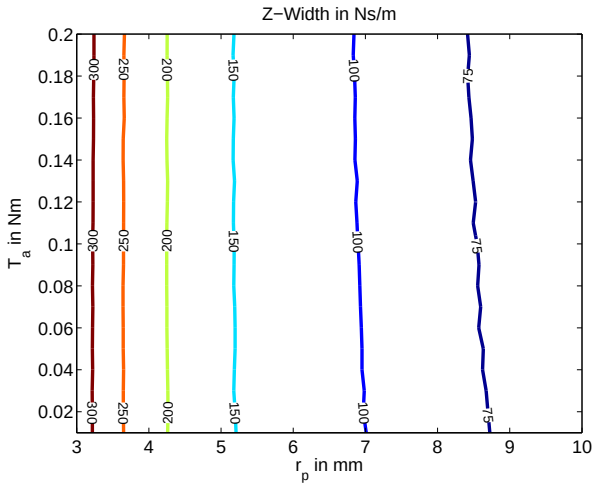

Figure 5.9: The Z-width as a function of the design variables.

In figure 5.10 an opposite trend is visible. The maximum Effective Stiffness Bandwidth is calculated using 3.28. It proves to be affected by both design variables. In contrast with the two figures before, a higher transmission ratio is diminishing the Effective Stiffness Bandwidth. Although the maximum stiffness might be higher, it is increasing the moving mass and therefore diminishing the useful frequency range. A stronger actuator is diminishing the bandwidth even more.

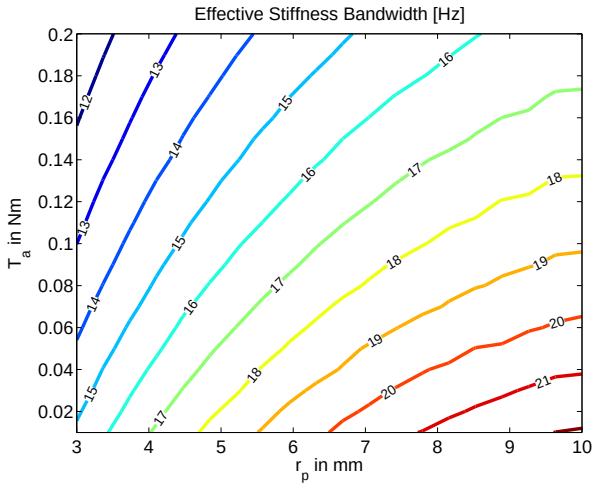

Figure 5.10: The maximum effective stiffness bandwidth as a function of the design variables.

The effect of actuator choice on maximum stable stiffness and Z-width does not seem to be that large. This is for a large extend due to the relatively low contribution of the actuator inertia to the total moving mass. The pulley-axis contains all components for fixing the capstan mechanism, and is made out of stainless steel, which explains the high inertia as compared to the actuator. In other configurations, the actuator inertia plays a larger role.

However, the haptic performance proved to be very sensitive to the variation in the radius of the pulley (and thus in the transmission ratio). The maximum stable stiffness can be improved three times over the considered domain, as can be seen in figure 5.8. In addition, the Z-Width in figure 5.9 follows the same trend: a larger transmission ratio improves the Z-Width. This seems mainly the result of the reduced quantization interval, since figure 5.6 and figure 5.9 have similar contour lines.

The parameters needed for maximum stable stiffness and maximum Z-Width seem to diminish the effective stiffness bandwidth in figure 5.10. The optimum of the bandwidth correlates to a point with

a small stiffness and bandwidth. However, the results seems reasonable, since literature suggests bandwidths from 10 to 30 Hz for haptic feedback[27, 29, 36, 45]. In figure 5.10 one can see that the effective stiffness bandwidth is well above 10 Hz in the entire workspace. However, this is only when rendering the maximum stiffness that is stably achievable. When rendering a lower stiffness, the Effective Stiffness Bandwidth will be lower too.

5.3. Optimization in Haptic Design, Two Examples

As seen in the previous figures, there are many conflicting interests in closed-loop haptic analysis. Different applications will result in different requirements, and thereby in completely different designs. For example, to maximize the Z-Width (figure 5.9) means that one will choose a configuration that will negatively affect the Effective Stiffness Bandwidth in figure 5.10. Another trend is the fact that a strong device, tends to be heavy, as one discovers in figures 5.4 and 5.7.

Since the analysis has two design variables, simple and insightful optimization problems are possible. Two examples will be considered: a rough and strong exploration robot, and a high precision assembly robot.

Example 1: the rough exploration robot

Imagine there has been a severe earthquake. Buildings are collapsed or about to. This Gemini act as master for a 1-DoF slave robot that is sent into one of these buildings. Goal of the slave is to find a save path into the building. This hypothetical slave is assumed to act as a perfect admittance-type manipulator without additional time delays.

This exploration system does not have to be very fast, a minimum effective stiffness bandwidth of 15 Hz will be sufficient. On the other hand, this teleoperation system must be strong. The operator should be able toe feel large stable stiffnesses. Therefore, the master should have the maximum stable stiffness that is possible. This results in the following optimization problem:

$$\begin{array}{lll} \text{Maximize} & K_{max}\,(T_a, r_p) & \text{(Objective function)} \\ \text{Subject to:} & \omega_{ES} \geq 15 \cdot 2\pi\,\text{rad}\,\text{s}^{-1} & \text{(Inequality constraint)} \\ & 0.01\,\text{N}\,\text{m} \leq T_a \leq 0.2\,\text{N}\,\text{m} & \text{(Design variable)} \\ & 3\,\text{mm} \leq r_p \leq 10\,\text{mm} & \text{(Design variable)} \end{array} \tag{5.4}$$

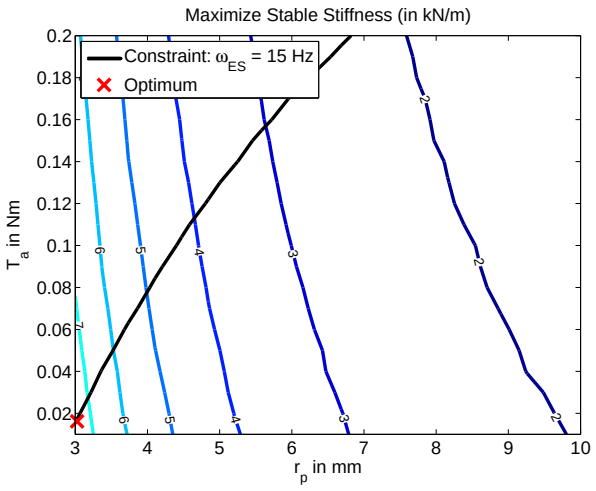

Figure 5.11: The first optimization problem visualized. The solid black line denotes the inequality constraint which divides the design space in the feasible and the infeasible domain. The legend is placed in the infeasible domain. This results in an optimum marked with the red cross.

The result of the optimization problem described here is visualized in figure 5.11. The black line represents the inequality constraints, where the feasible region is below the line (legend is in the infeasible

domain). The optimal solution for this case would be a very small actuator in combination with a very large transmission ratio, denoted with a red cross. Using appendix B, we see that the first one in table B.1, the Maxon RE25 118740, might be a suitable choice.

The optimum is bounded by the constraint and by the minimum size of the pulley. A smaller pulley would not be realizable in the haptic paddle configuration, but other ways of increasing the transmission ratio (for example multistage transmissions) might be interesting to consider for this problem, since it seems to be able to improve haptic performance even more.

Example 2: Precision assembly robot

In another application, the Gemini serves as the master device for a very precise assembly system. Once again, the slave is considered to be ideal: its time-delays by the mechanics or electrodynamics are neglectable. This assembly system requires very precise positioning, and therefore the effective stiffness bandwidth should be maximized. However, the parts that will be handled by the system require a minimal end-effector force of 5 N. This results in the following optimization problem:

$$\begin{array}{lll} \text{Maximize} & \omega_{ES}\,(T_a, r_p) & \text{(Objective function)} \\ \text{Subject to:} & F_{ee,max} \geq 5\,\text{N} & \text{(Inequality constraint)} \\ & 0.01\,\text{N m} \leq T_a \leq 0.2\,\text{N m} & \text{(Design variable)} \\ & 3\,\text{mm} \leq r_p \leq 10\,\text{mm} & \text{(Design variable)} \end{array} \tag{5.5}$$

The solution of the optimization problem in equation (5.5) is visualized in figure 5.12. Again, the black line divides the design space, and in this case the area above the line is feasible. The optimum is completely different than before: an actuator with a stall torque around 0.1 N m would be the ultimate choice. Again using appendix B would suggest for example the Maxon RE35 285794, number 83 from table B.3.

The transmission ratio should be as low as possible for this case. Again, the considered range of the design variable is limiting the optimum, suggesting that even better performance can be reached when lifting this constraint.

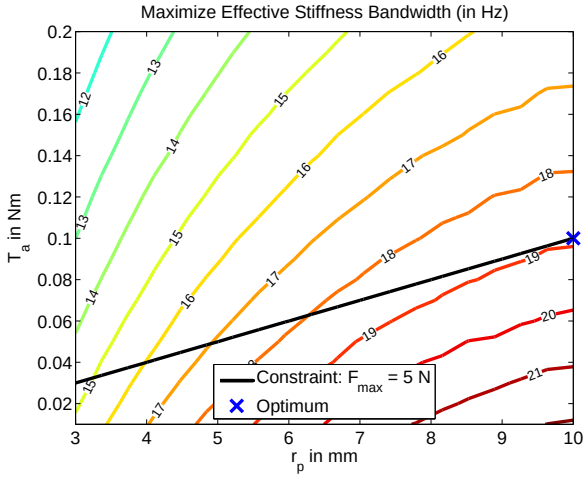

Figure 5.12: The second optimization problem visualized. The solid black line denotes the inequality constraint which divides the design space in the feasible and the infeasible domain. The legend is placed in the infeasible domain. This results in an optimum marked with the blue cross.

5.4. Discussion

This chapter was showed the possibilities of the model from the chapters before, using the Gemini haptic paddle as a case study. As a first step, the maximum stable stiffness of this device is predicted from its properties, and compared to measurements. The method for predicting the maximum stiffness is sufficient reliable, which is an important result towards optimization in haptic design.

The next step in this chapter, is to explore the design space of this haptic paddle, as a function of actuator choice and transmission ratio. It is shown that even small variations in one of the two design variables can lead to large variations in closed-loop haptic performance. The paddle seems more

sensitive to changes in the transmission ratio than to variation in the choice of actuator. In addition, the performance metrics are often conflicting. Especially a large effective stiffness bandwidth comes at the price of lower force, stiffness and Z-Width.

Furthermore, optimization of a design to desired haptic performance is demonstrated. Using two different examples, it is shown that different requirements can lead to complete different haptic paddle configurations. Therefore, potential impact of component level choices are demonstrated and the necessity and effectiveness of this method are proven.

Finally, this method obviously has its limitations:

- Actuator and amplifier saturation are not taken into account. A maximum stable achievable stiffness does not necessarily mean that an actuator will be able to deliver the force/torque that is needed.
- The mechanics are assumed to be stiff enough, to be able to neglect structural deformations.
- In both teleoperation examples for optimization to haptic performance, the slave dynamics are not taken into account.
- The change in transmission ratio is done by changing a single dimension. It might be more efficient to change multiple dimensions in the same time, to keep designs practically realizable.

6

Conclusions and Recommendations

6.1. Overall Conclusions

In this thesis a method is developed that relates component level choices to the main performance criteria in impedance-type haptic devices. This allows direct design trade-offs, enabling the designer to optimize for desired closed-loop haptic performance. This is done in three steps:

1. Determine the Key Parameters of Interest (KPI's).

   The quantification of closed-loop haptic performance.

2. Determine how the KPI's are affected by physical properties.

   Physical properties are the moving mass m, physical damping b, viscous friction c, time delay t_d, the quantization interval of the sensor Δ, and the properties of the velocity filter: cut-off frequency ω_c and order n.

3. Determine how the physical parameters are affected by component level choices.

   In this thesis, the choice of actuator and transmission ratio are the component level choices that are worked out extensively.

The first step: Closed-loop haptic performance is related to the device's capability to generate an impedance. When a free environment is simulated, it is desired to feel free. So the *free space impedance* (the impedance of the device itself) has to be low. On the other hand, when hard contact is simulated, the rendered impedance is desired to be as high as stably possible. In addition, the feedback force should be accurate. Those demands are quantified by the following Key Performance Indicators:

- The maximum stable stiffness of a haptic device. Limited by phase-lag due to actuator and amplifier time delay on one hand, and by energy generation of the quantization-error on the other hand.
- Z-Width: the stable range of achievable impedances. Limited by free space impedance as minimum and by the maximum stable impedance as maximum.
- Effective Stiffness Bandwidth: the upper limit of the useful frequency range. At lower frequencies, the resemblance between the desired and rendered impedance is good. At higher frequencies on the other hand, the device dynamics dominate.

The second step is to determine the influence of the physical properties on the key performance indicators. A clear relationship between the system parameters of a haptic device (mass, damping, friction, quantization interval and time delay) and the maximum stable stiffness is given in this report. Is is shown that the maximum achievable stiffness has two limiting factors: The first one is the sampled-data stability boundary, which is enlarged by a shorter time delay, a larger mass, and the filter-cut off frequency. The second limiting factor is the quantization error stability boundary, which is positively

affected by friction and smaller quantization interval. On the other hand, the free space impedance, is positively affected by a lower mass, damping and friction. This values diminish the upper stability boundary. The Z-Width is bounded by the free space impedance on one side, and by the maximum stable impedance on the other side. Therefore, for maximizing the Z-Width, the stable range of impedances, a trade-off is always needed. The same holds for the useful frequency range, bounded by the effective stiffness bandwidth, which is increased by the maximum stable stiffness, and decreased by the device's moving mass.

An important contradiction is discovered when comparing the above listed results with guidelines from literature. Conventional design guidelines for haptic device design are low moving mass, low damping and low friction[3, 30, 35, 36]. However, that proves to be not completely correct. Low moving mass, low damping and low friction are indeed beneficial for a low free space impedance, but are reducing the upper limit of the stable region. A mass-less device with no damping, as stated by many authors as the ideal design for force reproducibility, would be unstable[45].

Only two physical parameters are improving all haptic performance indicators: a lower time delay t_d and a smaller quantization interval Δ. All other parameters introduce trade-offs with regard to the capabilities of a haptic device (maximum stable stiffness and Z-Width) and the quality of the feedback force (Effective Stiffness Bandwidth). So choosing the fastest actuator and amplifier (minimize time delay) or the sensor with the finest resolution (smallest Δ), might suggest that such design achieves the best performance. However, this is not always feasible. Other properties could be limiting performance, or choosing the fastest motor might affect other properties and thereby diminish performance.

This method will give clear answers for the difficult interrelated problems. The method for testing stability is significantly improved. The computational time is reduced 50 times as compared to state-of-the-art methods by using Routh-Hurwitz stability criterion. This allows to easily compute these effects quantitatively.

The third step is to relate component level choices to changes in physical properties, and thereby to closed-loop haptic performance. It is shown that component level choices often come with interrelated physical properties: most component level choices affect multiple physical properties. Two component level choices are explicitly calculated in this thesis: the choice of actuator and the transmission ratio. It is demonstrated that both design choices not only determine the force capabilities of a haptic device, but have a significant effect on closed-loop haptic performance too.

It is shown that in a set of common DC-motors, there is a clear correlation between motor torque, motor inertia and time delay. Therefore, the choice of actuator affects the maximum end-effector force, the moving mass and the time delay. Those three physical properties have their effect on the closed-loop haptic performance.

Using a transmission the motor torque is amplified by the transmission ratio to the end-effector force. Since the motor and sensor are often co-located in haptic design, a higher transmission ratio decreases the quantization interval of the sensor. In addition, the moving mass of the haptic device is affected. All rotational inertia on the motor-axis contributes to the total mass, while multiplied with the transmission ratio squared.

Since the transmission ratio and actuator each affect three physical properties, their influence on closed-loop haptic performance is significant. This is demonstrated in this thesis by a case study.

6.2. Concussions Regarding Case Study

The Gemini[24] is developed at the Delft Haptics Lab as a 1-DoF haptic paddle, and is subject to the case study in this thesis. As a first and important step, the stable range of impedances is calculated. The stability boundary was calculated without physically testing the device. The properties where obtained with the use of data-sheets and CAD-software. The prediction of the stability boundary was good. The measured values were within 20% of the estimated stability boundary.

The two component level choices were implemented as two design variables: the motor torque and the lower radius in the transmission. Choosing a stronger motor (higher motor torque) represents a larger end-effector force, a longer time delay and a larger inertia. A larger transmission ratio (smaller radius) leads to a larger end-effector force, a smaller quantization interval and a larger mass.

Both design variables are varied around the original values of the Gemini to illustrate the effect of component level choices on haptic performance. Here, the following conclusions hold:

- Both actuator and transmission ratio have a significant effect on all performance indicators.
- The effect of the transmission ratio on maximum stable stiffness and Z-Width is larger than the effect of the actuator. The best performance is reached at a low transmission ratio, in combination with a small actuator.
- The Effective Stiffness Bandwidth, the upper limit of the useful frequency range, is highest for a small actuator and a small transmission ratio. This optimum is thus not coinciding with the optimum of the other performance indicators.
- The maximum end-effector force is not coinciding with the maximum stable stiffness.

As a final illustration, two example optimization problems demonstrate how this model can be used in combination with optimization techniques. The optimal component level choices can be found for desired closed-loop haptic performance. Here the effect of component level choices is visible, relatively small modifications on component level, can cause a significant change in closed-loop haptic performance.

In general, there are some important conclusions to draw from the case study:

- Both design variables depicted in this study, representing variation in actuator and transmission ratio, are affecting the closed-loop haptic performance. This effect is easily quantified with the methods presented in this thesis.
- When an impedance is stably achievable, it does not necessarily mean that this is achievable by the haptic device. Actuator- and power-amplifier-saturation can cause the force rendering capability to be a subset of the stable renderable regime.
- The two optimization problems demonstrate the effectiveness of this method to design for closed-loop haptic performance.

6.3. Recommendations for Further Research

One of the thing that keeps coming back in every step in this thesis, are the conflicting interests of physical properties or component level choices. Therefore, a logical step seems compensation of one of the diminishing effects. In this way a certain property can be used when needed, and compensated when it is diminishing performance.

For example, this study has shown that a higher mass is improving the maximum stable stiffness. On the other hand, it is diminishing the free space impedance and the useful frequency range. The same holds, to a lower extend, to the physical damping. It holds that damping has a stabilizing effect on the system, however it has been found to have a negative effect on an operator's opinion of the controllability of the system[29].

Therefore, compensation of inertia and damping in free space tasks will improve the Z-Width. However, to compensate dynamics the controller should know the inputs on the device, so a force sensor is needed. This would make the system more complicated, and more expensive. In addition, the complete control strategy will change to admittance-type controllers. It would be an interesting step to develop a similar method for this admittance-type devices.

Instead of compensating dynamics, physically reducing dynamics might therefore be a more convenient choice. This could for example be done by clutching mechanism, which is able to decouple heavy actuator in free space tasks. The clutched actuator developed by Plooij et al.[46] might be an interesting choice.

In addition, the same holds for the friction. In rendering the highest possible stiffness, friction proves to be indispensable. Hybrid designs seems to be a very interesting option for further research, with low friction in free space and some kind of braking mechanism that is increasing friction when rendering

harder virtual environments. An interesting choice might be the statically balanced braking mechanism developed for robotic application by Plooij et al.[47], which could generate a very large braking force in comparison with regular brakes.

The method in this thesis can be improved in multiple ways. For example, the maximum stable stiffness (and thereby the other performance indicators) is very sensitive to friction. Unfortunately, the estimation of the friction is not the most reliable part in this thesis. A better calculation of the friction will improve the method. Another example is the low-frequency approximation for the time delay in the transfer function. This approximation could be improved by taking higher orders of the Taylor series expansion of $e^{-t_d s}$ into account.

Another interesting thing to look at might be to incorporate different sensing techniques. The frequency filter and the position quantization are affecting the stable range of a haptic device. An alternative might be to incorporate direct velocity sensing, such that a more reliable velocity signal is obtained.

The case study has shown that a larger transmission ratio seems to be beneficial for rendering the maximum stable stiffness of the Gemini haptic paddle. Unfortunately, the transmission ratio was limited by the capstan drive mechanism. Therefore, other kinds of transmission systems might be an interesting choice or haptics, especially multistage transmissions to enlarge the applicable transmission ratio.

One of the motivations to study the effect of component level choices in the first place, was to economize haptic design. It might be very interesting to use this method to obtain certain "performance-to-cost" considerations.

In addition, task performance in haptic systems does not only depend on device performance. Human factors play an important role too. As an example, the study of Wildenbeest et. al.[23] was given, where one of the conclusions was that the high frequency content of the haptic feedback was barely improving task performance. There are numerous studies done on human factors. Therefore, combining those studies with the method of presented in this thesis to design for certain performance, could give more useable designs.

Appendices

A

Calculations and Numerical Methods

This appendix will discuss all calculations that are performed and that are not explicitly explained in the main part of this thesis.

A.1. The Characteristic Equation

The Loopgain of the haptic display was defined in (3.7) and given as follows:

$$L(s) = G(s)\, H_{VE}(s)\, D(s) \tag{A.1}$$

From equation (A.1), the characteristic equation is then as follows:

$$L(s) + 1 = 0 \tag{A.2}$$
$$G(s)\, H_{VE}(s)\, D(s) + 1 = 0 \tag{A.3}$$

For clarity, the ingredients of equation (A.3), equations (3.1)-(3.6), are repeated here:

$$G(s) = \frac{1}{ms^2 + bs} \tag{A.4}$$
$$H_{VE}(s) = K + B\ s\ H_f(s) \tag{A.5}$$
$$H_f(s) = \left(\frac{\omega_c}{s + \omega_c}\right)^n \tag{A.6}$$
$$D(s) \approx \frac{1}{1 + t_d s} \tag{A.7}$$

Combining the four equations with the general characteristic equation from (A.3) leads to the following characteristic equation:

$$\frac{K(s + \omega_c)^n + Bs\omega_c^n}{(ms^2 + bs)(s + \omega_c)^n (1 + t_d s)} + 1 = 0 \tag{A.8}$$

The order of the velocity filter is chosen to be minimal $n = 1$ and maximal $n = 4$ in equation (A.6), similar to literature[16]. This leads to minimal a fourth order characteristic equation, and maximal to a seventh order characteristic equation.

For sampled-data stability, the stability of the closed-loop transfer function should be evaluated. Therefore, the roots of equation (A.8) should be in the Left-Half-Plane, representing the location of the closed-loop poles. However, finding the roots of a seventh order characteristic equation can be

numerically very intensive. And in this case, it is not needed to know the exact location of the closed-loop poles, we are only interested in the binary question: Is the transfer function stable or not?

Therefore, the stability will be evaluated using Routh-Hurwitz Stability Criterion. It will not give any information on the exact pole location, but is a very cheap computational method to evaluate stability of a linear system with real coefficients[48].

The first step needed to apply Routh-Hurwitz stability criterion is to put the characteristic equation in its standard form. For a m^{th} order transfer function, the standard form is as follows:

$$\sum_{i=1}^{m} a_i s^i = a_m s^m + a_{m-1} s^{m-1} + \cdots + a_1 s + a_0 = 0 \tag{A.9}$$

For a higher order velocity filter, this involves the evaluation of a lot of terms, and therefore consists of a large risque of making mistakes. It consists of some simple and straightforward steps, and therefore it is easily implemented in Matlab's Symbolic Toolbox.

The steps are as follows:

1. Substitute the three terms in the loopgain of equation (A.1).
2. To get rid of fraction in the characteristic equation, a trick is applied: we recognize that $\frac{N}{D}+1=0$ is equivalent to $N+D=0$. Therefore, the second step is to split the numerator and denominator and add them.
3. Finally, expand all terms and collect the coefficients of s.

The following 12 lines of Matlab code extract the coefficients of the characteristic polynomial to put it in the standard form of equation (A.9). Here it is done for $n = 2$, but it works the same for other orders of the felocity filter. Term a in the last line returns a vector that contains the symbolic coefficients of s in the standard characteristic equation.

```
syms m b omeg t K B positive
syms s
n = 2;
P = 1/(m*s^2 + b*s); %Plant
VelFilt = omeg/(s+omeg); %Velocity Filter
H = K + B*s*VelFilt^n; %Virtual Environment
D = 1/(1+t*s); %Time delay

[N,D] = numden(P*H*D); %Extract nummerator and denominator

ChEq = expand(N + D); %1+L = 0 --> N + D = 0!
a = coeffs(ChEq,s); %Extract a_0, ..., a_n
```

This gives the following characteristic equations in standard form. A first order velocity filter results in a fourth order characteristic equation with the following coefficients:

$$\begin{aligned} a_4 &= m t_d \\ a_3 &= m + m\omega_c t_d + b t_d \\ a_2 &= m\omega_c + b + b\omega_c t_d \\ a_1 &= b\omega_c + K + B\omega_c \\ a_0 &= K\omega_c \end{aligned} \tag{A.10}$$

A second order velocity filter results in a fifth order characteristic equation. The coefficients of s are as follows:

$$\begin{aligned} a_5 &= m t_d \\ a_4 &= m + b\, t_d + 2\, m\, \omega_c\, t_d \\ a_3 &= b + 2\, m\, \omega_c + m\, {\omega_c}^2\, t_d + 2\, b\, \omega_c\, t_d \\ a_2 &= K + 2\, b\, \omega_c + m\, {\omega_c}^2 + b\, {\omega_c}^2\, t_d \\ a_1 &= 2\, K\, \omega_c + B\, {\omega_c}^2 + b\, {\omega_c}^2 \\ a_0 &= K\, {\omega_c}^2 \end{aligned} \tag{A.11}$$

A third order velocity filter results in a sixth order characteristic equation. The coefficients of s are as follows:

$$\begin{aligned}
a_6 &= m t_d \\
a_5 &= m + b\,t_d + 3\,m\,\omega_c\,t_d \\
a_4 &= b + 3\,m\,\omega_c + 3\,m\,{\omega_c}^2\,t_d + 3\,b\,\omega_c\,t_d \\
a_3 &= K + 3\,b\,\omega_c + 3\,m\,{\omega_c}^2 + 3\,b\,{\omega_c}^2\,t_d + m\,{\omega_c}^3\,t_d \\
a_2 &= 3\,K\,\omega_c + 3\,b\,{\omega_c}^2 + m\,{\omega_c}^3 + b\,{\omega_c}^3\,t_d \\
a_1 &= B\,{\omega_c}^3 + 3\,K\,{\omega_c}^2 + b\,{\omega_c}^3 \\
a_0 &= K\,{\omega_c}^3
\end{aligned} \tag{A.12}$$

And finally, fourth order velocity filter results in a seventh order characteristic equation. The coefficients of s are as follows:

$$\begin{aligned}
a_7 &= m t_d \\
a_6 &= m + b\,t_d + 4\,m\,\omega_c\,t_d \\
a_5 &= b + 4\,m\,\omega_c + 6\,m\,{\omega_c}^2\,t_d + 4\,b\,\omega_c\,t_d \\
a_4 &= K + 4\,b\,\omega_c + 6\,m\,{\omega_c}^2 + 6\,b\,{\omega_c}^2\,t_d + 4\,m\,{\omega_c}^3\,t_d \\
a_3 &= 4\,K\,\omega_c + 6\,b\,{\omega_c}^2 + 4\,m\,{\omega_c}^3 + 4\,b\,{\omega_c}^3\,t_d + m\,{\omega_c}^4\,t_d \\
a_2 &= 6\,K\,{\omega_c}^2 + 4\,b\,{\omega_c}^3 + m\,{\omega_c}^4 + b\,{\omega_c}^4\,t_d \\
a_1 &= B\,{\omega_c}^4 + 4\,K\,{\omega_c}^3 + b\,{\omega_c}^4 \\
a_0 &= K\,{\omega_c}^4
\end{aligned} \tag{A.13}$$

A.2. The Routh-Array

Now the characteristic equations are in the standard form, they can be substituted into a Routh-array. For a m^{th}-order polynomial as in (A.9), the Routh-Array has $m+1$ rows:

$$\begin{array}{llll}
a_m & a_{m-2} & a_{m-4} & \cdots \\
a_{m-1} & a_{m-3} & a_{m-5} & \cdots \\
b_1 & b_2 & b_3 & \cdots \\
c_1 & c_2 & c_3 & \cdots \\
\vdots & \vdots & \vdots & \ddots
\end{array} \tag{A.14}$$

The first two rows are filled with the coefficients of the characteristic equation. Both rows should be equal in length. If necessary, the last terms are zero. Every new entry in the following row consists of the determinant of the first terms of the two rows directly above and the two rows right from the new entry, divided by the first term of the row above, multiplied with minus one. Or mathematically, the terms entries of the third row, b_k, are composed as follows:

$$b_k = -\frac{\det \begin{vmatrix} a_m & a_{m-2k} \\ a_{m-1} & a_{m-2k-1} \end{vmatrix}}{a_{m-1}} \tag{A.15}$$

And for the fourth row, every new entry is calculated as follows:

$$c_k = -\frac{\det \begin{vmatrix} a_{m-1} & a_{m-2k-1} \\ b_1 & b_{k+1} \end{vmatrix}}{b_k} \tag{A.16}$$

And so on...
For a fourth order characteristic equation, the third row calculated as follows:

$$b_1 = -\frac{a_4 a_1 - a_2 a_3}{a_3} \quad \text{and} \quad b_2 = \frac{a_0 a_3}{a_3} \tag{A.17}$$

The fourth and fith row both contain one non-zero term:

$$c_1 = -\frac{a_3 b_2 - a_1 b_1}{b_1} \quad \text{and} \quad d_1 = \frac{b2c1}{c_1} \tag{A.18}$$

Therefore, the complete Routh-Array is as follows for a fourth order characteristic equation:

$$\begin{array}{lll} a_4 & a_2 & a_0 \\ a_3 & a_1 & 0 \\ -\frac{a_4 a_1 - a_2 a_3}{a_3} & \frac{a_0 a_3}{a_3} & 0 \\ -\frac{a_3 b_2 - a_1 b_1}{b_1} & 0 & 0 \\ \frac{b2c1}{c_1} & 0 & 0 \end{array} \tag{A.19}$$

The Routh-Hurwitz stability criterion is as follows: *The number of sign changes in the first column of the Routh array equals the number of roots of the polynomial in the Closed Right Half-Plane (CRHP)*

Therefore, since a_4 obviously is positive, all values in the the first column of (A.19) need to be positive. Working this out, this leads to three inequality constraints:

$$a_i > 0 \quad \text{for} \quad i = 0, 1, 2, 3, 4 \tag{A.20}$$

$$a_3 a_2 > a_4 a_1 \tag{A.21}$$

$$a_3 a_2 a_1 > a_4 a_1^2 + a_3^2 a_0 \tag{A.22}$$

Since all coefficients a_i in (A.9) are built up from summations of strictly positive physical values, the first inequality constraint (A.20) is always satisfied. The other two inequality constraints give the *necessary and sufficient* rules for stability of a haptic display:

$$(b + m\,\omega_c + b\,\omega_c\,t_d)\,(m + b\,t_d + m\,\omega_c\,t_d) - m\,t_d\,(K + B\,\omega_c + b\,\omega_c) > 0 \tag{A.23}$$

And:

$$(b + m\,\omega_c + b\,\omega_c\,t_d)\,(m + b\,t_d + m\,\omega_c\,t_d)\,(K + B\,\omega_c + b\,\omega_c) - m\,t_d\,(K + B\,\omega_c + b\,\omega_c)^2 \cdots - K\,\omega_c\,(m + b\,t_d + m\,\omega_c\,t_d)^2 > 0 \tag{A.24}$$

Although the two criteria from inequalities (A.23) and (A.23) look complicated, they consist of simple and low-level mathematics. Therefore, solving the two criteria is very cheap.

For higher order velocity filters, there will be more stability conditions and they will look more complicated. However, all stability criteria keep numerically very efficient. They all reduce the numerically intensive root-finding to simple multiplications, divisions, additions and subtractions.

Again, the Matlab Symbolic Toolbox is used complete a Routh-Array. The following lines of code complete the Routh Array for a seventh order in two steps:

1. The first two rows are filled with the coefficients a_i from the standard-form characteristic equations: the highest order in the upper left, on order lower under that item, and every additional term in the row is two orders lower.

2. Every next item in the rows below is calculated using the equations (A.15) and (A.16). This is done until the Routh Array has $m + 1$ rows.

```
syms a0 a1 a2 a3 a4 a5 a6 a7
RH = [a7 a5 a3 a1 0
    a6 a4 a2 a0 0];

%Insert next row: (n = 7, so 8 rows)
for h = 3:8; %rows
    for i = 1:4; %columns
        RH(h,i) = simplify((RH(h-1,1)*RH(h-2,i+1) - ...
                  RH(h-2,1)*RH(h-1,i+1))/RH(h-1,1));
    end
end
```

A.3. Line-Search Algorithm for Maximum Stiffness

The maximum stable renderable stiffness limited by sampled-data is discussed in section 3.3.1. In the previous section the mathematical criteria for the maximum stable stiffness are discussed and derived, using Routh-Hurwitz. It is shown that the evaluation of stability simply reduces to solving two or more inequalities, which are easy to solve in Matlab.
Calculating the inequalities from above is already a enormous improvement in computer time as compared to finding the roots of the characteristic equation. And instead of brute-forcing B and K (the initial strategy), an optimization algorithm is written. The flow diagram of the line-search algorithm is given in figure A.1. The strategy is simple. All parameters (m, b, ω_c, t_d, B) are fixed except for the virtual stiffness K.
The starting point for the virtual stiffness is always zero. Then the stability of K is evaluated. When this stiffness results in a stable closed-loop system (using the Routh-Hurwitz stability criterion as explained in section A.2), the stability of the next K is calculated, which is the previous K plus an additional step. When this value is unstable, the step is apparently too large and the same is tried with a smaller step. When the stepsize is smaller than a predefined tolerance, the maximum stable stiffness is determined within that tolerance.

All computations are performed in Matlab. Throughout this thesis, an initial stepsize `Kstep` is chosen to be $500\,\mathrm{N\,m^{-1}}$, and the tollerance `Tol` is set to $1\,\mathrm{N\,m^{-1}}$, which proved to give accurate results in a sufficient time.

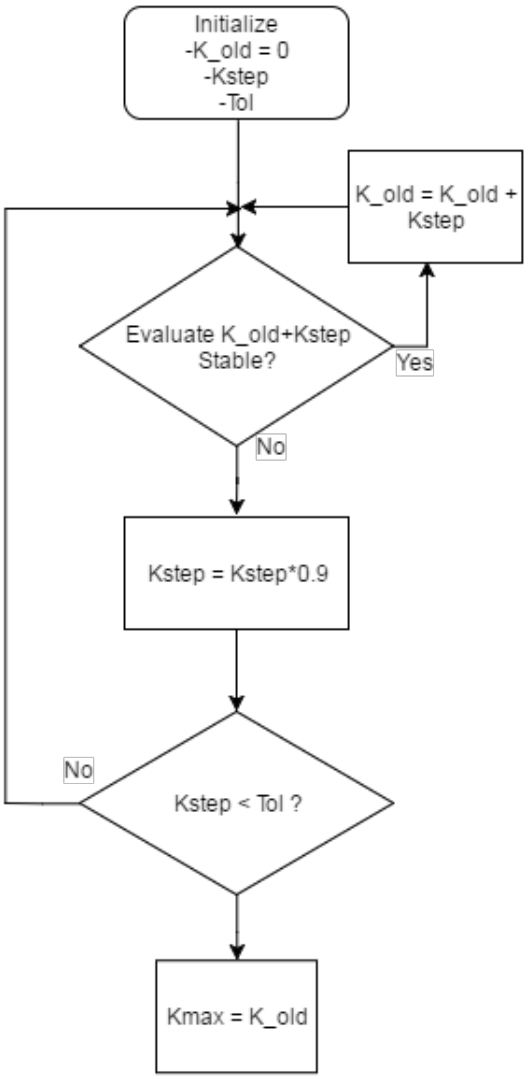

Figure A.1: Flow diagram of the optimization algorithm to find the maximum renderable stiffness.

A.4. The Gain-Margin Method

Instead of using Routh-Hurwitz stability criterion, multiple other control techniques were used to calculate stability. This could be seen in table 3.2. The only other method capable of evaluating stability of haptic devices *including* a velocity filter, is the gain-margin method, as introduced by Hulin[34] and used by Colonnese[16] among others.

It used the discrete time representation of a haptic master, using the bilinear transformation. Notation $G_d(z)$ is used for the discrete Zero-order-hold (ZOH) equivalent of the standard mass-damper.

$$G_d(z) = \mathrm{ZOH}\left(\frac{1}{ms^2 + b}\right) \tag{A.25}$$

The discrete derivative is calculated as follows:

$$D(z) = \frac{z-1}{Tz} \tag{A.26}$$

In addition, the velocity filter with a cut-off frequency ω_0 and order n is given in equation (A.27):

$$H_f(z) = \left(\frac{\left(1 - e^{-\omega_0 T}\right) z}{z - e^{-\omega_0 T}} \right)^n \tag{A.27}$$

The total time delay is considered a multiplicity k of the sample time, such that the time delay is as follows:

$$t_d = kT \quad \text{with} \quad k \in \mathbb{N} \tag{A.28}$$

Using this, the time delay is modeled as follows:

$$z^{-k} = \frac{1}{z^k} \tag{A.29}$$

The virtual environment is then given as follows:

$$H_{VE}(z) = \left[K + BD(z) H_f(z)\right] \frac{1}{z^k} \tag{A.30}$$

Based on the open-loop frequency response of a certain Loopgain $L(z)$ and a gain $K > 1$, the stability condition is as follows: the gain must be lower than 1 in the unstable region[49]. Or mathematically:

$$|KL(z)| < 1 \quad \text{at} \quad \angle L(z) = -180^\circ \tag{A.31}$$

The Gain Margin (GM) is the smallest amount by which the open loop gain can be raised before instability occurs in the closed loop system, so it is the gain at the frequency where the loop-gain crosses the -180°-line. Therefore, the stability criterion is as follows:

$$\mathrm{GM}\left[L(z)\right] > 1 \tag{A.32}$$

The loop-gain of a haptic device can be rewritten to use the gain-margin to calculate the maximum stable stiffness by sampled-data. The loop-gain is again simply the multiplication of all terms in the loop, in this case the haptic device from equation (A.25) and the virtual environment from (A.30):

$$L(z) = G_d(z) H_{VE} \tag{A.33}$$

Again, the characteristic equation is the loop-gain plus one, and therefore this can be rewritten as follows:

$$L(z) + 1 = 0 \tag{A.34}$$
$$G_d(z) H_{VE}(z) + 1 = 0 \tag{A.35}$$
$$G_d(z) K z^{-k} + G_d(z) BD(z) H_f(z) z^{-k} + 1 = 0 \tag{A.36}$$

This last equation (A.36) can be rewritten to obtain a kind of modified loopgain $L^*(z)$:

$$L^*(z) + 1 = 0 \tag{A.37}$$
$$\frac{KG_d(z) z^{-k}}{BD(z) H_f(z) z^{-k}} + 1 = 0 \tag{A.38}$$

And using the modified loop-gain, the maximum stable stiffness can be calculated as follows:

$$K_{max} = \mathrm{GM}\left(\frac{G(z) z^{-k}}{1 + G(z) z^{-k} BD(z) H(z)} \right) \tag{A.39}$$

A.5. Comparing the Two Methods: Routh-Hurwitz vs Gain-Margin

There are two methods to obtain the maximum stable stiffness:

- The gain-margin method from equation (A.39).
- The line-search algorithm based on Routh-Hurwitz stability criterion as explained in section A.3

Table A.1 shows the enormous improvement in computational effort that is achieved by implementing Routh-Hurwitz Stability Criterion. Using Routh-Hurwitz stability criterion lead to an improvement of 50 times in computational effort, with a better accuracy.

Table A.1: Two calculation methods compared. Giant leap in computational efficiency. These values are calculated on a computer with a dual core 2.8GHz processor, using Matlab 2014a 64bit.

	Steps in:				Computational time	
Method	**B**	ω_c	**n**	**Total steps**	**Total (s)**	**Per step (ms)**
Gain-margin	20	10	4	800	56.7	70.8
Routh-Hurwitz	100	20	4	8000	10.9	1.3

Using the Routh-Hurwitz stability criterion for calculating the stability boundary, might not be the most straightforward way, since it involves a lot of initial calculations to obtain the full table. However, once that has been done, this method has three major advantages over the other methods in table 3.2:

1. The Routh-Hurwitz stability criterion is a computational very efficient method.
2. In contrast with the other methods, the Routh-Hurwitz stability criterion allows electrodynamic time delays that are not necessarily multiples of the sample time.
3. The gain-margin method tends to give numerical errors, since higher order discrete transfer functions often have multiple $-180°$-crossings. This sometimes led to unreliable results.

A.6. Calculation of Z-Width

The Z-width is introduced in section 3.4 of this thesis, and calculated using equation (3.26), repeated here:

$$\mathbb{Z}_w = \frac{1}{\omega_1 - \omega_0} \int_{\omega_0}^{\omega_1} \left| \log_{10} \left[Z_{max} \left(\omega \right) \right] - \left[Z_{FS} \left(\omega \right) \right] \right| \mathrm{d}\omega \tag{A.40}$$

In other to approximate the value in (A.40) numerically in the computer, it is calculated with a trapezoid Riemann approximation:

$$\mathbb{Z}_w \approx \frac{1}{\omega_1 - \omega_0} \lim_{n \to \infty} \sum_{i=1}^{n-1} \frac{f\left(x_i\right) + f\left(x_{i+1}\right)}{2} \left(x_{i+1} - x_i \right) \tag{A.41}$$

With:

$$f\left(x_i\right) = \left| \log_{10} \left[Z_{max} \left(\omega_i \right) \right] - \left[Z_{FS} \left(\omega_i \right) \right] \right| \tag{A.42}$$

In practice, the value of $n = 1000$ proves to be sufficient large to give an accurate result, and small enough to be numerical efficient. As lower frequency 10^{-1} Hz is chosen, $\omega_0 = 2\pi \times 10^{-1}\,\mathrm{rad\,s^{-1}}$. The upper frequency is the point where the free space impedance and the rendered impedance cross, the effective stiffness bandwidth: $\omega_1 = \omega_{ES} = \sqrt{\frac{K}{m}}$.

B

List of Maxon and Faulhaber Actuators

All the motors used in this research are from two manufacturers of high-performance motors DC-motors, usually used in Haptic Devices. The data from the Maxon motors is retrieved from their digital database on the website[1]. The data of the motors made by Faulhaber are also retrieved from their website[2].

All motors are displayed in figure B.1. At the x-axis, the nominal torque is given, as a measure for the maximum continuous torque. The blue crosses are given with respect to the left y-axis, and represent the time delay. The green circles are given with respect to the right y-axis and represent the rotational inertia. The solid blue line is a linear trend in the torque vs time delay, and the dashed green line is a linear trend of torque vs inertia.

All actuators are sorted on nominal torque and listed in tables B.1, B.2 and B.3.

Quantitatively, two relations can be found. Least-square function fitting helps to put numbers to the relations. Symbol T_a denotes the actuator torque (the nominal torque of the actuator, as a measure for the maximum continuous torque), t_d is the time delay and I_a is the inertia of the actuator, all in SI-units. Then the relations, found by linear a least-squares estimation as in figure B.1, are as follows:

$$\begin{aligned} t_d &= a_1 \cdot T_a + a_2 \\ &\text{with:} \quad a_1 = 6.76 \times 10^{-3}\,\mathrm{s\,N^{-1}\,m^{-1}} \\ &\text{and:} \quad a_2 = 5.35 \times 10^{-4}\,\mathrm{s} \end{aligned} \tag{B.1}$$

and:

$$\begin{aligned} I_a &= a_3 \cdot T_a \\ &\text{with:} \quad a_2 = 7.07 \times 10^{-5}\,\mathrm{kg\,m\,N^{-1}} \end{aligned} \tag{B.2}$$

When $\rho(a_1, a_2)$ denotes the Pearson correlation between the variables a_1 and a_2, we show the following correlation between the motor parameters are all high, arround 80%:

$$\begin{aligned} \rho(T_a, t_a) &= 0.79 \\ \rho(T_a, I_a) &= 0.86 \\ \rho(t_a, I_a) &= 0.80 \end{aligned} \tag{B.3}$$

[1] http://www.maxonmotor.com/maxon/view/content/products, [50] checked in December 2015
[2] https://fmcc.faulhaber.com/category/PGR_13801_13601/en/GLOBAL/,[51] checked in December 2015

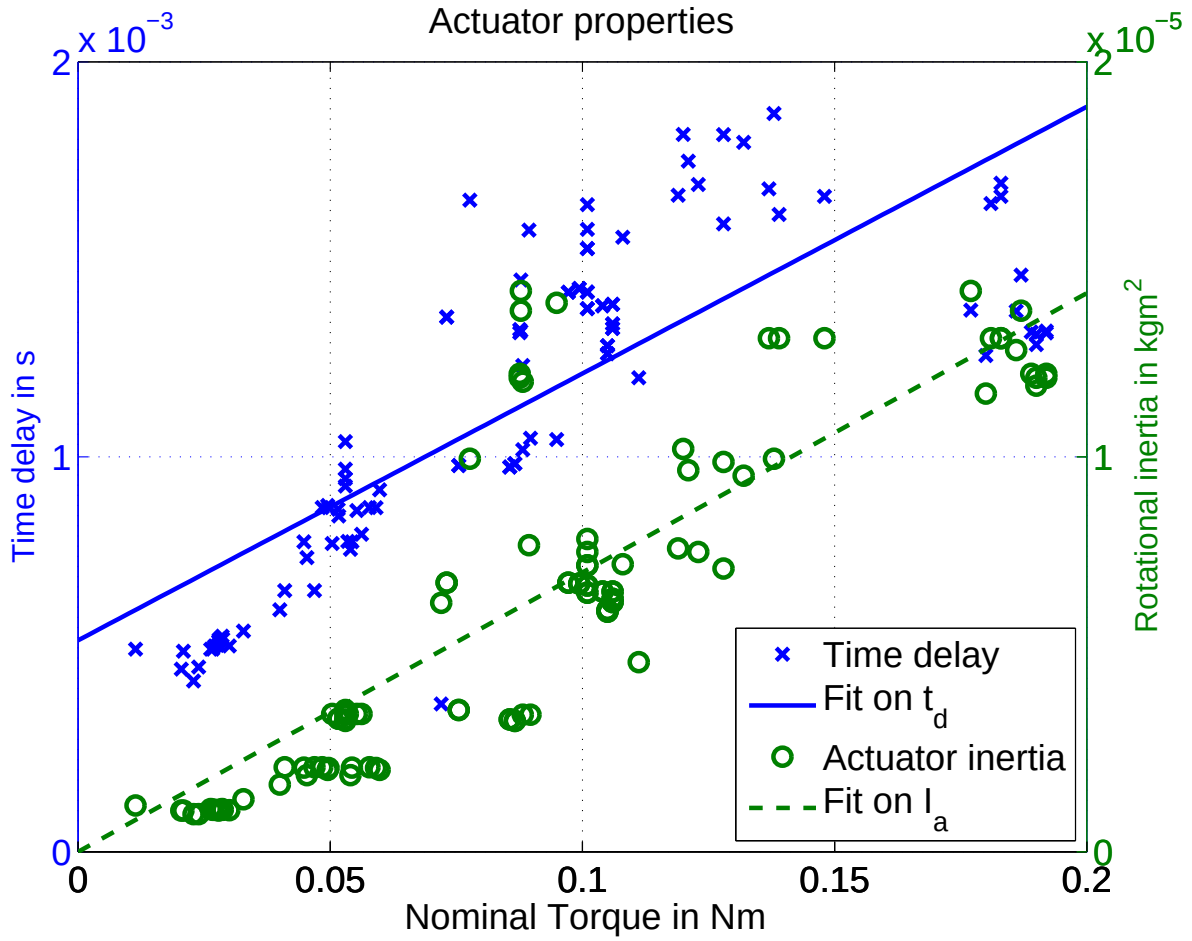

Figure B.1: All the actuators considered in this research. All low-power DC-motors. At the x-axis, the nominal torque is given, as a measure for the maximum continuous torque. The blue crosses are given with respect to the left y-axis, and represent the time delay. The green circles are given with respect to the right y-axis and represent the rotational inertia. The solid blue line is a linear trend in the torque vs time delay, and the dashed green line is a linear trend of torque vs inertia.

Table B.1: List of considered actuators and their properties, part 1 of 3. The first 15 actuators, sorted on torque.

no.	Manufacturer	Type	Torque in mN m	Inertia in gcm^2	Time delay in ms
1	Maxon RE25	118740	11.4	11.7	0.51
2	Maxon RE25	118750	20.5	10.4	0.46
3	Maxon RE25	118741	20.9	10.4	0.51
4	Maxon RE25	118751	22.9	9.5	0.43
5	Maxon RE25	118742	23.9	9.5	0.47
6	Maxon RE25	118752	26.3	10.8	0.51
7	Maxon RE25	118753	26.7	10.6	0.51
8	Maxon RE25	118754	27.1	10.6	0.52
9	Maxon RE25	302001	27.7	10.5	0.52
10	Maxon RE25	118747	27.9	10.5	0.53
11	Maxon RE25	118748	27.9	10.5	0.53
12	Maxon RE25	118746	28.0	10.5	0.54
13	Maxon RE25	118744	28.2	10.6	0.54
14	Maxon RE25	118743	28.6	10.8	0.55
15	Maxon RE25	118745	28.7	10.6	0.54

Table B.2: List of considered actuators and their properties, part 2 of 3. Actuators 16 upto 62, sorted on torque.

no.	Manufacturer	Type	Torque in mN m	Inertia in gcm^2	Time delay in ms
16	Maxon RE25	118757	30.0	10.5	0.52
17	Maxon RE25	339158	32.8	13.3	0.56
18	Maxon DCX26	12 V	41.0	21.4	0.66
19	Maxon DCX26	18 V	44.8	21.3	0.78
20	Maxon DCX26	36 V	45.4	19.4	0.74
21	Maxon DCX26	12 V	46.9	21.4	0.66
22	Maxon DCX26	24 V	48.4	21.4	0.87
23	Maxon DCX26	60 V	49.5	20.7	0.88
24	Maxon DCX26	48 V	49.7	21.2	0.87
25	Faulhaber	3264K048B	50.4	34.9	0.78
26	Maxon RE30	310005	51.6	33.7	0.87
27	Maxon RE30	268193	51.7	33.7	0.85
28	Maxon RE30	448595	53.0	33.1	0.97
29	Maxon RE30	448596	53.0	34.7	1.04
30	Maxon RE30	448594	53.0	33.5	0.94
31	Maxon RE30	448593	53.0	35.9	0.93
32	Faulhaber	3264K036B	53.5	34.9	0.79
33	Maxon DCX26	36 V	54.0	19.4	0.77
34	Maxon DCX26	18 V	54.3	21.3	0.78
35	Faulhaber	3264K024B	55.3	34.9	0.86
36	Faulhaber	3264K012B	56.2	34.9	0.80
37	Maxon DCX26	24 V	57.8	21.4	0.87
38	Maxon DCX26	48 V	59.1	21.2	0.87
39	Maxon DCX26	60 V	59.8	20.7	0.92
40	Faulhaber	3268G024BX4	72.0	63.0	0.37
41	Maxon RE35	273752	73.1	68.1	1.35
42	Maxon RE35	285785	73.1	68.1	1.35
43	Maxon RE30	268213	75.5	35.9	0.98
44	Maxon RE30	310006	75.5	35.9	0.98
45	Maxon DCX35	12 V	77.7	99.5	1.65
46	Maxon RE30	268214	85.6	33.5	0.97
47	Maxon RE30	310007	85.6	33.5	0.97
48	Maxon RE30	268215	86.6	33.1	0.98
49	Maxon RE30	310008	86.6	33.1	0.98
50	Maxon RE40	448591	87.6	121.0	1.32
51	Maxon RE40	448592	87.6	120.0	1.31
52	Maxon RE40	448588	87.8	142.0	1.32
53	Maxon RE40	448589	87.8	137.0	1.45
54	Maxon RE40	448590	88.2	119.0	1.23
55	Maxon RE30	268216	88.2	34.7	1.02
56	Maxon DCX32	12 V	89.4	77.6	1.57
57	Maxon RE30	310009	89.7	34.7	1.05
58	Maxon RE40	148866	94.9	139.0	1.04
59	Maxon RE35	273753	97.2	68.1	1.42
60	Maxon RE35	285786	97.2	68.1	1.42
61	Maxon RE35	273755	99.4	67.9	1.43
62	Maxon RE35	285788	99.4	67.9	1.43

Table B.3: List of considered actuators and their properties, part 3 of 3. Actuators 63 upto 108, sorted on torque.

no.	Manufacturer	Type	Torque in mN m	Inertia in gcm^2	Time delay in ms
63	Maxon RE35	273754	101	72.5	1.53
64	Maxon RE35	273756	101	67.4	1.42
65	Maxon RE35	273757	101	65.6	1.38
66	Maxon RE35	285787	101	72.5	1.53
67	Maxon RE35	285790	101	65.6	1.38
68	Maxon RE35	285789	101	67.4	1.42
69	Maxon RE35	323890	101	79.2	1.64
70	Maxon RE35	323891	101	79.2	1.64
71	Maxon DCX32	18 V	101	75.9	1.58
72	Maxon RE35	273758	104	65.9	1.38
73	Maxon RE35	285791	104	65.9	1.38
74	Maxon RE35	273762	105	61.2	1.28
75	Maxon RE35	273763	105	60.8	1.26
76	Maxon RE35	285795	105	61.2	1.28
77	Maxon RE35	285796	105	60.8	1.26
78	Maxon RE35	273759	106	65.9	1.39
79	Maxon RE35	273760	106	64.0	1.34
80	Maxon RE35	273761	106	63.2	1.33
81	Maxon RE35	285792	106	65.9	1.39
82	Maxon RE35	285793	106	64.0	1.34
83	Maxon RE35	285794	106	63.2	1.33
84	Maxon DCX32	24 V	108	72.8	1.56
85	Faulhaber	3274G024BP4	111	48.0	1.20
86	Maxon DCX32	36 V	119	76.8	1.66
87	Maxon DCX35	18 V	120	102.0	1.82
88	Maxon DCX35	24 V	121	96.6	1.75
89	Maxon DCX32	48 V	123	75.9	1.69
90	Maxon DCX35	36 V	128	98.7	1.82
91	Maxon DCX32	60 V	128	71.7	1.59
92	Maxon DCX35	60 V	132	95.2	1.80
93	Faulhaber	4490H048B	137	130.0	1.68
94	Maxon DCX35	48 V	138	99.5	1.87
95	Faulhaber	4490H036B	139	130.0	1.61
96	Faulhaber	4490H024B	148	130.0	1.66
97	Maxon RE40	148867	177	142.0	1.37
98	Maxon RE40	218009	180	116.0	1.26
99	Faulhaber	4490H036BS	181	130.0	1.64
100	Faulhaber	4490H024BS	183	130.0	1.66
101	Faulhaber	4490H048BS	183	130.0	1.69
102	Maxon RE40	218008	186	127.0	1.37
103	Maxon RE40	148877	187	137.0	1.46
104	Maxon RE40	218010	189	121.0	1.32
105	Maxon RE40	218011	190	120.0	1.31
106	Maxon RE40	218014	190	118.0	1.28
107	Maxon RE40	218012	192	121.0	1.32
108	Maxon RE40	218013	192	120.0	1.31

C

Experimental Validation

C.1. Experimental Setup

For the experiments, the Gemini Haptic Paddle is used[24]. A render of the setup is displayed in figure C.1.

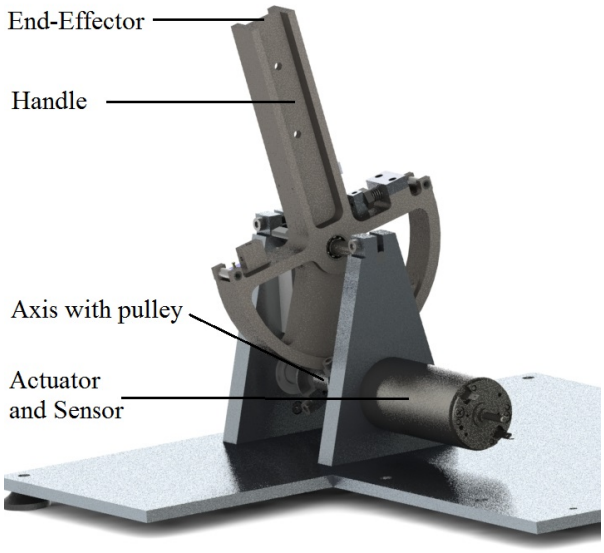

Figure C.1: A render of the Gemini, with the important components annotated.

The properties of the Gemini are listed in table C.1. Using equation (4.5), one can determine the mass lumped at the end-effector to be $m = 346\,\mathrm{g}$, and using an encoder with 4000 pulses per revolution and equation (4.7), the quantization interval is $\Delta = 16\,\mu\mathrm{m}$. The physical damping barely contributes, so it is assumed to be low: $b = 0.01\,\mathrm{N\,s\,m^{-1}}$ and the friction is assumed to be similar to existing devices (from which the data is listed in Diolaiti[26]): $c = 0.1\,\mathrm{N}$.

Table C.1: Dimensions and properties of the Gemini set-up, used for the performance analysis. One might notice that the inertia of the pulley is set to zero. This is because the inner and outer radius are the same. When varying r_p, it will be handled as an additional or subtracted inertia.

Part	**Dimensions and Properties**		
Handle	R_h	50	mm
	L_h	100	mm
	I_h	216890	gmm^2
Axis	I_{ax}	28971	gmm^2
Pulley	I_p	0	gmm^2
	r_{in}	5	mm
Actuator	Maxon	RE30-60W No. 268216	
	T_a	89.7	mN m
	t_a	1.05	ms
	I_a	3470	gmm^2

Using this values, the maximum stable stiffness can be determined according to the methods in section 3.3. This is visualized as the black line in figure C.3. At lower virtual damping, the sampled-data stability boundary dominates as limiting factor for the maximum stiffness, and at higher damping the quantization error dominates. Once again, it is visible that physical damping indeed barely contributes to the total damping. Even when the real physical damping would be ten times higher than this estimation, the virtual damping still is two orders higher.

The maximum stable stiffness of the is $K_{max} = 3800\,\mathrm{N\,m^{-1}}$ at damping $B = 10.9\,\mathrm{N\,s\,m^{-1}}$. These values are obtained using a second order velocity filter with a cut-off frequency of 100 Hz.

C.2. Experiment Description

The procedure is as follows: a virtual damping and stiffness are programmed, which are expected to be stable judged on modeling. The end-effector is moved manually from the equilibrium position, and then released. In the stable case, the device returns smoothly to its equilibrium position. In the unstable case, the release results in end-less limit cycles, which are only stopped manually. These two scenarios are visualized in figure C.2.

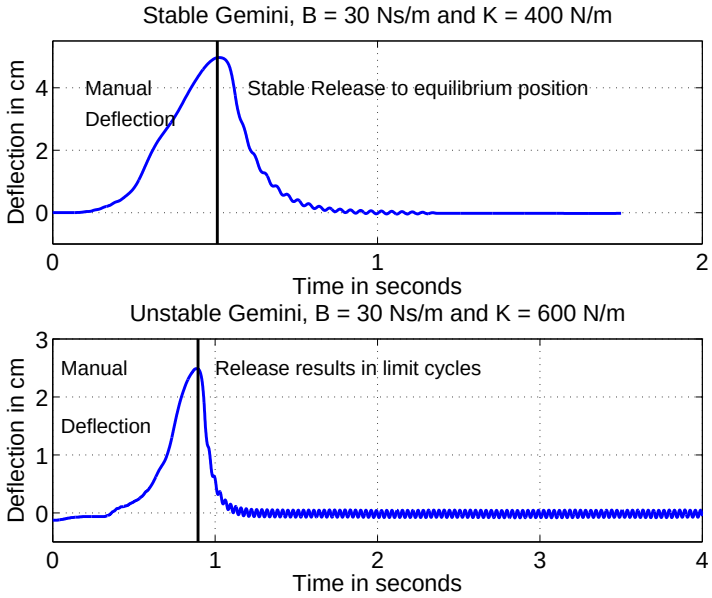

Figure C.2: The result of two individual tests, with the same virtual damping and a different virtual stiffness. The experimental procedure is simple: the end-effector is retracted from its equilibrium position, and released. The behavior is observed and measured: whether it is stable returning to its equilibrium position (the upper plot) or it results in limit cycles (the lower plot).

When the device proves to be stable for a certain B and K, the virtual stiffness is enlarged and the stability is tested again. The stiffness is increased with steps of $K = 500\,\mathrm{N\,m^{-1}}$ initially, and when the stability boundary is closer, in steps of $K = 100\,\mathrm{N\,m^{-1}}$. This is done at various values for the virtual damping in steps of $B = 2$ or $2.5\,\mathrm{N\,m^{-1}}$.

The resulting experimental determined stability boundary can be seen in figure C.3. The solid black line denotes the predicted stability boundary, and every red cross denotes the maximum stable stiffness at a certain damping. Every measurement is at least done three to five times, and every time, the same result was obtained. Therefore, no distribution is indicated in the figure.

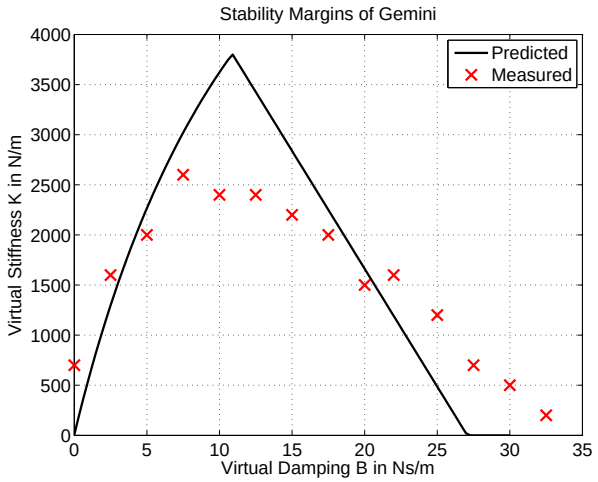

Figure C.3: Experimental results: The predicted stability boundary of the Gemini is solid black line, and the maximum stable points as tested on the device.

C.3. Results

Table C.2 gives an overview of the 82 tested conditions. At a fixed damping value, the stiffness is increased untill instability occurs. This is what can be seen in the table. An S denotes a stable response, LC stands for limit cycles. The maximum stable tested stiffness for each damping value is

given as a red cross in figure C.3. The log-files can be obtained by the secretary of the department Precision and Microsystems Engineering at the faculty of 3mE at Delft University of Technology, or by contacting the author[1].

Table C.2: Table listing all tested conditions and their outcome. The letter under the stiffness is the outcome corresponding to that value, where S denotes a stable response, and LC denotes limit cycles. In two occasions, stable behavior and limit cycles occurred at the same configuration, those cases are *not* considered to be stable. In the first column, the name of the data-file of the specific test is listed. Only logged results are taken into account.

logfile ***.mat**	**Damping** ($\mathrm{N\,s\,m^{-1}}$)	**Stiffness** ($10^2\,\mathrm{N\,m^{-1}}$)						
Exp1	0	5	7	10	15	20		
		S	S	LC	LC	LC		
	5	5	10	15	20	25	30	
		S	S	S	S	LC	LC	
	10	5	10	15	20	25		
		S	S	S	S	LC		
Exp2	10	5	10	15	20	22	24	25
		S	S	S	S	S	S	LC
Exp3	15	5	10	15	20	22	23	25
		S	S	S	S	S	LC	LC
Exp4	20	5	10	15	16	17	20	
		S	S	S	S	LC	LC	
Exp5	22	1	5	7	10	15	16	17
		S	S	S	S	S	S	LC
Exp6	25	10	12	13	15			
		S	S	LC	LC			
	27.5	5	7	8	9	10		
		S	S	S/LC	LC	LC		
Exp7	30	4	5	6	7	10		
		S	S	LC	LC	LC		
	32.5	1.5	2	3	4			
		S	S/LC	LC	LC			
Exp8	7.5	15	20	25	26	27		
		S	S	S	S	LC		
	12.5	20	23	24	25			
		S	S	S	LC			
	17.5	10	15	20	21	23	25	
		S	S	S	LC	LC	LC	
Exp9	2.5	5	10	15	16	17	20	
		S	S	S	S	LC	LC	

[1] E-mail: erikjansen90@gmail.com

D

Overview of Matlab Scripts

This appendix will give an overview of the Matlab scripts used in this research, which are given to secretary of the department Precision and Microsystems Engineering at the faculty of 3mE at Delft University of Technology. They could also be obtained by contacting the author[1]. All functions are listed in table D.1, and all other Matlab scripts are listed in table D.2.

Table D.1: List of Matlab-functions used in this research.

Name	Description
fig2eps	Used to save a Matlab-figure as color eps-file, ready to import in the report. Works only in my folder structure. Used in many Matlab-files.
HapticDisplayStable	This function evaluates the sampled-data stability of a fixed haptic device. Returns a Boolean which represents the stability as a function of mass, damping, time delay, velocity filter frequency and order, and virtual damping and stiffness. Used in `KmaxFixedDevice`.
KmaxFixedDevice	Function that calculate the stability boundary of a fixed haptic device as a function of the device parameters mass, damping, friction, quantization interval, time delay and sampling time. It returns the maximum stable stiffness and the corresponding damping and velocity filter. In addition, it returns the vector with damping values, and the stability boundary by both mechanism, and the total boundary. Uses `HapticDisplayStable`.
ReturnNumber	Function that returns the numerical value of a string that starts with a number and ends with an unit. Used to read in values from actuator datasheets, as in `MaxonMotor`.

[1]E-mail: erikjansen90@gmail.com

Table D.2: List of Matlab-scripts used in this research.

Name	Type	Description
EvaluateFinalResults	m-File	File used to interpretate the results of a full grid analysis as generated by `HapticGemini`. One of the datafiles `Data_all.mat` is used. Generates contourplots of max stable stiffness, effective stiffness, z-width and others,a s used in the report. Figures are saved using `fig2eps`.
Exp#.mat	Data-file	Data-file containing the successful results from the experiments, where # represents a number from 1 to 9, corresponding to the numbers in table C.2. The variable `data` contains the following signals, each in a row: time in s, angle in rad, applied torque in Nm, velocity in rad/s by filter, velocity in rad/s by sensor, desired torque in Nm, B in 1e-4 Ns/m, K in 1e-4 N/m, velocity filter cut-off in Hz.
HapticGemini	m-File	File used for a full grid analysis of the haptic Gemini. Uses the properties of the Gemini and variations in transmission and actuator to evaluate the effect of component level choices. Uses `KmaxFixedDevice`. Generates contour plots of affected physical properties of the device.
HapticGeminiIdentification	m-File	File used to compare the predicted stability boundary with the measured values and saves the resulting figure for the report.
Optimization	m-File	File used to generate the figures to simulate the optimization problems from chapter 5.
PlotsForPresentation	m-File	File used to generate a lot of figures used in the paper, the report and the presentation.
PlotsInPaper	m-File	File used to generate a lot of figures used in the paper and the report.
Results19-5 20x20 grid_Gemini	Folder	Folder containing the results of a full grid analysis by `HapticGemini`. It contains all data in `Data_All.mat`, and for every iteration the logged data in `Data_i_#_j_#.mat` and a figure `Imp_i_#_j_#.png`, where the symbol # represent a number between 1 and 20.
Results12-4 7x7grid	Folder	idem
Results20-5 10x10grid-Needle	Folder	idem
Results24-4 10x10 grid	Folder	idem
Results26-4 12x12 grid	Folder	idem
RouthHurwitcSymbolic	m-File	File used to obtain the symbolic representation of the characteristic equations and the Routh-Array. The resulting inequalities are used in `HapticDisplayStable`.

E

Literature Overview and Research Background

This appendix is written in finalized in december 2015, and is meant to give an overview of the literature which formed the basis of this research. Some objectives might be outdated, but it gives a overview of the context of this research.

E.1. Haptics, What and Why?

A haptic interface is a kinesthetic link between a human operator and a virtual environment/computer generated environment[25].

In Hayward [3] haptic interfaces are defined as follows: *"Haptic interfaces comprise hardware and software components aiming at providing computer-controlled, programmable sensations of mechanical nature, i.e., pertaining the sense of touch."* The word Haptic comes from the Greek verb $\alpha\pi\tau\varepsilon\sigma\theta\alpha\iota$ or *haptesthai*, which means to touch.

Hayward distinguishes four methods to create the haptic sensation:

- Vibrotactile devices: the buzzing feeling in mobile phones and game controllers.
- Haptic Force-feedback: the reproduction of forces by mechanism with sensors, actuators and a control system. It is often explained as in figure E.2: on the left we see an operator touching an object with an infinitely stiff and mass-less stick. The operator feels like he is touching the object directly. In haptic force feedback, the stiff, mass-less stick is replaced by a mechanism with senors, actuators and a control system. A block diagram is given in figure E.2b: the goal is that the operator still has the experience of touching the object directly, by reproduction of the forces. This picture also shows the typical non-collocated behavior of haptic devices.
- Surface displays: a device where the sensation of touching a surface is simulated.
- Distributed tactile displays: a device that provides spatial distributed sensations to the skin surface.

The focus of this research will be the haptic force feedback. Adams[25] distinguishes the historical one-directional human-computer interaction (from computer to human through sound and vision, vice versa via keyboard and mouse) and two-directional haptic interaction.

Haptics is the science and technology of experiencing and creating touch sensations in human operators. [5]. In Haptic rendering, a user can interact with a virtual or remote environment and feel the sensation of touch.

Haptic rendering (in impedance systems) is the process of computing the force required by contacts with virtual objects based on measurements of the operator's motion[5].

Telemanipulation is performing an action, over a distance. It consists of a pair of robot manipulators: one to be handled by the operator (the master) and one operating in a remote environment (a slave), that reconstructs the human actions of the operator[1]. When forces of the remote environment

felt by the slave, are reconstructed at the master side, this is called 'Haptic Force Feedback'. The slave in a remote environment can be replaced by a virtual environment for virtual reality. Figure E.1 shows the three scenarios: direct operation, teleoperation and virtual reality. Haptic telemanipulation has become a topic of extensive study, judging on the many universities devoting courses to the subject[9].

The two main applications for rendering virtual environments are education, in flight simulators or medical simulators[1], and entertainment, such as the the Novint Falcon[44]. Two main applications for haptic teleoperation are minimal invasive surgery[52] and contact with hostile environments (e.g. robots for dismantling bombs or robots in radioactive environments, such as the exploration robot in Fukushima. In addition, a combination of a remote and virtual environment can be found in shared control[53]. Haptic feedback based on a virtual model is used to help the operator control a device in a remote environment.

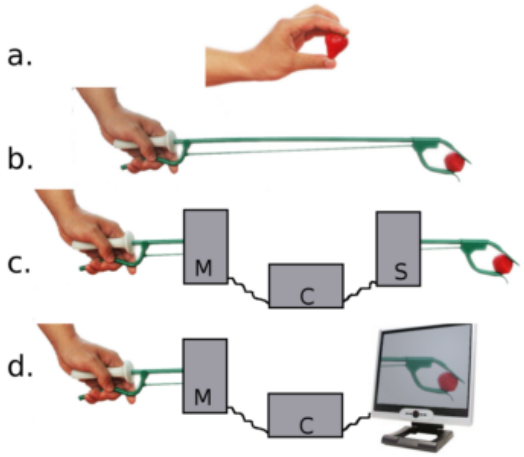

Figure E.1: The four different ways in interaction and manipulation, where M stands for Master, C for Controller and S for slave. Situation a gives direct manipulation, b is indirect manipulation, c gives teleoperation and d is virtual reality. Figure adapted from Christiansson[2].

In the ideal case, the operator is not able to distinguish haptic telemanipulation from direct manipulation [29]. A device with that properties is called 'transparent'[30]. Qualitatively, the ideal haptic device is mass-less and infinite stiff[3, 30]. In addition, it has low friction, zero or low backslash, high force bandwidth and high dynamic range of impedances[6, 14, 35]. This ensures a high force bandwidth, enabling the master to construct the slave's forces accurately.

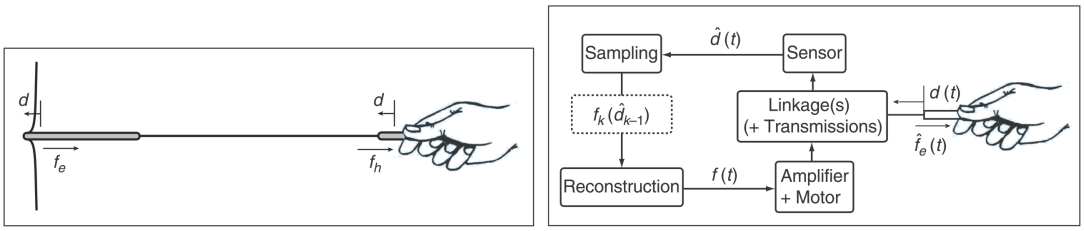

(a) Idealized teleoperator.

(b) Block diagram of haptic interface

Figure E.2: Figure (a) shows the idealized teleoperator. The tool on the left is connected to the operator with an infinitely stiff mass-less stick. The experience for the operator would be the same as holding the tool directly. In (b) the block diagram of an haptic interface is given. The stiff and massless stick is replaced by a mechanism, sensors, actuators and a control system. Both figures are adapted from [3]

Another role for haptic feedback is that it offers an additional communication channel, recognizing that there is not much communication bandwidth left in conventional channels like sound and vision[54].

[1]Like the Simodont Dental Trainer, a machine allowing dental students to train dental surgeries in a virtual mouth http://www.acta.nl/en/studying-at-acta/student-services/simodont/index.aspx, viewed 04-12-2015.

E.2. Abstract Performance Metrics of Haptic Systems

The need for universal performance metrics is first acknowledged by Hayward[28]. According to him, the bi-directionality of information and energy flows is the most distinguishable factor for haptics as compared to other robotics devices. Therefore, performance metrics are not straightforward. His motivation for performance metrics is as follows:

- Device performance (and price) can be matched in an informed fashion to the task they meant to address.
- Devices can be specified before they are built.
- The improvements applied to a particularly device or technology can be tracked in a systematic fashion.
- Devices with different designs can be compared.
- The importance of certain particular factors can be ascertained with respect to application areas.
- Progress in the field can be monitored.

Generally, in commercial Haptic devices, only static properties are given[44, 55], such as size of the workspace, maximum force or stiffness, and resolutions. Due to differences in kinematics and degrees of freedom, comparing devices is difficult. In addition, the relation between design choices and performance is not very straightforward, making design for certain performance difficult.

Roughly three strategies are used to evaluate haptic devices: a comparison between two or more devices, task-specific performance metrics, and physical performance measures, which will be discussed next.

E.2.1. Direct Comparison of Haptic Devices

Direct comparison of haptic devices is the easiest method for the evaluation of haptic devices, but also the most limited one. One simply takes two or more haptic devices, and performs the same test on all devices. This gives a quantitative comparison between the devices. However, this is a limited result, since it is not very generalizable.

An example study is performed by Rose et. al.[9], where the different haptic paddles by different universities are compared. One of their conclusions is the fact that a haptic paddle with a capstan drive has a larger range of achievable impedances than the ones with a friction drive. Another example is done by Harders et. al. [11], where they compared three different 6DoF devices on completion time and mean forces.

Another comparison is done by Vanacken[56]. He compares the two low-cost devices Phantom Omni[55] and Novint Falcon[44], based on system identification: identified mass and damping and a resulting bode plot. In addition, both master devices are used to perform a certain task and compared on their task performance. A similar study is performed by Martin[10]: system identification is used to obtain the properties of the Novint Falcon. Again, a posteriori.

A disadvantage of this method is the fact that it is only possible after designs are realized. It is not possible to evaluate the effect of design parameters on the performance. In addition, designs with different architectures are hard to compare.

E.2.2. Task-Specific Performance Metrics

There are standardized tests, such as the the one by Ruffaldi[13]. He uses 3D-information of an object in combination with motion and forces experienced by a probe. In addition, different control methods can be compared on one device, when a certain task is performed. An example study of this is done by Wildenbeest[23]. In his research to the impact of the frequency of haptic feedback on teleoperation tasks, he uses *task completion time* as task performance metric. In addition, the *maximum input force* and *reversal rate* (amount of steering corrections) are metrics for the teleoperator's control effort. Finally, he uses the scores of two sorts of questionnaires filled in by the operator as a metric.

In line with this, Samur[45] dedicates a book chapter on *Performance Evaluation based on Psychological tests*. He again uses standardized peg-in-the-hole tasks and hardness perception. An addition

to this is the 'Toy Problem', introduced as a benchmark problem[12]. Here a construction in LEGO is used as a benchmark test for teleoperation. Finally, questionnaires to the operator like NASA's Cooper-Harper test can also be used to evaluate the Human workload[57].

Using task-specific or psychological performance metrics, it is hard to evaluate design choices. Tests are only possible after a design is finished. To evaluate the influence of component level choices, many tests are necessary, since all design variations must be built. In addition, comparing different designs would require testing all of them, in exactly the same conditions. This will be very time consuming. In addition, a designer is unable to evaluate design decisions a priori, in the design phase.

Therefore, this study will focus on physical performance measures. It will be up to a haptic device designer to link certain task specific requirements to physical requirements which can be used in the design phase. Then it would be possible to use my design tool.

E.3. Physical Metrics as Performance Indicators

One of the limitations of haptic devices is their general high costs. Therefore, the they are not used very much yet. To understand the design aspects where money can be saved, without diminishing performance, a good model is needed. In contrast with the two other group of performance metrics, one can define physical performance metrics a priori in the design phase. Comparison of devices and task specific measures can only be determined a posteriori, when a device is physically there.

Several studies have been performed to investigate the influence the effect of a certain aspect in a haptic device on a performance metric. The aspects in haptics devices that are evaluated in papers are visible in figure E.2b, and are the following:

- **Mechanics**: the mechanical part of the device, with its mass, stiffness, damping and kinematics.
- **Viscous Damping**: Physical damping in the mechanics of a device.
- **Virtual Environment**: the rendered mass, stiffness and damping of the device.
- **Sensor**: In most papers, especially the discretization in sensors is evaluated.
- **Filter**: The velocity filter which is used to obtain the velocity from position measurements.
- **Sampling**: The sampling rate of the digital control domain of the device.
- **Delay**: the complete actuation (power amplifiers and actuators) is often simplified as one time delay only.
- **Actuation**: Everything else in the actuation, in a bit more detail than just a time delay.

These aspects are used in the following paragraphs to categorize studies on the influence of component level choices on overall performance.

E.3.1. Z-width

Every haptic device can be seen as a generator of impedances. One of the first metrics specific for haptics is the **Z-width**[6]: the dynamic range of achievable impedances that can be rendered by a haptic display. Most of the studies on haptic performance aim on improving the z-width, without diminishing stability and transparency.

In most studies, the impedance can be seen as a combination of the elementary building blocks: masses, springs and dampers[25]. Other studies focus on a special case: an unilateral constraint in the form of a virtual wall, for which stability can be an issue[32].

A selection of papers were the Z-width is optimized, are given in table E.1.

E.3.2. Passivity

In control systems and circuit network theory, a passive component or circuit is one that consumes energy, but does not produce energy. The coupling of dynamic systems is guaranteed to be stable[14].

Colgate states that to achieve passivity in an active systems, some physical dissipation is needed[14]. This can be mathematically expended to the following explanation.

Table E.1: Papers considering Z-width in Haptics. One can see that there is a lack of research on the actuation side of haptic devices.

	Influence of:							
Source	Mechanics	Visc. Damp.	Virt. Env	Sensor	Filter	Sampling	Delay	Actuation
(Colonnese *et al.*, 2015), [8]			x			x	x	
(Colonnese and Okamura, 2015), [16]			x	x	x	x	x	
(Adams and Hannaford, 1999), [25]		x	x			x		
(Colgate and Brown, 1994), [6]		x	x			x		
(Gil and Sanchez, 2009), [15]	x	x	x				x	
(Chawda *et al.*, 2014), [37]			x	x	x			
(Lawrence and Chapel, 1994), [30]	x	x	x					x
(Shayan-Amin *et al.*, 2013), [58]	x				x	x		
(Christiansson and van der Helm, 2007), [59]	x		x					

Edward Colgate[60]: A necessary and sufficient condition for passivity of the haptic interface model is:

$$b > \frac{T}{2}\frac{1}{1-\cos\omega T}\Re\left\{\left(1-e^{-j\omega T}\right)H\left(e^{j\omega T}\right)\right\} \quad \text{for} \quad 0 \leq \omega \leq \omega_N \tag{E.1}$$

Where b stands for physical damping, T is the sampling time, and ω the frequency. Using a virtual spring-damper system (with K being the virtual stiffness and B the virtual damping), equation E.1 reduces to:

$$b > \frac{KT}{2} + |B| \tag{E.2}$$

From which one can conclude:

- To achieve passivity, some physical dissipation is essential.
- With other variables (b and B) fixed, the maximum achievable virtual stiffness is proportional to the sampling rate.
- The maximum achievable virtual damping for zero stiffness is independent of the sampling rate.
- With other variables (b and T) fixed, higher virtual stiffness can be achieved at lower values of virtual damping.

After the introduction of passivity in Haptics by Colgate, many follow-up studies have been performed. A selection is given in table E.2

E.3.3. Stability

One important note of passivity is the fact that it is very conservative[32]. A passive system is stable, but not all stable system are necessarily passive. In control theory are more tools to check stability. Several studies on stability have been performed in Haptics, which is summarized in table E.3. The

Table E.2: Papers considering passivity in Haptics. One can see that there is a lack of research on the actuation side of haptic devices.

	Influence of:							
Source	Mechanics	Visc. Damp.	Virt. Env	Sensor	Filter	Sampling	Delay	Actuation
(Colonnese and Okamura, 2015), [16]			x	x	x	x	x	
(Adams and Hannaford, 1999), [25]		x	x			x		
(Colgate and Brown, 1994), [6]		x	x			x		
(Gil and Sanchez, 2009), [15]	x	x	x				x	
(Diolaiti *et al.*, 2006), [26]	x	x	x	x		x	x	

ones only considering passivity (and thus only give the conservative measure for stability) are omitted here.

Since the haptic device actively generates physical energy, instabilities can damage the hardware or cause injuries to the user. The stability of the system is, thus, crucial. Furthermore, instabilities degrade transparency in haptic simulation. A transparent haptic interface should be able to emulate any environment, from free space to infinitely stiff obstacles.

A general study on stability analysed using Routh-Hurwitz Criterion is performed by Gil et al. in 2004[31].

Table E.3: Papers considering stability in haptics. One can see that there is a lack of research on the actuation side of haptic devices.

	Influence of:							
Source	Mechanics	Visc. Damp.	Virt. Env	Sensor	Filter	Sampling	Delay	Actuation
(Colonnese and Okamura, 2015), [16]			x	x	x	x	x	
(Daniel and McAree, 1998), [61]	x	x			x			
(Gil and Sanchez, 2009), [15]	x	x	x				x	
(Chawda *et al.*, 2014), [37]			x	x	x			
(Diolaiti *et al.*, 2006), [26]	x	x	x	x		x	x	
(Hulin *et al.*, 2006), [34]		x					x	
(Shayan-Amin *et al.*, 2013), [58]	x				x	x		
(Christiansson and van der Helm, 2007), [59]	x		x					

E.3.4. Transparency: Difference between rendered and desired dynamics

Brooks[29]: an ideal teleoperation system would create a man-machine interface of such high fidelity that the human operator could not detect that he was remotely located from the task. A haptic device with those properties is called 'Transparent'[30]. Greater transparency translates to closer force and position signal matching between master and slave devices. To render realistic virtual environments, the difference between desired and rendered dynamics must be small.[8].

Recent research regarding transparency is done by Nick Colonnese from Stanford[8]. He claims:

This work informs the design of haptic displays by modeling how the closed-loop system is affected by haptic device dynamics, time delay, and low-pass filtering. By understanding the actual mechanical dynamics of the display, and demonstrating the influence of those dynamics on human perception, we form a foundation for future work to rigorously analyze human perception of haptic qualities.

Accurate haptic displays should feel exactly as desired, with no unwanted effects from a multitude of sources such as device dynamics (i.e., inherent inertia and friction), analog to digital (A/D) and digital to analog (D/A) conversions, aggressive low-pass filtering to mitigate noise, and amplifier or transport time delay.

Nick Colonnese[8], about the influence of time delay on rendered stiffness and damping: *The theoretical and experimental analyses show that time delay strongly affects rendered and characterized damping, but does not have a significant affect on effective or characterized stiffness. In other words, the actual stiffness of the haptic display does not significantly change with time delay. For the human user studies, we observed that the effect of time delay on perceived damping and stiffness was well predicted by the characterized results: time delay affects perceived damping, but not perceived stiffness.*

However, this research stays at device level. The whole actuation path is modeled as a time delay, but in my vision it plays a more important role, and affects the mass/inertia of the device too. The research must be done on component level.

Papers focusing on transparency are given in table E.4.

Table E.4: Sources focusing on transparency in Haptics. One can see that there is a lack of research on the actuation side of haptic devices.

Source	Mechanics	Visc. Damp.	Virt. Env	Sensor	Filter	Sampling	Delay	Actuation
(Colonnese *et al.*, 2015), [8]			x			x	x	
(Adams and Hannaford, 1999), [25]		x	x			x		
(Lawrence and Chapel, 1994), [30]	x	x	x					x
(Christiansson and van der Helm, 2007), [59]	x		x					

E.4. Models to Analyze Physical Metrics

E.4.1. Admittance and Impedance Approach

A virtual or remote environment can be modeled using two approaches: the admittance and impedance approach. In general, one can distinguish two different approaches, the impedance approach and the admittance approach, both showed in figure E.3. The picture and the description are adapted from Hayward 2007 [3].

In the Admittance control, a force is applied on the environment, which responds by a movement. This approach is not used very often, due to the fact that expensive force sensors are needed. In add. One example however is the Haptic Master[62]. The impedance approach is used more often. The environment is modeled as an impedance. This virtual environment can be built up from a combination of the elementary building blocks: masses, springs and dampers.

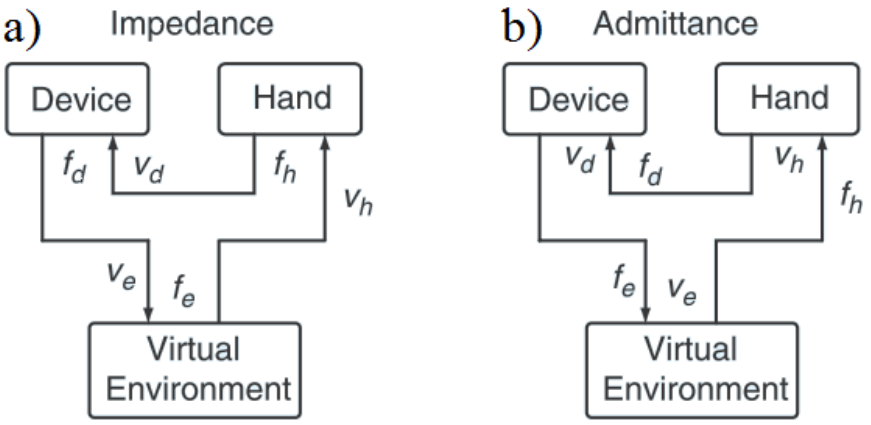

Figure E.3: Block diagrams of the two approaches in haptics: impedance approach and the admittance approach. The v's denote velocity and the f's denote forces. Figure adapted from [3]

There are two main models in use, the two-port model introduced by Hannaford (section E.4.2), and the feedback model as introduced by Colgate(section E.4.3). Many other models are variations of one of the two.

E.4.2. Two-Port Model Hannaford

The so-called two-port model is originally introduced as design framework for haptic teleoperation[1].

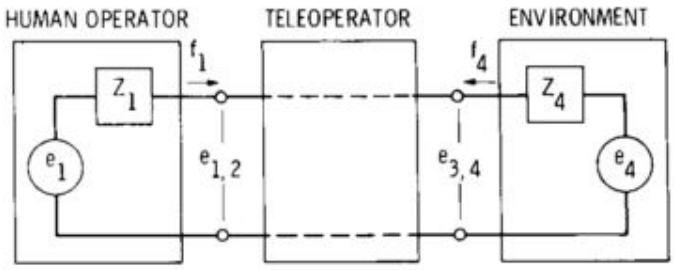

Figure E.4: The two-port model of teleoperation as introduced by Hannaford[1].

This two-port Hybrid parameters are defined as efforts and flows, analogue to electrical network theory. The input and output effort are the the input and output force f. The flows are the velocities v. The two-port Hybrid Matrix is then as follows:

$$\begin{bmatrix} f_{in} \\ v_{out} \end{bmatrix} = \begin{bmatrix} h_{11} & h_{12} \\ h_{21} & h_{22} \end{bmatrix} \begin{bmatrix} v_{in} \\ f_{out} \end{bmatrix} \tag{E.3}$$

Then, the interpretation of the h parameters is then as follows:

$$h = \begin{bmatrix} Z_{in} & \text{Rev. Force Scale} \\ \text{Velocity Scale} & \frac{1}{Z_{out}} \end{bmatrix} \tag{E.4}$$

Ideally, one has a very small impedance of the master and a small admittance of the slave. In addition, the force and velocity transfer would have infinite bandwidth. Therefore, the h matrix representing an ideal teleoperator is as follows:

$$h = \begin{bmatrix} 0 & 1 \\ -1 & 0 \end{bmatrix} \tag{E.5}$$

Samur adjusted the two-port model for teleoperation to a model valid for haptic rendering of a virtual environment[45]. Since force and velocity are modelled as effort and flow, one is able to use the

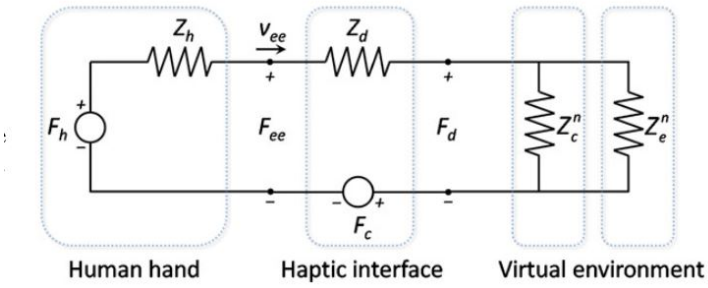

Figure E.5: Electrical model by Samur[45].

electrical equivalents current adn force. The electrical equivalent of the two-port model for operating in a virtual environment is given in figure E.5.

Using this model, the uncontrolled haptic device dynamics are as follows (with a complete derivation in [45]):

$$\begin{bmatrix} F_h \\ F_{ee} \end{bmatrix} = \begin{bmatrix} Z_h + Z_d & H_f \\ Z_d & H_f \end{bmatrix} \begin{bmatrix} v_{ee} \\ F_d^n \end{bmatrix} \tag{E.6}$$

Where F_{ee} and F_d^n are the rendered end-effector force and the desired one, v_{ee} is the end effector velocity and F_h is the voluntary human muscle force. Furthermore, Z_d and Z_h are the device and the human impedance and H_f is the force transfer function.

In addition, he gives a model with different components on place, which is displayed in figure E.6. The upper horizontal path is considered to be the sensing actuation transfer function H_S and the lower horizontal path is the force or actuation transfer function H_f. In most other sources, the actuation transfer function is only modeled as a time delay. Obviously, both ideal transfer functions are 1.

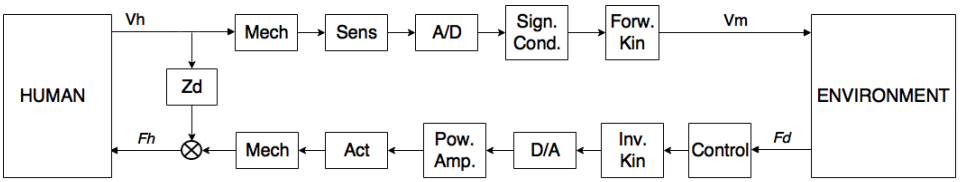

Figure E.6: The model of a haptic master Samur[45], slightly modified.

E.4.3. Colgates Model

Another frequently used model is the feedback model introduced by Colgate[14], displayed in figure E.7. The device is modeled as an impedance with perfect (but quantized) sensing. The actuation is only modeled as a zero-order-hold.

This model is used to examine the influence of sensor quantization, damping, stiffness and sampling rate. It does not consider any other non-linearities in the sensing or actuation part.

This model is used in many other studies ([8, 34, 63, 64] among others). However, in most cases the actuation is not taken into account or simplified to a time delay only.

E.5. Closed-Loop Analysis by Samur

In an impedance-type haptic device, users feel the combined forces from the dynamics and statics of the device and the simulated environment in response to moving the device[3]. Therefore, mass is an undesired property of haptic devices.

Samur[45] gives an expression for the force at the end effector of an haptic device F_{ee} as a function of the applied motion v_{ee}. In the ideal case, this end effector force is simply a function of the programmed virtual environment Z_{VE}^d (where the superscript d denotes the discrete model of the virtual environment):

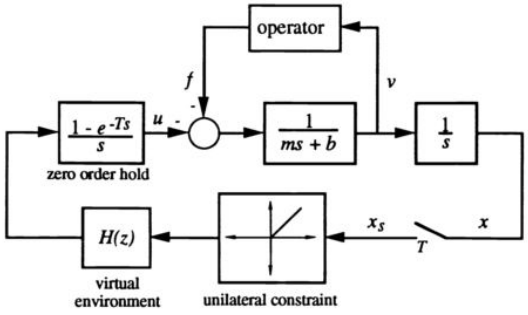

Figure E.7: Colgates model of a one degree-of-freedom haptic interface. m is the inherent mass of the display, b is inherent damping, v is velocity, x is position, X is the sampled potion, T is the sampling rate, u is the control effort, and f is the force applied by the operator. From [14].

$$F_{ee} = Z^d_{VE} v_{ee} \tag{E.7}$$

However, an operator also experience the effect of the device impedance Z_d, which can partly compensated by the discrete model of this device impedance Z^d_d. Two additional transfer functions play a role in the formula for the haptic feedback: the force transfer function, H_f, from desired end effector force to applied force and the velocity transfer function H_v, from the real end effector velocity to the measured end effector velocity. The information above leads to the total end effector force, felt by the operator:

$$F_{ee} = \left(Z_d - H_f Z^d_d H_v + H_f Z^d_E H_v\right) v_{ee} \tag{E.8}$$

The end effector force from (E.8) is in the ideal case equal to the one from (E.7). One can derive that this is the case when the following conditions are fulfilled:

1. Large resemblance between the measured and real velocity of the end effector ($H_v \approx 1$).
2. Large resemblance between the desired and the applied end effector force ($H_f \approx 1$).
3. Small device impedance ($Z_d \approx 0$, equivalent to quantitative statements of [3, 25, 30, 35, 36, 61, 65], etc)
4. Large resemblance between modeled and real impedance, for environment as well as device ($Z^d_{VE} \approx Z_{VE}$ and $Z^d_d \approx Z_d$)

It is the challenge of the engineer to design a haptic device such that conditions 1 till 4 are fulfilled.

On item 1: Several studies are done to the influence of sensor properties on the stability or transparency. Examples are the influence of sensor quantization on stability[16] and transparency[8], or the influence of the velocity filter [37].

On item 2: This is the condition where there is not a lot of attention yet, and therefore the focus of this research.

On item 3: A lot of quantitative statements are made, and the goal is simple to understand (but not easy to achieve): the device impedance must be as low as possible. The ideal device according to this condition is the trivial one: the infinite stiff, mass-less stick[3].

On item 4: The resemblance between real-world and simulated impedances is a challenge for the software engineer, and therefore not a focus of this research.

A final note of importance, is the asymmetry of the human sensitory system[29]. The applied motion by the human is in the order of magnitude of 5 Hz, but the sensing requires a bandwidth of 10-20 Hz.

E.6. Problem with Actuation Modeling

E.6.1. Low-Cost Haptics

Recent interest in haptics by universities led to the development of simple, 1DOF, low-cost, haptic interfaces to use for educational purposes. Most of these devices are so-called 'Haptic Paddles': university demonstrators. The first Haptic Paddle is developed by Stanford University in 1997 and is used

in undergraduate dynamics courses[18]. Other universities use the haptic paddle for courses in control, haptics and programming. An extensive overview of and comparison between the different haptic paddles is given by Rice University[9]. Figure E.8 shows the haptic paddle from Rice University, as an example of haptic paddles and their components.

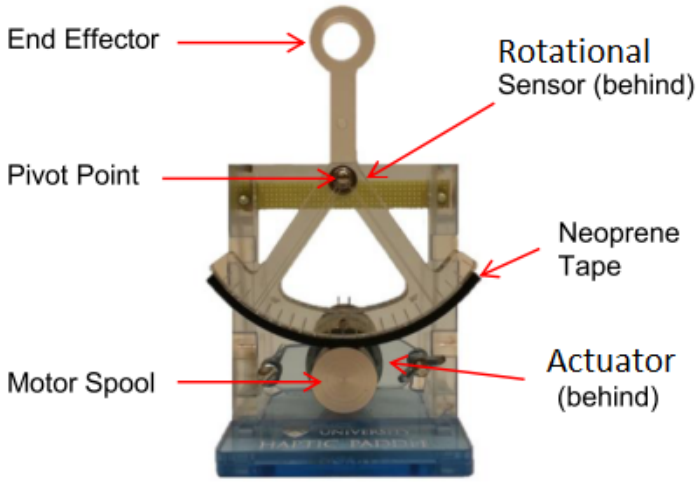

Figure E.8: The Haptic Paddle from Rice University[9], as a typical example of the haptic paddle.

Apart from the Haptic Paddles, other parties acknowledge the need for low-cost haptic devices. Several strategies are used. Italian scientists designed the 2-Dof OSHAP[19], with the motivation to develop an alternative for expensive commercial interfaces, and two use open-source, low-cost electronic prototyping environments as the Arduino and the Rasberry Pi. The Arduino micro-controller was also used by Beni et al.[20]. They use and compare different programming strategies in the Arduino to cancel the torque ripple of an low-cost stepper motor. Another strategy is followed in [21]: Lawrence et al. use low-cost hardware, but increases the complexity in control to preserve performance. As an alternative, Eilering developed a method to build 3D-printed miniatures of an industrial robot as an input device for teleoperation: the Robopuppet[22]. Here the financial benefit is in the production.

E.6.2. Actuation Modeling

As stated in a design paper[38]: the actuator is what bounds the performance from above. In [5] however is stated, that the effect of actuator and amplifier dynamics and D/A resolution on system stability is typically negligible in comparison to position sensor resolution and sampling rate for most haptic devices.

Numerous studies have been performed on the influence of components on overall haptic performance(see table E.1, E.2, E.3, E.4). However, the influence of the actuation part of the loop is only examined as a time delay, when examined at all. As a consequence of the general statements in the previous alinea, and the lack of knowledge of the influence of the actuation properties on overall performance, the actuator is over-engineered. An engineer typically chooses the best and therefore most expensive actuator, to be on the safe side.

This study fills in the gap and will give more insight in the influence of design choices in the actuation part on haptic performance.

The effect of actuator and amplifier dynamics and D/A resolution on system stability is typically negligible in comparison to position sensor resolution and sampling rate for most haptic devices. [5].

In the area of force feedback devices, the actuator performance is what bounds the performance above. [38].

Colonnesse[8]: *Describing the effect of system parameters (e.g., device damping and mass, and time delay) on the closed-loop properties would be a valuable tool in haptic display design.* In my opinion

however, this is oversimplified. Instead of studying the influence of 'vague' properties like mass, damping and time delay, the complete device should be studied. The electrodynamics are reduced to a time delay in this case, but it plays a more important role. Therefore, the research question is as follows: what is the influence of component level choices on the overall haptic device performance.

E.6.3. Why Precise Modeling

Jeroen Wildenbeest et al.[23] showed that *overall task performance is substantially improved providing low-frequency haptic feedback, while further increasing the haptic feedback quality yields only marginal improvements, even if a full natural spectrum of haptic feedback is provided.* In economics, this phenomena is called *diminishing returns*[2]: the performance shows only marginal improvements, with major effort. Therefore, it is an indication that it is possible to make a simpler and therefore more economical design, without suffering from lower performance.

E.6.4. Application: the Rotating Bar

Why is this shape a realistic choice?

- An Haptic master ideally has low mass/inertia, maintaining high stiffness[35]. This ensures the master to have an high force bandwidth, enabling it to reconstruct the slave's forces accurately.As stated in many papers, a parallel mechanism seems to be the ultimate choice for haptic master[3, 19, 36], due to the combination of low moving mass and high structural stiffness[42]. The rotating bar is used as input in many parallel mechanisms, such as the Delta Robot[43], as used in the Novint Falcon [44]. In addition, it is used in low-cost applications as the Munin developed in our department (a twin pantograph) [66], and in Teun's demonstrator[67]. In addition, it is used in many four-bar- and five-bar-mechanisms.
- Therefore: results expendable to multidof.
- The Hapkit is used at many universities in many different configurations[9, 18, 41]

E.6.5. Difficulties to Consider

The requirements on the forward motion channel, and the feedback force channel are different. As stated by Fischer[36]: *In particular the forward bandwidth (from master input device to slave manipulator arm) relates to a powertransfer channel and is much lower (around 10Hz) than the reverse bandwidth (from slave manipulator arm to master input device) which is primarily an information channel with a bandwidth extending into the kHz range.*

This is what Brooks mentions as the asymmetry in human perception[29].

On transparency: what is needed? Lawrence et al. experimentally explored accuracy in haptic displays by investigating the ability of humans to detect differences in impedances[68].

E.7. Rough Content of Paper

In impedance controlled force feedback, the haptic device responds to a movement by generating a force. A virtual environment can be modeled as an impedance consisting of springs and dampers, the elementary building blocks of every impedance[4]. With this impedance approach, users feel the combined forces from the dynamics and statics of the device and the simulated environment in response to moving the device[3]. This gives a trade off. In free space motion, the ideal impedance is as low as possible. However, the same device must be able to render large impedances, for which large actuators are needed, with typically larger inertia. This large dynamic range of impedances is called 'z-width' in haptic literature, a term introduced by Colgate[6]. In addition to render a wide range of impedance, the challenges in haptic device engineering are maintaining stability[7] and transparency[68]: the quality of the rendered force[8].

The main question in engineering haptic devices is: what is the influence of component level choices on overall haptic device performance?

[2]The exact definition according to the Encyclopedia Britannica (2014) is as follows: economic law stating that if one input in the production of a commodity is increased while all other inputs are held fixed, a point will eventually be reached at which additions of the input yield progressively smaller, or diminishing, increases in output.

The ideal haptic device has a low mass in combination with high stiffness. To achieve this, parallel mechanisms are considered to be a good choice[3]. However, this introduces the typical non-collocated designs for sensors and actuators.

Problems:

1. Users feel the combined forces from the dynamics and statics of the device and the simulated environment in response to moving the device.[3]
2. Z-Width: achievable range of impedances[6, 14]. Very large and very low impedance necessary.
3. Stability [7, 69]
4. Maintaining quality of force feedback[8, 68].

However, in general, most haptic devices on the market are very expensive and therefore not commonly used yet. The growing interest in low-cost haptic devices raises the question: how to economize haptic devices without diminishing performance? What is the influence of component-level choices on the overall haptic device performance?

This paper will focus on the actuator part of this question, since it is generally acknowledged as the limiting factor in haptics[38].

Traditionally, a number of design guidelines is given qualitatively. Ellis[35] comes with a extensive list, like high stiffness, low mass, low friction, zero backslash, high backdrivability etc. This paper gives a method to study the quantitative influence of those guidelines on the final device performance.

Relation between technical performance measures and task completion time for example researched by Wildenbeest[23]. But how to know what the technical performance measures are? This paper gives a method to study the performance measures, based on a design. What is the influence of component-level choices on overall haptic design performance?

E.8. Conclusions and Focus

The ideal haptic device is stiff and has a low moving mass, to be able to generate a large dynamic range of impedances. Therefore, parallel mechanisms are a convenient choice. However, this generates the typical location of the sensors and actuators in haptic devices: non-collocated with the end effector.

This non-collocated behavior, in addition to the bi-directional flow of power and information, makes haptic devices difficult to analyze. The most important performance metrics are Z-Width (achievable range of impedances), passivity, stability, and transparency.

Numerous studies have been performed on the influence of components on overall haptic performance(see table E.1, E.2, E.3, E.4). However, the influence of the actuation part of the loop is only examined as a time delay, when examined at all. As a consequence of the general statements in the previous alinea, and the lack of knowledge of the influence of the actuation properties on overall performance, the actuator is over-engineered. An engineer typically chooses the best and therefore most expensive actuator, to be on the safe side.

This study fills in the gap and will give more insight in the influence of design choices in the actuation part on haptic performance.

The model of Samur (of which parts are shown in figure E.5 and figure E.6) will be taken as a basis for this research.

Bibliography

[1] B. Hannaford, *Design framework for teleoperators with kinesthetic feedback,* IEEE Transactions on Robotics and Automation **5**, 426 (1989).

[2] G. A. V. Christiansson, *Hard Master, Soft Slave Haptic Teleoperation*, Ph.D. thesis, TU Delft (2007).

[3] B. Y. V. Hayward and K. E. Maclean, *Do It Yourself Haptics: Part I,* IEEE Robotics & Automation Magazine **14**, 88 (2007).

[4] L. Rosenberg and B. Adelstein, *Perceptual decomposition of virtual haptic surfaces,* Proceedings of 1993 IEEE Research Properties in Virtual Reality Symposium (1993), 10.1109/VRAIS.1993.378264.

[5] B. Hannaford and A. M. Okamura, *Haptics,* in *Springer Handbook of Robotics* (Springer Handbooks, 2008) pp. 719–739.

[6] J. Colgate and J. Brown, *Factors affecting the Z-Width of a haptic display,* Proceedings of the 1994 IEEE International Conference on Robotics and Automation , 3205 (1994).

[7] D. a. Lawrence, *Stability and transparency in bilateral teleoperation,* IEEE Transactions on Robotics and Automation **9**, 624 (1993).

[8] N. Colonnese, A. Siu, C. Abbott, and A. Okamura, *Rendered and Characterized Closed-loop Accuracy of Impedance-type Haptic Displays,* IEEE Transactions on Haptics **1412**, 1 (2015).

[9] C. G. Rose, J. A. French, and M. K. O'Malley, *Design and characterization of a haptic paddle for dynamics education,* IEEE Haptics Symposium, HAPTICS , 265 (2014).

[10] S. Martin and N. Hillier, *Characterisation of the Novint Falcon Haptic Device for Application as a Robot Manipulator,* in *Australian Conference on Robotics and Automation (ACRA)* (2009).

[11] M. Harders, A. Barlit, K. Akahane, and M. Sato, *Comparing 6dof haptic interfaces for application in 3d assembly tasks,* Proc. of EuroHaptics' , 3 (2006).

[12] Y. Yokokohji, Y. Iida, and T. Yoshikawa, *"Toy problem" as the benchmark test for teleoperation systems,* Proceedings. 2000 IEEE/RSJ International Conference on Intelligent Robots and Systems (IROS 2000) , 996 (2000).

[13] E. Ruffaldi, D. Morris, T. Edmunds, F. Barbagli, and D. Pai, *Standardized Evaluation of Haptic Rendering Systems,* 2006 14th Symposium on Haptic Interfaces for Virtual Environment and Teleoperator Systems , 225 (2006).

[14] J. E. Colgate, M. C. Stanley, and G. Schenkel, *Dynamic range of achievable impedances in force reflecting interfaces,* in *Proc. SPIE Telemanipulator Technology and Space Telerobotics Conference*, Vol. 2057 (1993) pp. 199–210.

[15] J. J. Gil and E. Sanchez, *Stability Boundary for Haptic Rendering: Influence of Damping and Delay,* Journal of Computing and Information Science in Engineering **9**, 11005 (2009).

[16] N. Colonnese and A. Okamura, *Stability and quantization-error analysis of haptic rendering of virtual stiffness and damping,* The International Journal of Robotics Research **Oktober 6** (2015), 10.1177/0278364915596234.

[17] J. J. Gil and E. Sanchez, *Stability Boundary for Haptic Rendering: Influence of Damping and Delay,* IEEE International Conference on Robotics and Automation , 124 (2007).

[18] C. Richard, A. M. Okamura, and M. R. Cutkosky, *Getting a Feel for Dynamics: using haptic interface kits for teaching dynamics and controls,* ASME Symposium on Haptic Interfaces for Virtual Environment and Teleoperator Systems (Haptics) , 15 (1997).

[19] A. Lavatelli, P. Milano, F. Ferrise, D. Meccanica, and M. Bordegoni, *Design of an Open-Source Low Cost 2DOF Haptic Device,* in *Mechatronic and Embedded Systems and Applications (MESA), 2014 IEEE/ASME 10th International Conference on* (2014) pp. 1–6.

[20] N. Beni, M. Grottoli, F. Ferrise, and M. Bordegoni, *Rapid prototyping of low cost 1 DOF haptic interfaces,* 2014 IEEE Haptics Symposium (HAPTICS) , 479 (2014).

[21] D. A. Lawrence, A. C. White, L. Y. Pao, and W. Xu, *Low cost actuator and sensor for high-fidelity haptic interfaces,* in *Proceedings - 12th International Symposium on Haptic Interfaces for Virtual Environment and Teleoperator Systems, HAPTICS* (2004) pp. 74–81.

[22] A. Eilering, G. Franchi, and K. Hauser, *ROBOPuppet : Low-Cost , 3D Printed Miniatures for Teleoperating Full-Size Robots,* in *International Conference on Intelligent Robots and Systems (IROS 2014)* (IEEE, Chicaco, IL, USA, 2014) pp. 1248–1254.

[23] J. G. W. Wildenbeest, D. a. Abbink, C. J. M. Heemskerk, F. C. T. Van Der Helm, and H. Boessenkool, *The impact of haptic feedback quality on the performance of teleoperated assembly tasks,* IEEE Transactions on Haptics **6**, 242 (2013).

[24] R. Kuiper, L. Boerefijn, W. Heij, M. Flipse, W. Vreugdenhil, and K. Wang, *Gemini - 1 dof telemanipulator,* `http://www.delfthapticslab.nl/device/gemini-1dof-master-slave/` (2014), accessed: 09-May-2016.

[26] N. Diolaiti, G. Niemeyer, F. Barbagli, and J. K. Salisbury, *Stability of haptic rendering: Discretization, quantization, time delay, and Coulomb effects,* IEEE Transactions on Robotics **22**, 256 (2006).

[25] R. Adams and B. Hannaford, *Stable haptic interaction with virtual environments,* IEEE Transactions on Robotics and Automation **15**, 465 (1999).

[27] H. Z. Tan, B. Eberman, M. A. Srinivasan, and B. Cheng, *Human Factors for the Design of Force-Reflecting Haptic Interfaces,* in *Proceedings of the ASME Dynamics Systems and Control Division*, Vol. 55, edited by C. J. Radcliffe (1994) pp. 353–359.

[28] V. Hayward and O. R. Astley, *Performance Measures for Haptic Interfaces,* in *International Symposium In Robotics Research* (1996).

[29] T. Brooks, *Telerobotic response requirements,* in *IEEE International Conference on Systems, Man, and Cybernetics Conference Proceedings* (IEEE, 1990) pp. 113–120.

[30] D. Lawrence and J. Chapel, *Performance trade-offs for hand controller design,* Proceedings of the 1994 IEEE International Conference on Robotics and Automation (1994), 10.1109/ROBOT.1994.351076.

[31] J. J. Gil, A. Avello, acAngel Rubio, and J. Flórez, *Stability analysis of a 1 DOF haptic interface using the Routh-Hurwitz criterion,* IEEE Transactions on Control Systems Technology **12**, 583 (2004).

[32] J. J. Abbott and A. M. Okamura, *Effects of position quantization and sampling rate on virtual-wall passivity,* IEEE Transactions on Robotics **21**, 952 (2005).

[33] M. Minsky, O.-y. Ming, O. Steele, F. P. Brooks, and M. Behensky, *Feeling and seeing: issues in force display,* ACM SIGGRAPH Computer Graphics **24**, 235 (1990).

[34] T. Hulin, C. Preusche, and G. Hirzinger, *Stability Boundary for Haptic Rendering: Influence of Physical Damping,* Spring , 1570 (2006).

[35] R. Ellis, O. Ismaeil, and M. Lipsett, *Design and evaluation of a high-performance haptic interface,* Robotica **14**, 321 (1996).

[36] P. Fischer, R. Daniel, and K. Siva, *Specification and design of input devices for teleoperation,* in *Proceedings., IEEE International Conference on Robotics and Automation* (IEEE Comput. Soc. Press, 1990) pp. 540–545.

[37] V. Chawda, O. Celik, and M. K. O'Malley, *A Method for Selecting Velocity Filter Cut-Off Frequency for Maximizing Impedance Width Performance in Haptic Interfaces,* Journal of Dynamic Systems, Measurement, and Control **137**, 024503 (2014).

[38] G. Millet, S. Haliyo, S. Regnier, and V. Hayward, *The ultimate haptic device: First step,* Proceedings - 3rd Joint EuroHaptics Conference and Symposium on Haptic Interfaces for Virtual Environment and Teleoperator Systems, World Haptics 2009 , 273 (2009).

[39] V. Hayward, O. R. Astley, M. Cruz-Hernandez, D. Grant, and G. Robles-De-La-Torre, *Haptic interfaces and devices,* Sensor Review **24**, 16 (2004).

[40] P. Berkelman, *Tool-Based Haptic Interaction with Dynamic Physical Simulations using Lorentz Magnetic Levitation,* Interface , 1 (1997).

[41] M. R. Cutkosky, T. Morimoto, A. Okamura, and P. Blikstein, *Hapkit by stanford university,* http://hapkit.stanford.edu/index.html (2015), accessed: 03-Dec-2015.

[42] J.-P. Merlet, *Civil Engineering*, Vol. 208 (Springer, 2006) p. 415.

[43] R. Clavel, *Device for the movement and positioning of an element in space,* (1990).

[44] N. T. Inc., *Novint falcon technical specifications,* http://www.novint.com/index.php/novintxio/41 (2015), accessed: 03-Dec-2015.

[45] E. Samur, *The Springer Series on Touch and Haptic Systems* (Springer Handbooks, London, 2012).

[46] M. Plooij, M. Van Nunspeet, M. Wisse, and H. Vallery, *Design and evaluation of the Bi-directional Clutched Parallel Elastic Actuator (BIC-PEA),* Proceedings - IEEE International Conference on Robotics and Automation **2015-June**, 1002 (2015).

[47] M. Plooij, T. Van Der Hoeven, G. Dunning, and M. Wisse, *Statically balanced brakes,* Precision Engineering **43**, 468 (2016).

[48] S. Bakshi, *Feedback Control Systems* (Technical Publications, 2009).

[49] K. Åström and R. Murray, *Feedback Systems, An Introduction for Scientists and Engineers*, version v2.11b ed. (Princeton University Press, 2012).

[50] MaxonMotor, *Maxon motor online catalog,* urlhttp://www.maxonmotor.com/maxon/view/catalog/ (2016), accessed: Jan-2016.

[51] FaulhaberGroup, *Faulhaber brushless dc-motors,* https://fmcc.faulhaber.com/type/PGR_13814_13801/PGR_13822_13814/en/GLOBAL/ (2016), accessed: Jan-2016.

[52] U. Hagn, R. Konietschke, B. Kübler, U. Seibold, A. Tobergte, M. Nickl, S. Jörg, and G. Hirzinger, *Telemanipulator for remote minimally invasive surgery,* IEEE Robotics and Automation Magazine **15**, 28 (2008).

[53] D. A. Abbink and M. Mulder, *Neuromuscular Analysis as a Guideline in designing Shared Control,* in *Advances in Haptics* (INTECH, 2010) pp. 499–516.

[54] K. MacLean and V. Hayward, *Do It Yourself Haptics: Part II,* IEEE Robotics & Automation Magazine **15**, 104 (2008).

[55] Sensable, *Phantom omni technical specifications,* http://www.dentsable.com/haptic-phantom-omni.htm (2015), accessed: 07-Dec-2015.

[56] L. Vanacken, J. De Boeck, and K. Coninx, *The Phantom versus the Falcon: Force feedback magnitude effects on user's performance during target acquisition,* in *Haptic and Audio interaction design*, Vol. 6306 LNCS (Springer Berlin Heidelberg, Berlin, 2010) pp. 179–188.

[57] M. Khan, S. Sulaiman, A. M. D. Said, and M. Tahir, *Exploring the quantitative and qualitative measures for haptic systems,* Proceedings 2010 International Symposium on Information Technology - Visual Informatics, ITSim'10 **1** (2010), 10.1109/ITSIM.2010.5561305.

[58] S. Shayan-Amin, L. L. Kovacs, and J. Kovecses, *The role of mechanical properties on the behaviour and performance of multi-dof haptic devices,* 2013 World Haptics Conference (WHC) , 725 (2013).

[59] G. a. V. Christiansson and F. C. T. van der Helm, *The Low-Stiffness Teleoperator Slave - a Trade-off between Stability and Performance,* The International Journal of Robotics Research **26**, 287 (2007).

[60] J. Colgate and G. Schenkel, *Passivity of a class of sampled-data systems: application to haptic interfaces,* Proceedings of 1994 American Control Conference - ACC '94 **3**, 37 (1994).

[61] R. Daniel and P. McAree, *Fundamental Limits of Performance for Force Reflecting Teleoperation,* The International Journal of Robotics Research **17**, 811 (1998).

[62] R. V. D. Linde, P. Lammertse, E. Frederiksen, and B, *The HapticMaster, a new high-performance haptic interface,* Proc. EuroHaptic, Edinburgh, UK , 1 (2002).

[63] N. Colonnese, S. M. Sketch, and A. M. Okamura, *Closed-loop stiffness and damping accuracy of impedance-type haptic displays,* 2014 IEEE Haptics Symposium (HAPTICS) , 97 (2014).

[64] D. W. Weir and J. E. Colgate, *Stability of Haptic Displays,* Haptic Rendering: Foundations, Algorithms, and Applications (2008), 10.1201/b10636-9.

[65] B. Hannaford, *Stability and performance tradeoffs in bi-lateral telemanipulation,* Proceedings, 1989 International Conference on Robotics and Automation , 1764 (1989).

[66] G. a. V. Christiansson and E. C. Fritz, *A novel planar 3-DOF hard-soft haptic teleoperator,* Proceedings - Second Joint EuroHaptics Conference and Symposium on Haptic Interfaces for Virtual Environment and Teleoperator Systems, World Haptics 2007 , 361 (2007).

[67] A. Hoevenaars, *Parallel haptic master device for needle steering, delft haptics lab,* `http://www.delfthapticslab.nl/device/parallel-haptic-master-device-for-needle-steering/` (2015), accessed: 07-Dec-2015.

[68] D. a. Lawrence, L. Y. Pao, M. a. Salada, and A. M. Dougherty, *Quantitative Experimental Analysis of Transparency,* in *Fifth Annual Symposium on Haptic Interfaces for Virtual Environment and Teleoperator Systems* (Atlanta, GA, USA, 1996) pp. 441–449.

[69] R. J. Adams, M. R. Moreyra, and B. Hannaford, *Stability and Performance of Haptic Displays : Theory and Experiments,* Proceedings ASME International Mechanical Engineering Congress and Exhibition , 227 (1998).